



Control of Grid Side Inverter in a B2B Configuration for WT Applications

Master Thesis

by

George Alin RADUCU

PED10-1015b

Aalborg University, 2008

Preface

This present Master Thesis ‘Control of Grid Side Inverter in a B2B Configuration for WT Applications’ is written by group 1015b at the 10th semester at Aalborg University, Institute of Energy Technology, Department of Power Electronics and Drives. The project period is from 1.02.2008 to 11.06.2008. The report consists of two parts: a main part and an appendix part. The main part consist of six parts (1-6), defining the demands for the applications in which the control schemes are to be used, and describing and modeling the test systems. The systems are modeled and control schemes are designed and implemented. Conclusions will be drawn concerning the accuracy of the developed models and achieved results. The appendix part contains 2 parts (A-B). Appendix A includes information about the reference frame theory, in appendix B can be found the simulation and implementation models. Equations are numbered in format (X.Y) and figures are numbered in format figure X.Y, where X is the chapter number and Y is the number of the item. The enclosed CD contains the report in Adobe PDF format, documentations used throughout the report and Simulink Models and their implementation in dSPACE platform. Author would like to thanks to the supervisors Florin IOV for the support and ideas provided throughout the project period.



TITLE: Control of Grid Side Inverter in a B2B Configuration for WT Applications

PROJECT PERIOD: 1.02.2008 to 11.06.2008

PROJECT GROUP: PED10-1015b

AUTHORS:

George Alin RADUCU

SUPERVISOR:

Florin IOV

NUMBER OF COPIES: 3

NUMBER OF PAGES

Report: 96

COMPLETED:

11.06.2008

ABSTRACT

The increase interest in renewable energy production together with higher and higher demand from the energy distribution companies (TSO) regarding grid energy injection and grid support in case of a failure raises new challenges in terms of control for wind turbine (WT) systems. Due to the above mentioned, grid side inverter control in WT systems is one of the main issues in decentralized power production units.

This project deals with the design and implementation of one control method for the grid side converter in a back-to-back configuration.

This project will review different control techniques for grid inverters systems and an overview of the grid codes will be included. Targeted applications are decentralized grid connected systems, wind turbines in this case, but motor/generator applications may also be considered. A particular control method has been selected and implemented in laboratory using a dSpace setup. The control strategy chose is *Voltage Oriented Control (VOC)* where the active and reactive power are regulated by controlling the i_d and i_q current components.

Table of Contents

1. Introduction	Page 1
1.1. Background of Wind Energy Systems.....	Page 3
1.2. Project description.....	Page 6
1.3. Project goals.....	Page 7
2. Power Electronics based WT	Page 10
2.1. Grid code overview.....	Page 11
2.2. Power converters in grid connected applications.....	Page 23
2.2.1 Control strategy for grid side converter.....	Page 28
3. Modeling	Page 39
3.1. Introduction.....	Page 40
3.2. Plant model	Page 40
3.2.1 Grid side converter.....	Page 41
3.2.2 Space vector modulation.....	Page 43
3.2.3 LCL filter.....	Page 45
3.2.4 Grid model.....	Page 49
3.2.5 DC link circuit.....	Page 50
4. Control strategies design	Page 51
4.1 Introduction.....	Page 52
4.2 Control method.....	Page 52
4.3 Phase locked loop.....	Page 56
4.4 The d axis and q axis current controller.....	Page 58
4.5 DC voltage controller.....	Page 60
5. Simulation and experimental results	Page 65
5.1 Introduction.....	Page 66
5.2 Simulation results	Page 66
5.3 Implementation and experimental evaluation.....	Page 70
5.4 Experimental results.....	Page 74
6. Conclusions and future work	Page 79
6.1. Conclusions.....	Page 79
6.2. Future work.....	Page 81
References	Page 83
Nomenclature	Page 87
Abbreviations	Page 89
Appendix A	Page 91
Appendix B	Page 95

Chapter 1

1. Introduction

Abstract

This project deals with the design of the grid side converter control in a back to back configuration for wind turbine application. In the first chapter a short background of the wind energy system is given and a description of the project and goals is presented. Then, an overview of the grid codes and control strategies for the grid side converter is presented.

1.1. Background of Wind Energy Systems.....	Page 3
1.2. Project description.....	Page 6
1.3. Project goals.....	Page 7

1.1. Background of Wind Energy Systems

The global energy consumption is rising and an increasing attention is being paid to alternative methods of electricity generation. The very low environmental impact of the renewable energies makes them a very attractive solution for a growing demand. In this trend towards the diversification of the energy market, wind power is probably the most promising sustainable energy source. The progress of wind power in recent years has exceeded all expectations, with Europe leading the global market [1]. Recent progress in wind technology has led to cost reduction to levels comparable, in many cases, with conventional methods of electricity generation.

Power electronics are nowadays used to efficiently interface renewable energy systems to the grid [2]. They are playing a very important role in modern wind energy conversion system (WECS) especially for MW-size wind turbines (WT) concentrated in large wind farms. Control of WECSs, performed by means of power electronics, allow the fulfilment of grid requirements, a better use of the turbine capacity and the alleviation of aerodynamic and mechanical loads that reduce the lifetime of installation [1]. Furthermore, with WECSs approaching the output rating of conventional power plants, control of the power quality is required to reduce the adverse effects of their integration into the grid. Even though active control has an immediate impact on the cost of wind energy, it leads to high performance that is essential to enhance the competitiveness of wind technology.

1.1.1 Power control capability

WECSs have to cope with the intermittent and seasonal variability of the wind. By this reason they begin to work when the wind speed is above the cut-in speed so that power is injected into the utility grid; moreover they include some mechanisms to limit the captured power at high wind speeds to prevent overloading. Three control strategies can be used for captured power control [2] [1]:

- stall control;
- pitch control;
- active stall control.

The stall control is based on a specific design of the blades so that stall occurs when the wind speed exceeds a certain level; it means that the captured power is automatically limited in the rated power range. This method is simple, robust and cheap but it has low efficiency at low wind speed.

In case of pitch control, blades can be tuned away from or into the wind as the captured power becomes too high or too low; this is performed by rotating the blades, or part of them, with respect to their longitudinal axes. Below rated wind speed, blades are pitched for optimum power extraction whereas above the rated wind speed blades are pitched to small angle of attack for limiting the power. Advantages of this type of control are good power control performance, assisted start-up and emergency power reduction; the biggest disadvantage is the extra complexity due to the pitch mechanism.

In case of active stall control, the stall is actively controlled by pitching blades to larger angle of attack with wind speed above the rated value.

1.1.2 Speed control capability

Beyond the captured power controllability, another important feature is the speed controllability.

Based on this, WTs are classified into two main categories [2][3]:

- Fixed speed WTs;
- Variable speed WTs.

Fixed speed WTs are equipped with induction generator (squirrel cage induction generator SCIG or wound rotor induction generator WRIG) directly connected to the grid and a capacitor bank for reactive power compensation. This is a very reliable configuration because of the robust construction of the standard IG. The IG synchronous speed is fixed and determined by the grid frequency regardless of the wind speed; this implies that such WTs can obtain maximum efficiency at one wind speed. As power electronics is not involved in this configuration, it is not possible to control neither reactive power consumption nor power quality; in fact due to its fixed speed, wind fluctuations are converted into torque fluctuations, slightly reduced by small changes in the generator slip, and transmitted as power fluctuations into the utility grid yielding voltage variations especially in weak grids.

Variable speed WTs are equipped with an induction or synchronous generator connected to the grid through a power converter. The variable speed operation, made possible by means of power electronics, allows such WTs to work at the maximum conversion efficiency over a wide range of wind speeds. The most commonly used WT designs can be categorized into four categories [2][3][1][4]:

- fixed speed WTs (FSWT);
- partial variable speed WTs with variable rotor resistance (PVSWT);

- variable speed WTs with partial-scale frequency converter, known as doubly-fed induction generator-based concept (DFIGWT);
- variable speed WTs with full-scale power converter (FSPCWT).

Fig.1.1 shows the structure of the above concepts. They differ in the generating system (electrical generator) and the way used to limit the captured aerodynamic power above the rated value. Fixed speed WTs are characterized by a squirrel cage induction generator (SCIG) directly connected to the grid by means of a transformer [2]. The rotor speed can be considered locked to the line frequency as very low slip is encountered in normal operation (typically around 2%). The reactive power absorbed by the generator is locally compensated by means of a capacitor bank following the production variation (5-25 steps) [2]. A soft-starter can be used to provide a smooth grid connection.

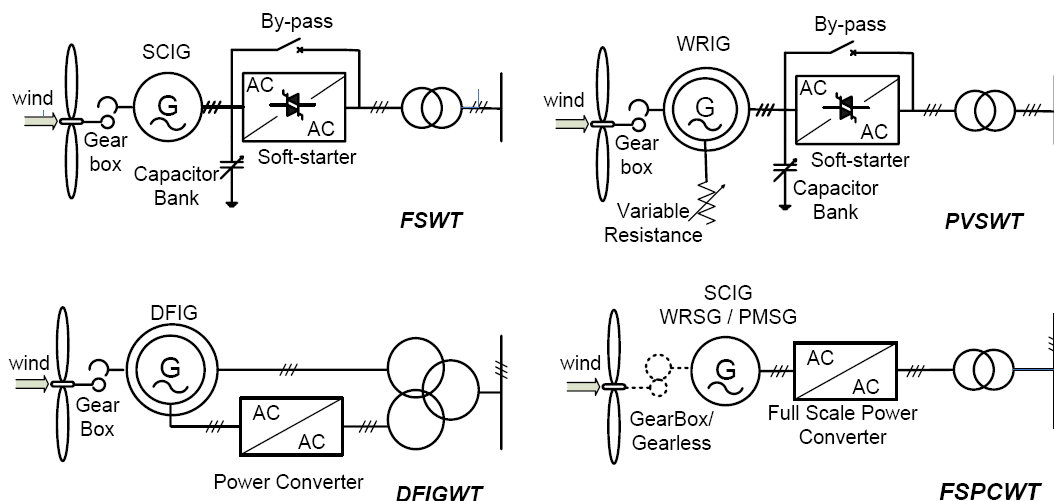


Fig.1.1 Wind turbine concepts

This configuration is very reliable because of the robust construction of the standard SCIG and the simplicity of the power electronics [2][1].

Partial variable speed WTs with variable rotor resistance use a WRIG connected to the grid by means of a transformer [2][1][5]. The rotor winding of the generator is connected in series with a controlled resistance; it is used to change the torque characteristic and the operating speed in a narrow range (typically 0 – 10% above the synchronous speed) [2]. A capacitor bank performs the reactive power compensation and smooth grid connection occurs by means of a soft-starter.

For a DFIGWT, the stator is directly coupled to the grid while a partial scale power converter controls the rotor frequency and, thus, the rotor speed [2][1][5][6]. The partial scale power converter is rated at 20% – 30% of the WRIG rating so that the speed can be varied within $\pm 30\%$

of the synchronous speed. The partial scale frequency converter makes such WTs attractive from the economical point of view. However, slip rings reduce the reliability and increase the maintenance.

Variable speed FSPCWTs are characterized by the generator connected to the grid by means of the full-scale frequency converter [2][1][5]; the converter performs the reactive power compensation and a smooth grid connection [7][8]. Synchronous generators have so far dominated the market for variable speed wind turbines; now induction generators are becoming more popular in WECS industry and also for variable speed applications [7][1].

1.1.3 Control Objectives

WECSs connected to the grid must be designed to minimize the cost of supplied energy ensuring safe operation, acoustic emission and grid connection requirements. Control objectives involved in WECSs are [1]:

- energy capture;
- mechanical load;
- grid connection requirements.

1.2. Project description

This project deals with grid side converter control in a back to back configuration for wind turbine application. The increase interest in renewable energy production together with higher and higher demand from the energy distribution companies (TSO), regarding grid energy injection and grid support in case of a failure, raises new challenges in terms of control for wind turbine systems. According to [2], FSPCWT it is the second most common WT concept in the MW range on the market while the most common is the concept based on the DFIGWT. However, the concept FSPCWT has the chance in the next future to become the best solution as the higher cost is balanced by the power quality, harmonic compensation and full grid support by 100% reactive current injection during grid events [2][7].

Due to the above mentioned, grid side inverter control in WT systems is one of the main issues in decentralized power production units. This is due to the presence of some filtering means at the inverter output, which will introduce system stability problems.

The real system of the FSPCWT is represented in Fig 1.2. The SCIG is connected to the ac grid through a frequency converter, the so called back-to-back PWM-VSI; it is a bi-directional power converter consisting of two conventional PWM-VSCs (generator and grid side converters).

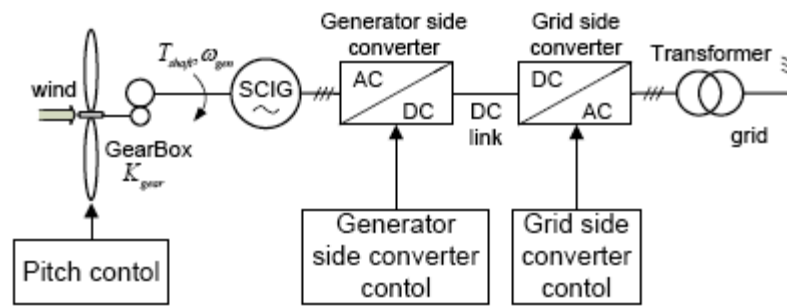


Fig.1.2 Layout of the real system

Since that the wind turbine and generator side converter are not the main issue for this project the modified layout of the system can be represent in Fig 1.3 where is represented only the grid side converter connected to the grid by means of a passive filter and a transformer.

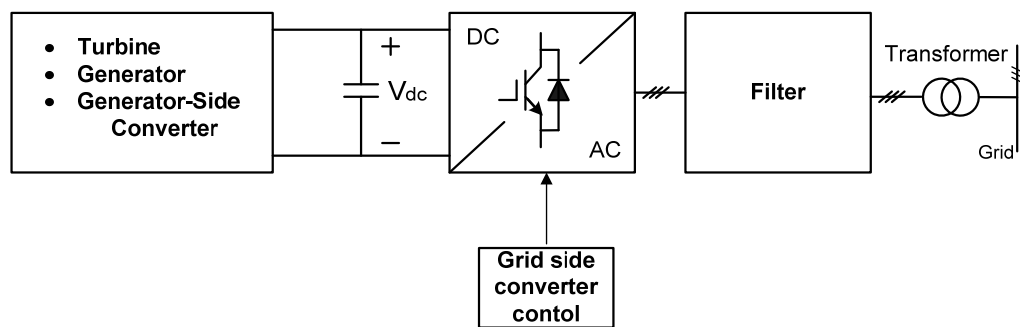


Fig.1.3 Modified layout of the real system

1.3. Project goals

This project will review different control techniques for grid inverters systems. Targeted applications are decentralized grid connected systems, WT in this case, but motor/generator applications may also be considered. Control techniques for the grid inverter must be modeled and simulated, followed by a comparative analysis. A particular control method must be selected and implemented in laboratory using dSpace setup.

The goals of this project are summarized below:

- Implement a control technique for the grid side inverter including a passive filter
- Harmonic compensation techniques

1.4. Project limitation

Due to the physical limitations, the following rating for the PWM rectifier is being considered:

- Grid voltage: $e=3 \times 400\text{V}$;
- Output voltage: $V_{dc}=700\text{V}$;
- Nominal output power: $P_{out}=3\text{kW}$;
- Nominal output current: $I_{out}=4.3\text{A}$;
- Power factor: $PF=1$;

Chapter 2

Power Electronics based WT

Abstract

In this chapter, an overview of the grid codes and control strategies for the grid side converter are presented. Power converters in grid connected applications and topologies for the wind turbines will be described on the end of this chapter.

2.1. Grid code overview.....	Page 11
2.2. Power converters in grid connected applications.....	Page 23
2.2.1 Control strategy for grid side converter.....	Page 28

2.1 Grid codes overview

Early wind power plant in Europe was connected to distribution networks, but, in recent years, more and larger wind farms have been connected to transmission networks. Each of these network levels has specific requirements when connecting wind power. The connection issues for the network are related to grid stability which is influenced by power flows and wind farm behaviour in case of network faults. Grid operators (transmission, distribution) develop rules (grid codes) for connecting generators. Their grid codes have been complemented by specific codes for wind power plants, and the wind turbine manufacturers have responded to these requirements by design measures, mainly in the area of wind turbine control and electrical system design. During the last few years, there has been a special interest on the grid integration of wind turbines. This has led to a re-definitions of the grid connection conditions by the system operator (SO) in different countries. The aim of the requirements is to ensure that wind farms do not adversely affect the power system operation with respect to security of supply, reliability and power quality [9][10]. Essential grid code requirements are related to frequency, voltage and wind turbine behaviour in case of grid faults. The most common requirements concern [9]:

- *active power control*: several grid codes (GCs) require the active control of the wind farm output power in order to participate to the energy dispatch as conventional power plants and to prevent overloading of lines.
- *frequency control*: some GCs require WTs to participate to the frequency control as conventional power plants; the frequency is kept within acceptable limits to ensure the security of supply, prevent the overloading of electric equipment and fulfil the power quality standards.
- *frequency and voltage ranges*: ranges of voltage amplitude and frequency are provided for continued operation in case the system is in trouble (i.e. voltage and frequency stability problems).
- *voltage control*: some GCs require WTs to perform the voltage control as conventional power plants; this is performed by controlling the reactive power.

- *voltage quality*: a whole set of different requirements is included in national GCs with respect to rapid changes, flicker and harmonics.
- *tap-changing transformers*: some grid codes (i.e. E.on Netz, ESBNG) require that wind farms are equipped with tap-changing grid transformer in order to be able to vary the voltage ratio between the wind farm and the grid when needed.
- *fault ride-through capability*: some GCs require WTs to remain connected and, in some cases, to support the power system by injecting sufficed reactive power in order to ensure the system stability.
- *wind farm modelling and verification*: some GCs require wind farm owners/developers to provide models and system data, to enable the TSO to investigate by simulations the interaction between the wind farm and the power system. They also require installation of monitoring equipment to verify the actual behaviour of the farm during faults and to check the model.
- *communications and external control*: most GCs require that the wind farm operator provide on-line measurement of some important variables for the system operator to enable proper operation of the power system (i.e. voltage, active and reactive power, operating status and wind speed). Only in few cases (i.e. Denmark and E.on), it is required the possibility to connect and disconnect the wind turbines externally.

According to [13] the main topics for RES interconnection are presented:

- Active power/frequency control.
- Reactive power/voltage control
- Design voltages and frequencies.
- Fault ride-through capability.
- Power quality issues.

In the following paragraphs an overview of the most important Danish, Irish and German connection requirements for wind turbines to electrical network with voltages below 100 kV is presented based on [13].

2.1.1 Denmark

2.1.1.1 Voltage level

In the Table2.1 is presented the voltage levels of the electrical network in Denmark.

	Nominal voltage	Lower limit U_L	Lower limit full load U_{LF}	Upper-limit full-load U_{HL}	Upper limit U_H
Distribution	0.4 kV	360 V	380 V	440 V	440 V
	10 kV	9.5 kV	10 kV	11 kV	12 kV
	15 kV	13.5 kV	14.5 kV	16.5 kV	17.5 kV
	20 kV	18 kV	20 kV	22 kV	24 kV
	30 kV	27 kV	28.5 kV	33 kV	26 kV
	50 kV	45 kV	47.5 kV	55 kV	60 kV
	60 kV	54 kV	57 kV	66 kV	72.5 kV
Transmission	132 kV	119 kV	125 kV	145 kV	155 kV
	150 kV	135 kV	146 kV	170 kV	180 kV
	400 kV	320 kV	360 kV	420 kV	440 kV

Table2.1: Voltage levels for electrical network in Denmark

2.1.1.2 Active power/frequency control

According to this demand the wind turbines must be able to control the active in the Point-of-Common-Coupling (PCC) in a given range. The active power is typically controlled based on the system frequency [14]. Because the wind can not be controlled, the output power of the wind turbine can be controlled by most modern turbines through the ability of the generators to increase/decrease the output power in order to support system frequency during an unexpected demand or after a loss of a network element.

The requirement of frequency control includes frequency response capability, limitation of ramp rates and active power output. A typical characteristic for the frequency control in the Danish grid code is shown in Fig.2.1 [14].

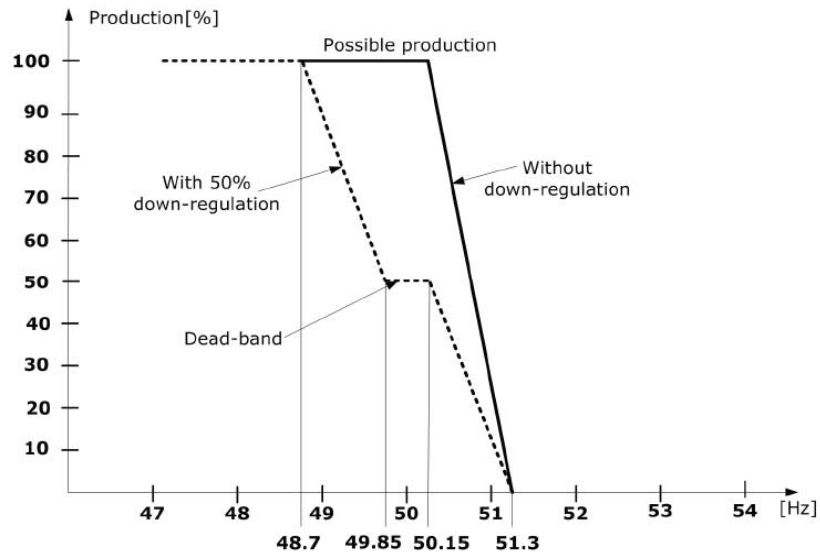


Fig.2.1 Frequency control characteristic for the wind turbines connected to the Danish grid

The nominal frequency is the same throughout a synchronously-operated system and is normally maintained within a narrow band. Any deviation from the planned production or consumption moves the frequency away from its nominal value. If the deviation is large enough, the frequency falls out of its normal. Abnormal frequencies increase the operating temperatures of generator windings, shorten the lifetime of insulation, and can damage power electronics [9].

Currently, Denmark has the most demanding requirements regarding the controllability of the produced power. Wind farms connected at the transmission level shall act as a conventional power plant providing a wide range of controlling the output power based on Transmission System Operator's (TSO) demands and also participation in primary and secondary control [14].

2.1.1.3 Reactive power/voltage control

Reactive power is typically controlled in a given range. The grid codes specify in different ways this control capability. The Denmark's grid code gives a band for controlling the reactive power based on the active power output as shown in Fig.2.2 [14]. The reactive power flow between the wind turbine including the transformer and the electrical network must be calculated as an average value over 5 min within the control band [13][14].

The capability of a wind turbine to control voltage and reactive power depends on its generator type. A squirrel cage induction generator applied in fixed speed wind turbines is a consumer of reactive power and needs additional equipment to provide fast control of reactive power (i.e. Static VAR compensators – SVCs or STATCOMs). This can be implemented as centralised compensation equipment of the wind farm or by individual wind turbines. Modern MW size fixed

speed wind turbines are mostly equipped with these devices, but the older machines of this type would need modification in order to be able to provide reactive power control. [9]

A doubly-fed induction generator (DFIGWT) is capable of reactive power control, fulfils the requirement of the leading power factor of 0.925 without difficulties, but may have problems with the maximum power output when the lagging power factor of 0.85 is required. Compliance with this requirement demands increased frequency converter rating and possibly increased ratings of rotor and stator conductors.[9]

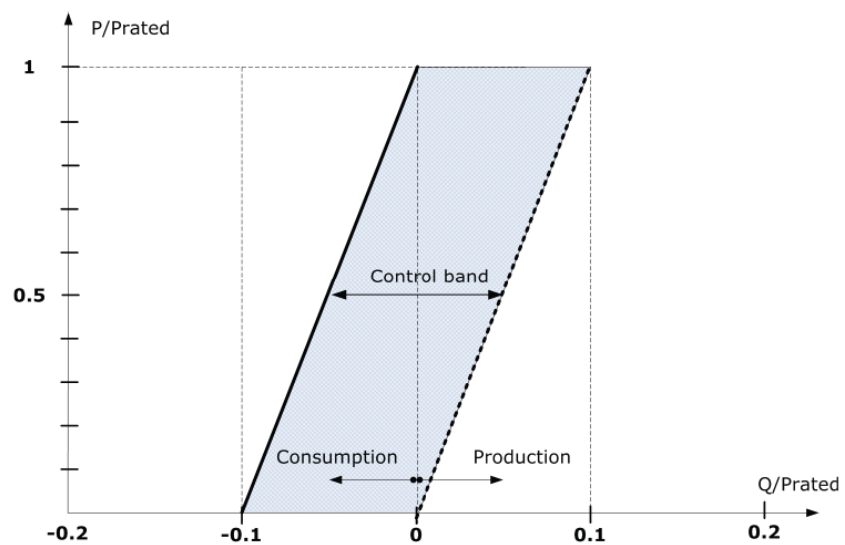


Fig.2.2 Danish grid code demands for the reactive power exchange in the PCC[14]

2.1.1.4 Power quality

Power quality is a concept used to characterise an essential set of parameters that determine the impact of wind turbines on the voltage quality of an electric power network. It applies in principle both to transmission and distribution networks, but is far more essential for the medium voltage networks[9]. The relevant parameters are active and reactive power, including maximum value, voltage fluctuations (flicker), number of switching operations (and resulting voltage variations), harmonic currents and related quantities. A schedule of individual harmonics distortion limits for voltage are also given based on standards or in some cases e.g. Denmark custom harmonic compatibility levels are defined and interharmonics may also be considered. [14].This levels are presented in Fig.2.3.

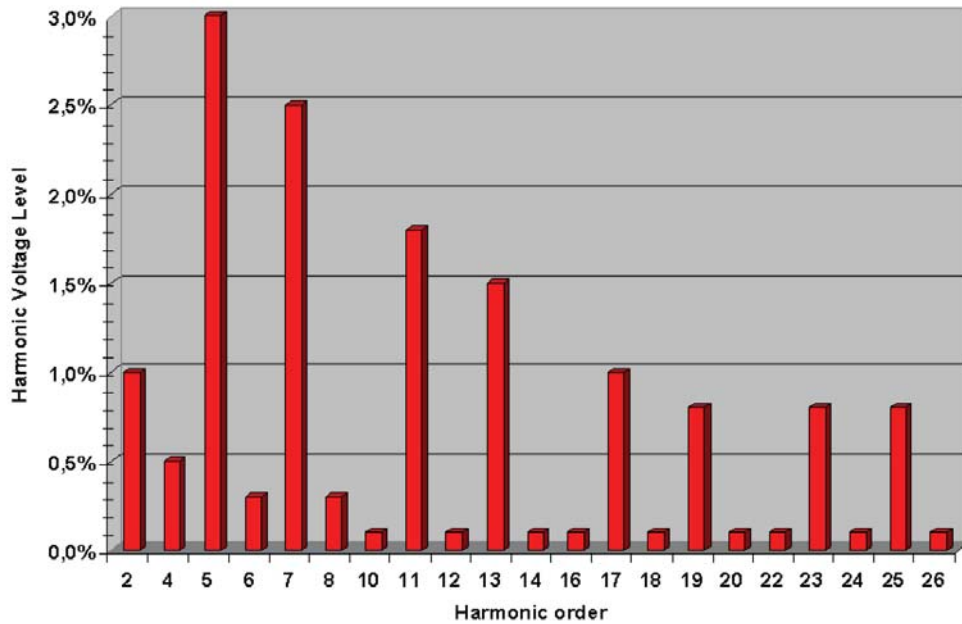


Fig.2.3 Harmonics level [14]

2.1.1.5 Fault ride-through requirements

A particular concern of some TSOs is the ability of generators to remain stable and connected to the network when faults occur on the transmission network. This is known as fault ride-through capability (FRT) or low-voltage-ride-through capability. The capability of wind farms to support the grid in case of voltage dips in the system is an area that is still under development.[9]

All considered grid codes require fault ride-through capabilities for wind turbines. Voltage profiles are given specifying the depth of the voltage dip and the clearance time as well. One of the problems is that the calculation of the voltage during all types of unsymmetrical faults is not very well defined in some grid codes. The wind turbine shall be disconnected from the electrical grid, according to [13], as shown in Fig.2.4

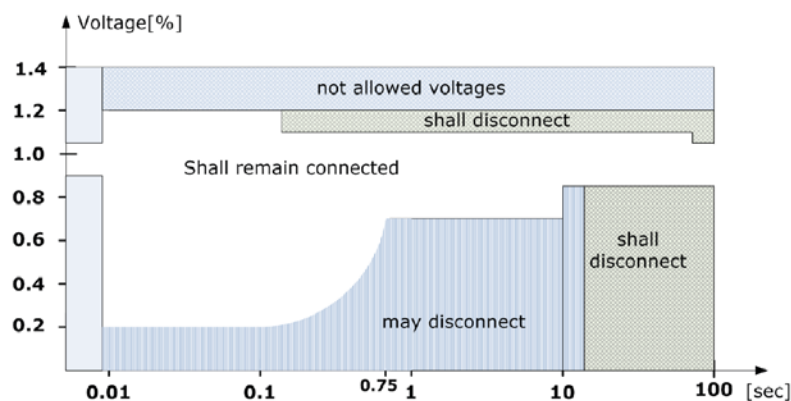


Fig.2.4 Requirements for disconnection of wind turbines under voltage dips/sags

In some special situations when a WT shall not be disconnected from the electrical network are specified according to [13].

- 3-phase short-circuit for 100 msec;
- 2-phase short-circuit with or without ground for 100 msec followed after 300-500 msec by a new short-circuit of 100 msec duration.

2.1.2 Ireland

2.1.2.1 Voltage level

The DS in Ireland includes networks operating at the nominal voltages as shown in Table 2.2

	Nominal voltage	Upper limit	Lower Limit	Neutral treatment
Low Voltage (LV)	230 V phase to neutral	244 V	207 V	-
	400 V phase to phase	424 V	360 V	-
Medium Voltage (MV)	10 kV	10,75 kV	Variable according to operating conditions.	Isolated neutral ¹⁾
	20 kV	21,5 kV		Earthed through a 20 ohms resistor which limits eart fault current to 500 A
High Voltage (HV)	38 kV	41,35 kV		Earthed through an arc suppression coil at source 110 kV substations
	110 kV	120 kV		Effectively earthed

Table2.2: Voltage levels for electrical network in Ireland

2.1.2.2 Active power/frequency control

According to [13] the Wind Farm Power Stations(WFPS) from Ireland must have the capability to:

- Operate continuously at normal rated output at frequencies in the range 49.5 Hz to 50.5 Hz;
- Remain connected to the DS at frequencies within the range 47.5 Hz to 52 Hz for duration of 60 min.
- Remain connected to the DS at frequencies within the range 47.0 Hz to 47.5 Hz for a duration of 20 sec required each time the frequency is below 47.5 Hz;
- Remain connected to the DS during rate of change of frequency of values up to and including 0.5 Hz/sec.

The WTs shall be able to operate at reduced power level based on the TSO demands. The frequency control characteristic is represented in Fig.2.5.

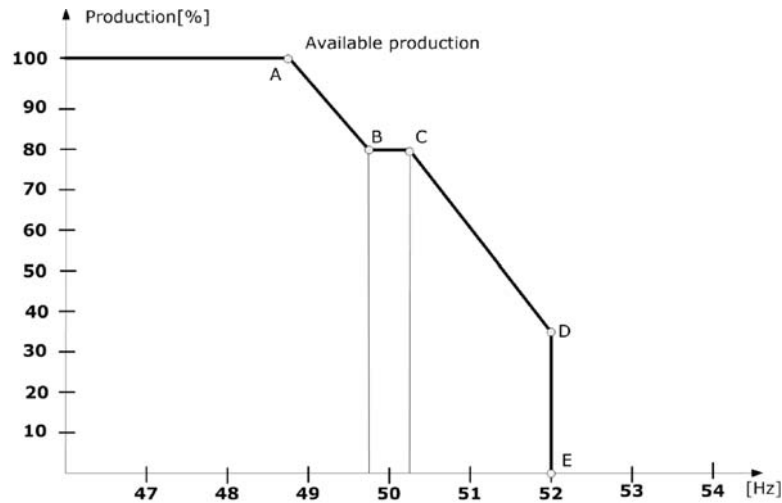


Fig.2.5 Frequency control characteristic [13]

Frequency [Hz]		Available Active Power [%]		
			5 MW ≤ MEC ≤ 10 MW	MEC ≥ 10 MW
F _A	47.0÷51.0	P _A	100	50÷100
F _B	49.5÷51.0	P _B	100	50÷100
F _C		P _C		
F _D	50.5÷52.0	P _D	20÷100	20÷100
F _E		P _E	0	0

Table2.3: Frequency and active power ranges for Fig.2.5

No time delay other than those necessarily inherent in the design of the Frequency Response System (FRS) shall be introduced. The response rate of the WT shall be a minimum of 1% of the rated capacity per second. Also, the frequency is continuously monitored. If the frequency is above the line D-E the WT may disconnect and shall be brought back as fast as technical feasible [13].

2.1.2.3 Reactive power/voltage control

Voltage control is required for WFPS connected at 100 kV bus. These power stations shall have a continuously-variable and continuously-acting Voltage Regulator System (VRS) with similar response characteristics to a conventional Automatic Voltage Regulator and shall perform generally as described in BS4999 part 140 or equivalent European Standards. The voltage step emissions limits are according with the IEC standard 61000-3-7/1996 Assessment of Emission limits for fluctuating loads in MW and HV power systems. The slope setting of the VRS shall be capable of being set to any value in the range 0% to 10%. WFPS must keep power factor between 0.92 and 0.95 as measured in the PCC such that reactive power is absorbed by the WT from the DS

[13]. Some of the WFPS shall remain connected to the DS for step changes in the 100 kV voltage of up to 10%.

The reactive power capability of WFPS is summarized in Fig.2.6:

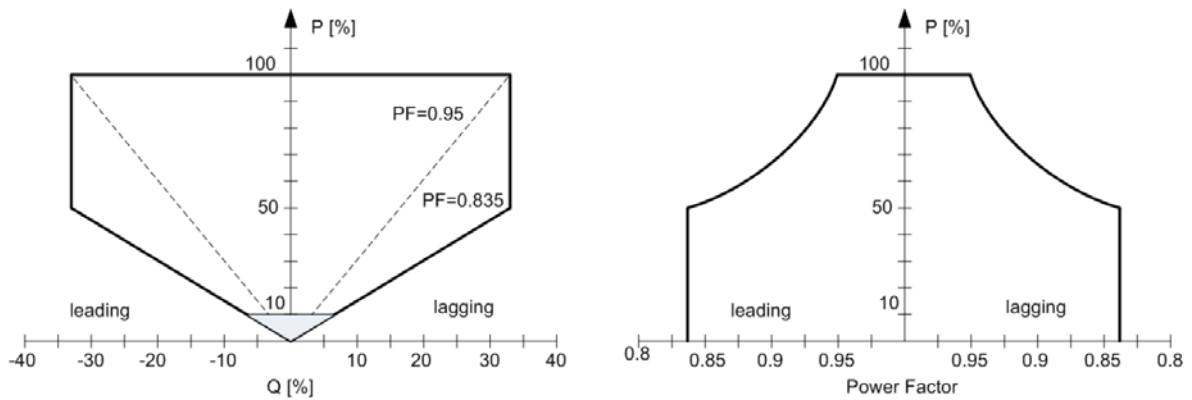


Fig.2.6 Reactive power capability of WFPS in Ireland [13]

2.1.2.4 Fault ride-through requirements

The fault ride-through capabilities of the WFPS connected at the distribution system are given in Fig. 2.7. The WFPS shall remain connected to the DS for voltage dips on any or all phases. During the voltage dip the WFPS shall have the technical capability to provide [13], [14]:

- Active power in proportion to retained voltage and maximize reactive current to the DS without exceeding the WT limits for at least 600 msec or until the DS voltage recovers to the normal operational range;
- At least 90% of its maximum available active power as quickly as the technology allows and in any event within 1 sec of the DS voltage recovering to the normal operating range.

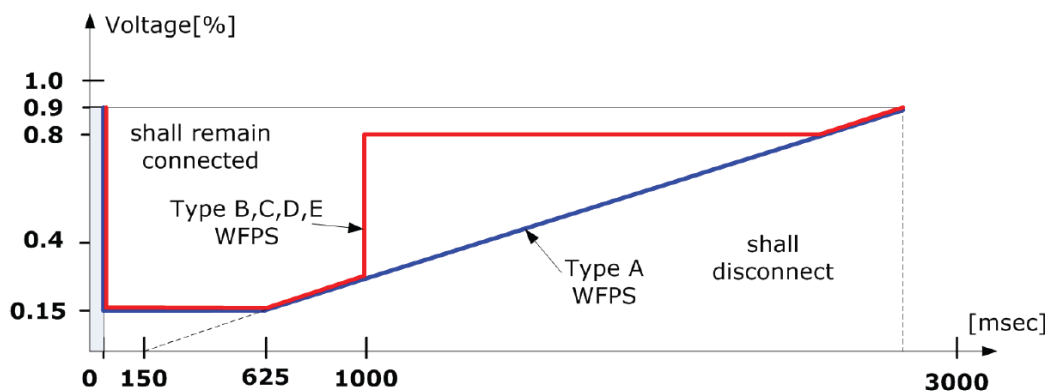


Fig.2.7 Fault ride-through requirements for WFPS in Ireland [13]

2.1.3 Great Britain

2.1.3.1 Voltage level

The frequency in the GB grid shall be nominally 50 Hz with a control range between 49.5 and 50.5 Hz. The frequency can rise to 52 Hz or fall to 47 Hz in exceptional circumstances[13].

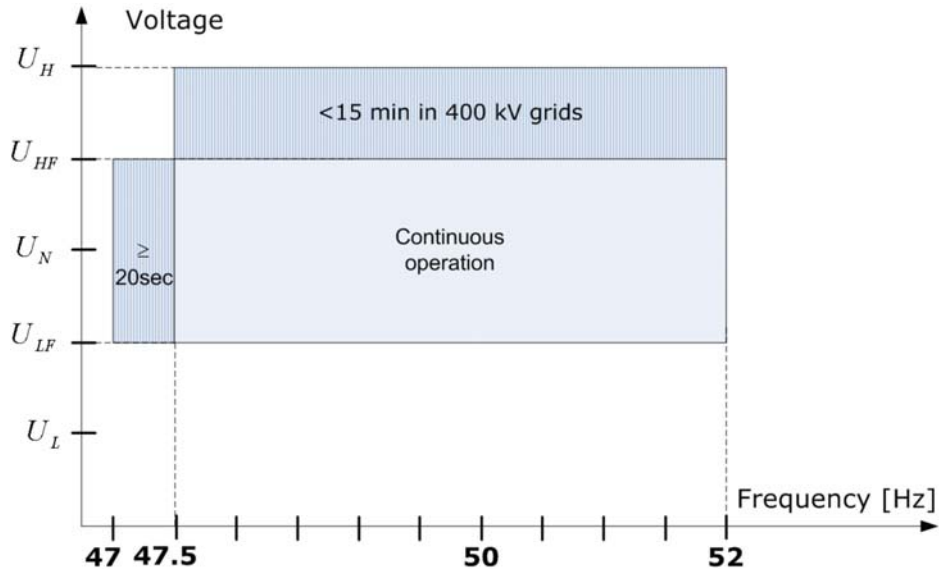


Fig.2.8 Frequencies and voltages in GB grid [13]

The voltage levels in the transmission system as well as the variations allowed are given in Table 2.4.

	Nominal voltage	Lower limit U_L	Lower limit full load U_{LF}	Upper-limit full-load U_{HL}	Upper limit U_H
Transmission	< 132 kV	-	(-6%)	(+6%)	-
	132 kV	-	(-10%)	(+10%)	-
	275 kV	-	(-10%)	(+10%)	-
	400 kV	360 kV (-10%)	380 kV (-5%)	420 kV (+5%)	440 kV (+10%)

Table2.4: Voltage levels in the transmission system

2.1.3.2 Active/reactive power flow in the PCC

All generating units other than synchronous ones with a Completion date after 1 January 2006 should be able to support an active reactive power flow as shown in Fig.2.9:

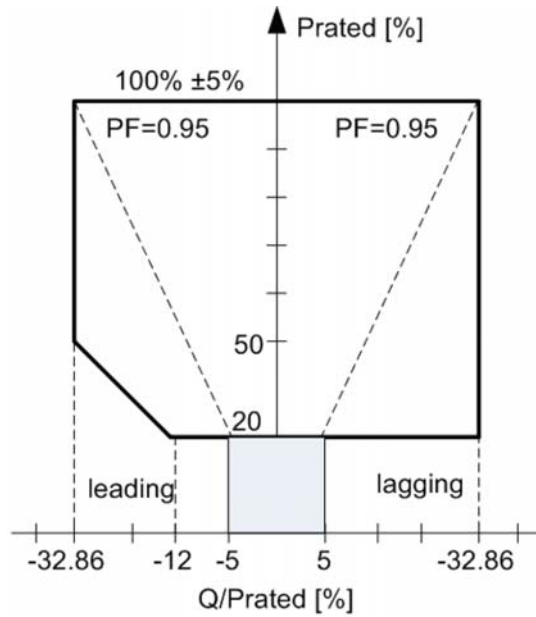


Fig.2. 9 Active /reactive power flow in the PCC [13]

These requirements are valid at the Grid Entry Point in England and Wales or at the HV side of the 33/132 kV or 33/275 kV or 33/400 kV transformer for Generators directly connected to the TS in Scotland [13].

Each generating unit using an intermittent power source where the mechanical power input will not be constant over time shall be able to:

- Continuously maintain constant active power output for the frequency range 49.5 Hz to 50.5 Hz
- Keep the power with a drop of maximum 5% when the system frequency is 47 Hz as specified in Fig.2.10 [13]

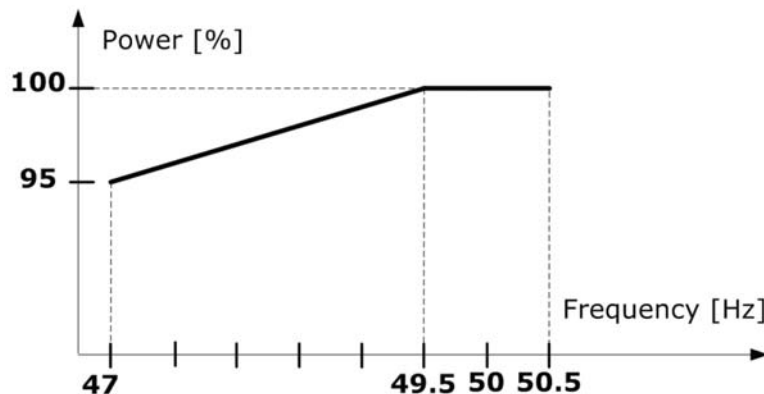


Fig.2.10 Frequency control characteristic [13]

Each generating unit with completion date after 1 January 2006 must be capable of contributing to frequency control by continuous modulation of active power. The frequency control device shall operate with an overall speed droop of between 3% and 5% and a dead-band of maximum 0.03 Hz (± 0.015 Hz) [13].

2.1.3.3 Reactive power/voltage control

The reactive power output under steady state conditions should be fully available within the voltage range $\pm 5\%$ at 400 kV, 275 kV, and 132 kV and lower voltages except the distributed generation if embedded at 33 kV and below where the requirements shown in Fig.2.11 are applied.

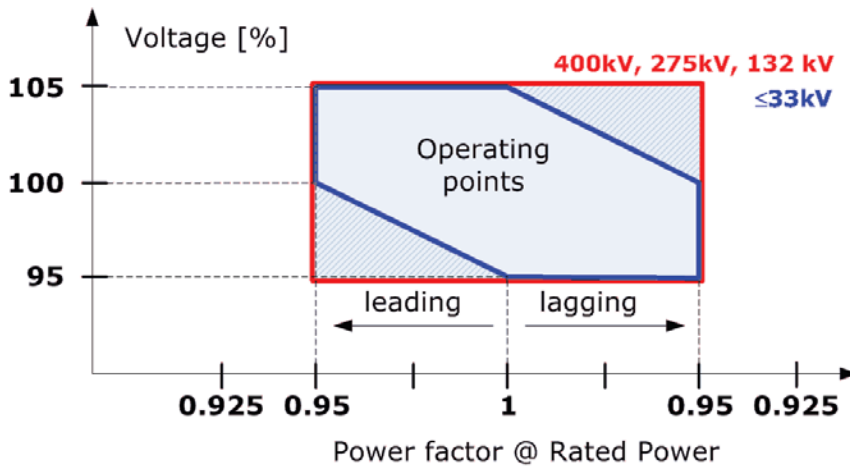


Fig.2.11 Reactive power control characteristic [13]

2.1.3.4 Fault ride-through requirements

The following requirements are valid for generating units in the GB grid according with [13]:

- Generating units shall remain connected and transiently stable without tripping for a close up solid three-phase short circuit fault or any unbalanced short-circuit fault on the transmission system operating at super grid voltages for a total fault clearance time of up to 140 msec. The duration of zero voltage is dependent on local protection and circuit breaker operating times. This duration and the fault clearance time will be specified in the individual agreement between TSO and the owner of the production unit. Following fault clearance, recovery of the super grid voltage to 90% may take longer than 140 msec as illustrated in Fig.2.12
- Same requirements as above are valid for voltage dips greater than 140 msec in duration.
- In order to avoid unwanted island operation the generating units in Scotland shall be tripped for the following conditions:

- Frequency above 52 Hz for more than 2 sec;
- Frequency below 47 Hz for more than 2 sec;
- Voltage as measured in the PCC below 80% for more than 2 sec;
- Voltage as measured in the PCC above 120% (115% for 275 kV) for more than 1sec.

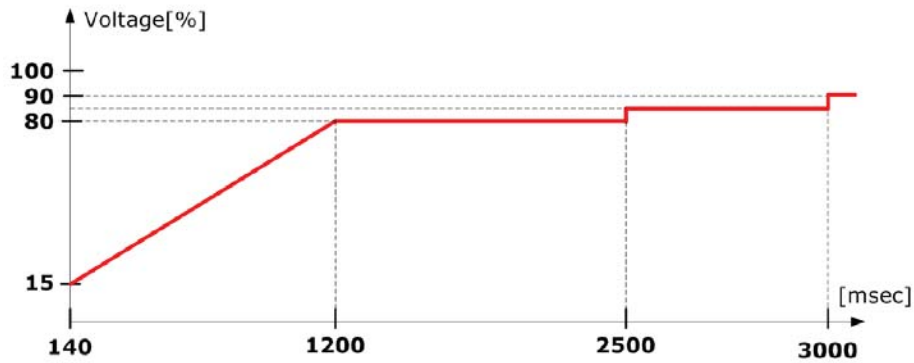


Fig.2.12 Fault ride-through capability [13]

2.2. Power converters in grid connected applications

In this paragraph the commonly used converters topologies are presented. The analyzed topologies are two-level, three-level and multi-level converters.

2.2.1 Two-level converter

The two-level inverter is a very commonly used topology. The layout is shown on Fig.2.13, and it shows, that a three phase inverter consists of six switches. The capacitor models a ripple-free DC-link voltage.

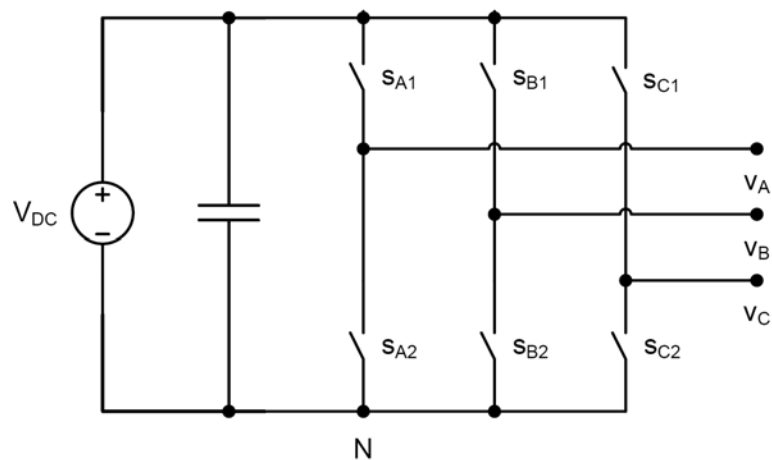


Fig.2.13 Two-level three phase converter schematic

By controlling the switches, for instance by Space Vector Modulation (SVM) and Pulse With Modulation (PWM), and filtering the output, a quasi-sinusoidal waveform is obtained. However without the filter, the output voltage would be a square wave. To ensure, that short circuits do not occur, dead time is normally incorporated, meaning that two switches in one leg of the inverter is never turned on at the same time.

2.2.2 Three-level converter

The three-level inverter is an alternative to the two-level inverter, and have some advantages, that makes it better suited for a medium voltage application. But a trade off is, that it consist of twice as many transistors as its two level counterpart. Fig.2.14 shows the schematic of a three-level three phase inverter.

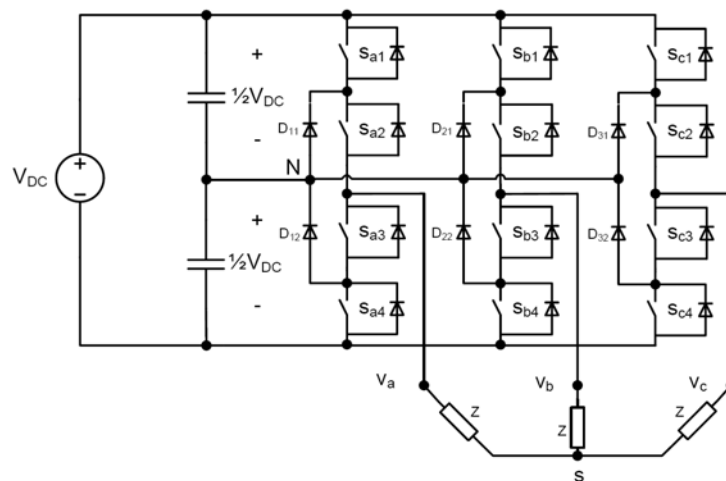


Fig.2.14 Three-level three phase converter schematic with star connected load

One of the advantages of the three-level inverter is, that the transistors always turn on and off in pairs. This means, that the full DC-link voltage will always be shared by two switches, where the two level inverter switches has to be able to block the full DC-link voltage. The switching scheme of a three-level inverter has three states; first one where switch 1 and 2 are turned on, second state where the middle switches 2 and 3 are on, and the last one where switch 3 and 4 are turned on.

2.2.3 Multi-level converter

Currently there is an increasing interest in multilevel power converters especially for medium to high-power, high voltage wind turbine applications. Multilevel inverters consist of six or more switches pr. leg, and the main idea is to create an even higher number of output sinusoidal voltage levels, than the three-level inverter, further decreasing the harmonic content. Since the development of the neutral-point clamped (NPC) three-level converter, several alternative

multilevel converter topologies have been reported in the literature. According with [14] the different proposed multilevel converter topologies can be classified in the following five categories and these are represented in Fig.2.15:

- multilevel configurations with diode clamps (a)
- configurations with bi-directional switch interconnection (b)
- multilevel configurations with flying capacitors (c)
- multilevel configurations with multiple three-phase inverters (d)
- multilevel configurations with cascaded single phase H-bridge inverters (e)

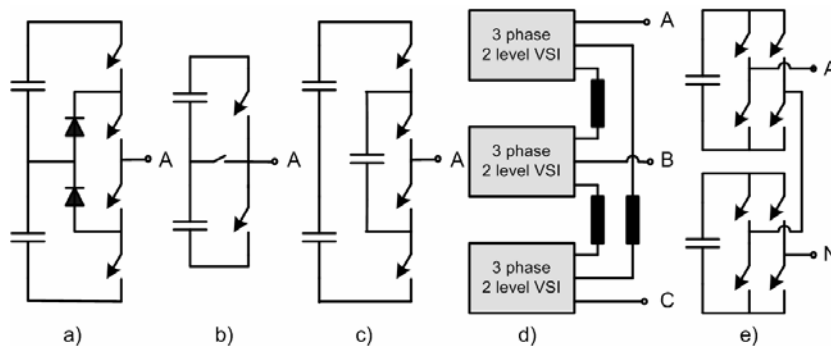


Fig.2.15 Multi-level topologies [14]

Because the multilevel inverter consists of many switches, the control of the inverter is more complex. Also, the NPC voltage becomes harder to control, because the number of neutral points increase.

2.2.4 Power converters topologies for wind turbines

Basically two power converter topologies with full controllability of the generated voltage on the grid side are used currently in the wind turbine systems [13]. These power converters are related with PVSWT and DFIGWT wind turbine concept.

2.2.4.1 Bidirectional back-to-back two-level power converter

This topology is state-of-the-art especially in large DFIG based wind turbines. The back-to-back PWM-VSI is a bi-directional power converter consisting of two conventional PWM-VSCs. The topology is shown in Fig.2.16.

To achieve full control of the grid current, the DC-link voltage must be boosted to a level higher than the amplitude of the grid line-line voltage. The power flow of the grid side converter is controlled in order to keep the DC-link voltage constant, while the control of the generator side is set to suit the magnetization demand and the reference speed [13].

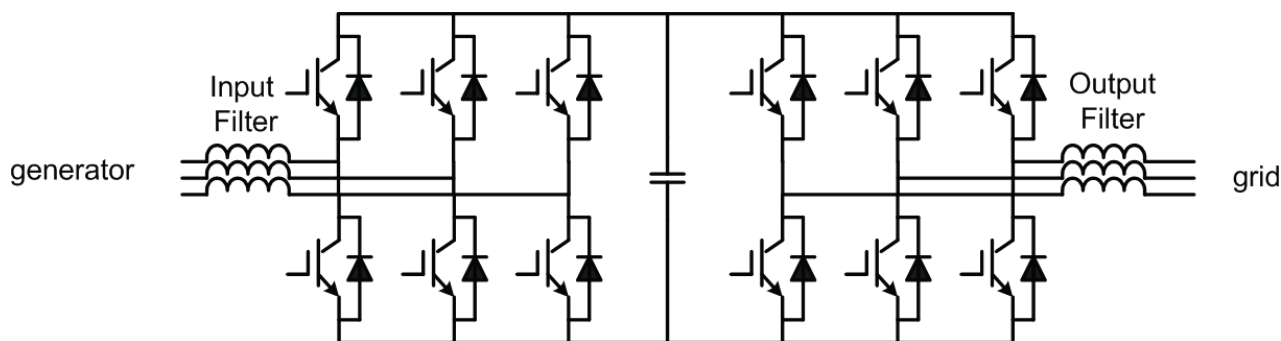


Fig.2.16 Structure of the back-to-back Voltage Source Converter.

A advantage of the PWM-VSC is the capacitor decoupling between the grid inverter and the generator inverter. Besides affording some protection, this decoupling offers also separate control of the two inverters, allowing compensation of asymmetry both on the generator side and on the grid side, independently. The inclusion of a boost inductance in the DC-link circuit increases the component count, but a positive effect is that the boost inductance reduces the demands on the performance of the grid side harmonic filter, and offers some protection of the converter against abnormal conditions on the grid [13], [14].

On the other hand, in several papers concerning adjustable speed drives, the presence of the DC-link capacitor is mentioned as a drawback, since it is heavy and bulky, it increases the costs and maybe of most importance, - it reduces the overall lifetime of the system [13]. Another important drawback of the back-to-back PWM-VSI is the switching losses. Every commutation in both the grid inverter and the generator inverter between the upper and lower DClink branch is associated with a hard switching and a natural commutation. Since the back-to-back PWM-VSI consists of two inverters, the switching losses might be even more pronounced. The high switching speed to the grid may also require extra EMI-filters.

In order to achieve variable speed operation the wind turbines equipped with a permanent magnet synchronous generator (PMSG) will required a boost DC-DC converter inserted in the DC-link.

2.2.4.2 Unidirectional power converter

A wound rotor synchronous generator requires a simple diode bridge rectifier for the generator side converter as shown in Fig.2.17

The diode rectifier is the most common used topology in power electronic applications. For a three-phase system it consists of six diodes. The diode rectifier can only be used in one quadrant, it is simple and it is not possible to control it. It could be used in some applications with a dc-bus.

The variable speed operation of the wind turbine is achieved by using an extra power converter which fed the excitation winding.

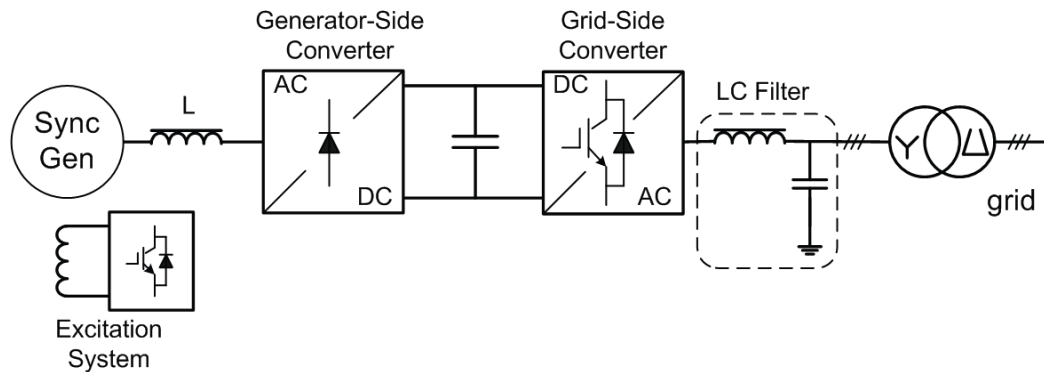


Fig.2.17 Variable-speed WT with synchronous generator and full scale power converter

The grid side converter will offer a decoupled control of the active and reactive power delivered to the grid and also all the grid support features. These wind turbines can have a gearbox or can be direct-driven.

2.2.4.3 Modular power converters

However, at low wind speeds and hence low level of the produced power, the full scale power converter concept exhibits low utilization of the power switches and thus increased power losses. Therefore, a new concept in which several power converters are running in parallel is used as show in Fig.2.18 [13].

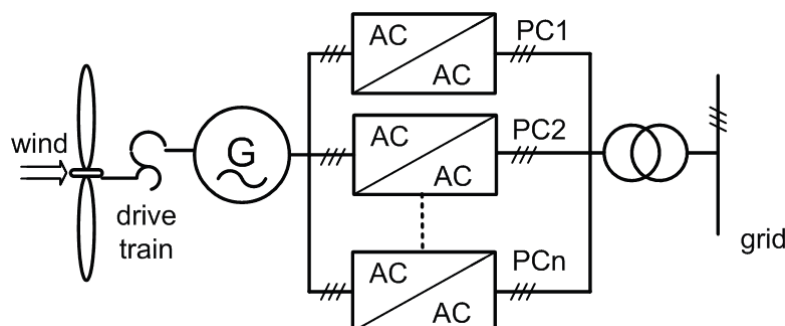


Fig.2.18 Full scale power converter wind turbine with n-parallel converters

By introducing power electronics many of the wind turbine systems get similar performances with the conventional power plants. Modern wind turbines have a fast response in respect with the grid operator demands however the produced real power depends on the available wind speed.

The reactive power can in some solutions, e.g. full scale power converter based wind turbines, be delivered without having any wind producing active power. These wind turbines can also be active when a fault appears on the grid and where it is necessary to build the grid voltage up again; having the possibility to lower the power production even though more power is available in the wind and thereby act as a rolling capacity for the power system. Finally, some systems are able to work in island operation in the case of a grid collapse [13], [14].

2.3. Control strategies for grid side converter

According with the project description the system considered for modeling and implementation can be represented in Fig.2.19.

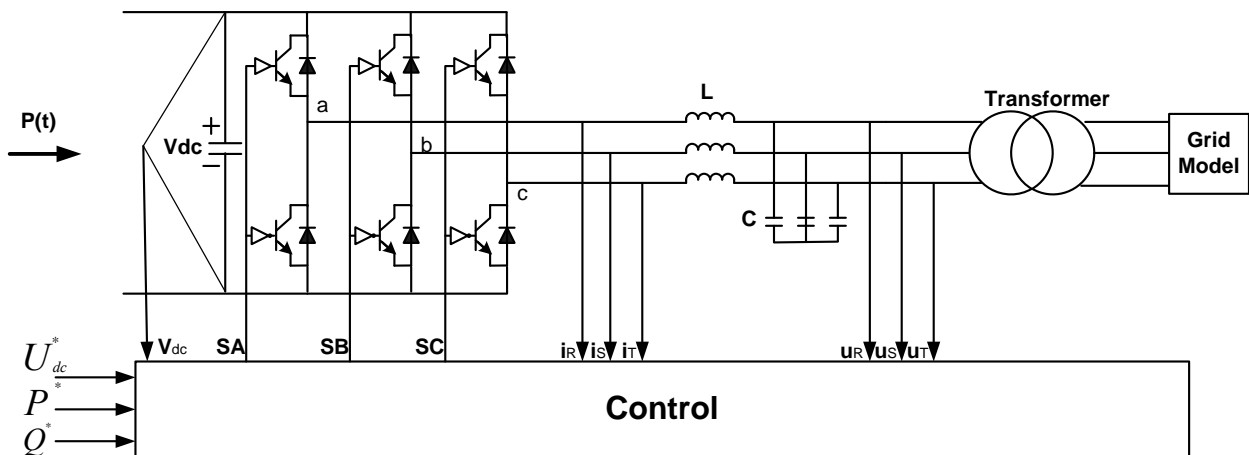


Fig.2.19 Block diagram of the considered system

As it can be seen the system consists in:

- an IGBT based VSC
- an LC filter
- a transformer
- grid

The generator and the generator side converter are not included in this model and a variable power source $P(t)$ is fed into the DC-link of the grid side converter.

The optimum control strategy for the grid inverter control must be chosen based on the characteristics of known control methods. The control methods to be investigated should be as a

minimum Voltage Oriented Control (VOC), Virtual Flux Oriented Control (VFOC) and Direct Power Control (DPC).

First a short description of the synchronization methods will be presented followed by the description of the control strategies for grid side converter.

2.3.1 Phase Locked Loop (PLL)

Phase, amplitude and frequency of the utility voltage are critical information for the operation of the grid-connected inverter systems. In such applications, an accurate and fast detection of the phase angle, amplitude and frequency of the utility voltage is essential to assure the correct generation of the reference signals and to cope with the standard requirements for the grid-connected converters. Grid-connected operations are controlled to work close to the unity power factor in order to reach the standards. It requires the use of a synchronizing algorithm which is able to synchronize the reference current of the H-bridge VSI inverter with the grid voltage.[12]

There are two basic synchronization methods:

- Filtered Zero Cross Detection (ZCD);
- Phase Locked Loop (PLL).

The first method is based on the detection of the zero crossing of the grid voltage while the second one, PLL, is a feedback control system that automatically adjusts the phase of a logical generated signal to match the phase of an input signal. The PLL is used to synchronize the inverter current angle, ϑ_{inv} , with the angle of the grid voltage, ϑ_{grid} , to obtain a power factor as close to 1 as possible. The angle ϑ_{inv} is used to calculate the reference current that is compared to the actual output current of the inverter.

PLL requires two orthogonal voltages which can easily get for three phase systems representing the voltage space vector \bar{v}_{abc} in a rotating reference frame (dq). For single phase systems the classical solution was the filtered ZCD. Now the trend is to use the PLL creating virtual orthogonal components. The main idea in the PLL is that it changes the inverter current frequency, ω_{inv} , if the inverter current and the grid voltage are out of phase. If the current lags the grid voltage the PLL will decrease ω_{inv} until the inverter current is in phase with the grid voltage, but if the inverter current leads the grid voltage ω_{inv} is increased until they are in phase.

2.3.1.1 Three phase PLL structure

The most common PLL technique applied to three phase grid connected systems is based on an algorithm implemented in synchronous reference frame (dq). The structure of the dq PLL algorithm is represented like in Fig1.22

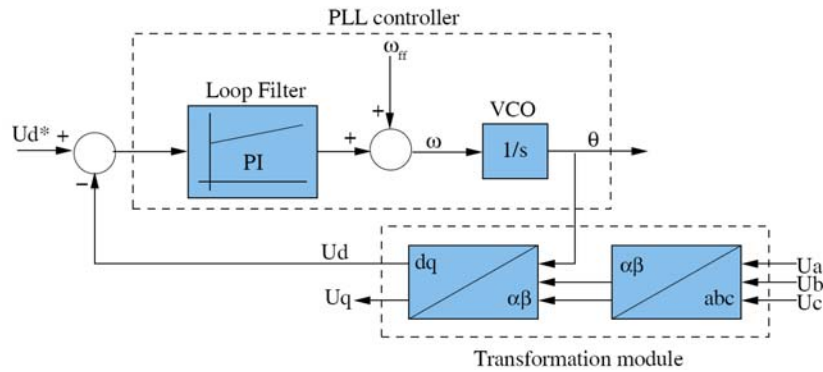


Fig.2.20 Three-phase PLL structure [15]

The grid voltages are the input into the algorithm and they are transformed into synchronous reference frame by means of $abc \rightarrow dq$ transformation module. The phase locking is realized by controlling the d-voltage to be zero. A regulator, usually PI, can be used to control this variable and the output of this regulator is the grid frequency. After the integration of the grid frequency, the utility voltage angle is obtained, which is fed back into the \hat{d} -dq transformation module in order to transform into the synchronous rotating reference frame [15], [16].

This structure of PLL consists of two major parts, the phase detection and the loop filter. The phase detection can be easily implemented by using abc -dq transform in the three phase system. On the other hand, the loop filter determines the dynamics of the system. Therefore, the bandwidth of the filter is a trade off between the filtering performance and the time response. As a consequence, parameters of the loop filter have a significant influence on the lock quality and the PLL dynamics. In this way, the phase angle of grid voltage ϑ is detected and this is the output of the algorithm.

2.3.1.2 Single phase PLL structure

The structure of the single phase PLL is depicted in Fig.2.21. This algorithm artificially creates the orthogonal component of the grid voltage used to obtain the phase error between the phase of the real grid voltage and the estimated one by the PLL.

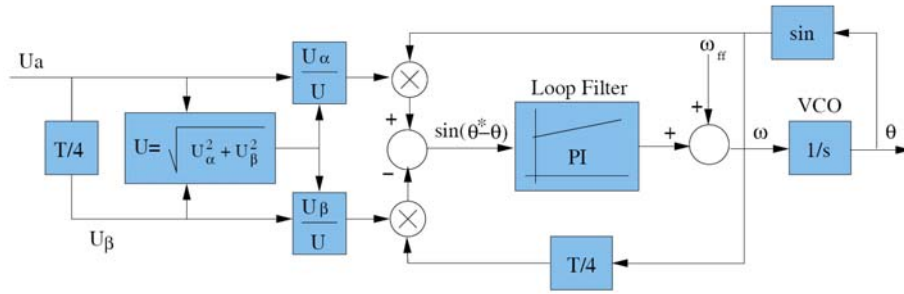


Fig.2.21 Single-phase PLL structure [15]

In the case of three phase grid converters, three such PLL structures (one for each phase) are necessary. The output of the three systems will follow their respective grid voltage phase angle and, as a consequence, the reference currents will be in phase to their corresponding voltages. Hence, independent synchronization can be implemented using three such PLLs [15].

2.3.2 Synchronous VOC-PI with PLL

This control strategy is well-proven being used for a long time in applications like active rectifiers, active filters or grid converters. The grid converter structure to be simulated is depicted in Fig.2.22.

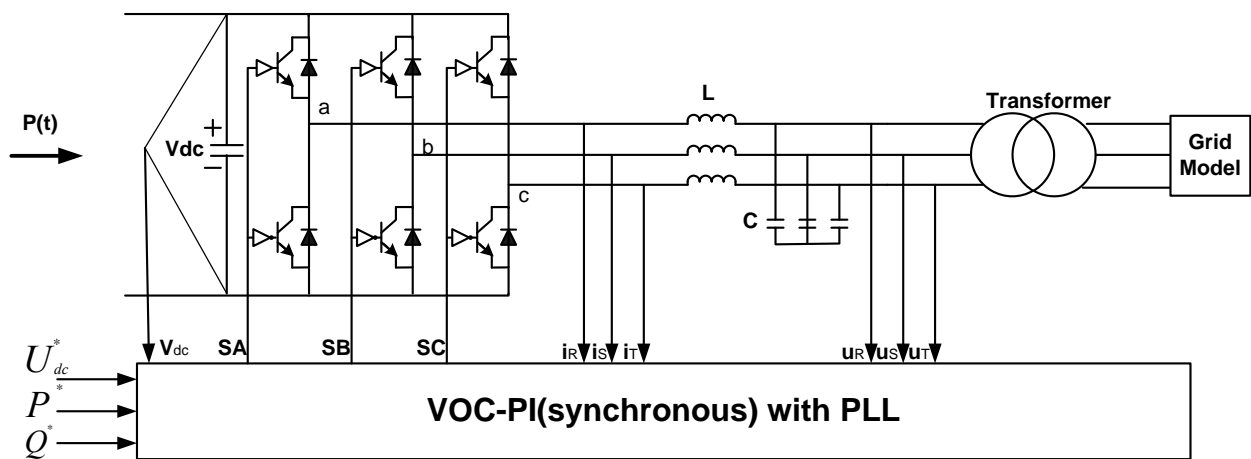


Fig.2.22 Diagram of the VOC-PI with PLL

In this strategy the current is oriented along the active voltage V_d and normally V_q and this is also the reason why this strategy is called voltage oriented control. A conventional PLL is used to detect the phase grid angle ϑ , grid frequency and grid voltage. The frequency and the voltage are needed in order to monitor the grid conditions and to comply with the control requirements while the grid angle is required for transformations to the synchronous frame. The currents are

transformed from stationary (abc) to synchronous frame (dq) and conventional PI controllers are used. Decoupling of the cross-coupled d and q axis is performed as it is shown in Fig.2.23. To decouple the grid voltage from the output of the current controllers a voltage feed forward is used. A standard PI controller is used also for the DC voltage and its output is feed-forwarded to the output of the P controller to obtain the reference for the active current i_d^* and another PI controller is used to obtain the reference for the reactive current i_q^* .

The biggest disadvantage is the low performance in case of unbalanced or faulty grid where the grid angle is difficult to define.

This strategy can be also implemented in the stationary frame replacing PI controllers with the resonant controllers like in Fig.2.24. In this situation can be reach the advantage of less complexity due to the less need of transformations and no need of decoupling and voltage feed-forward.

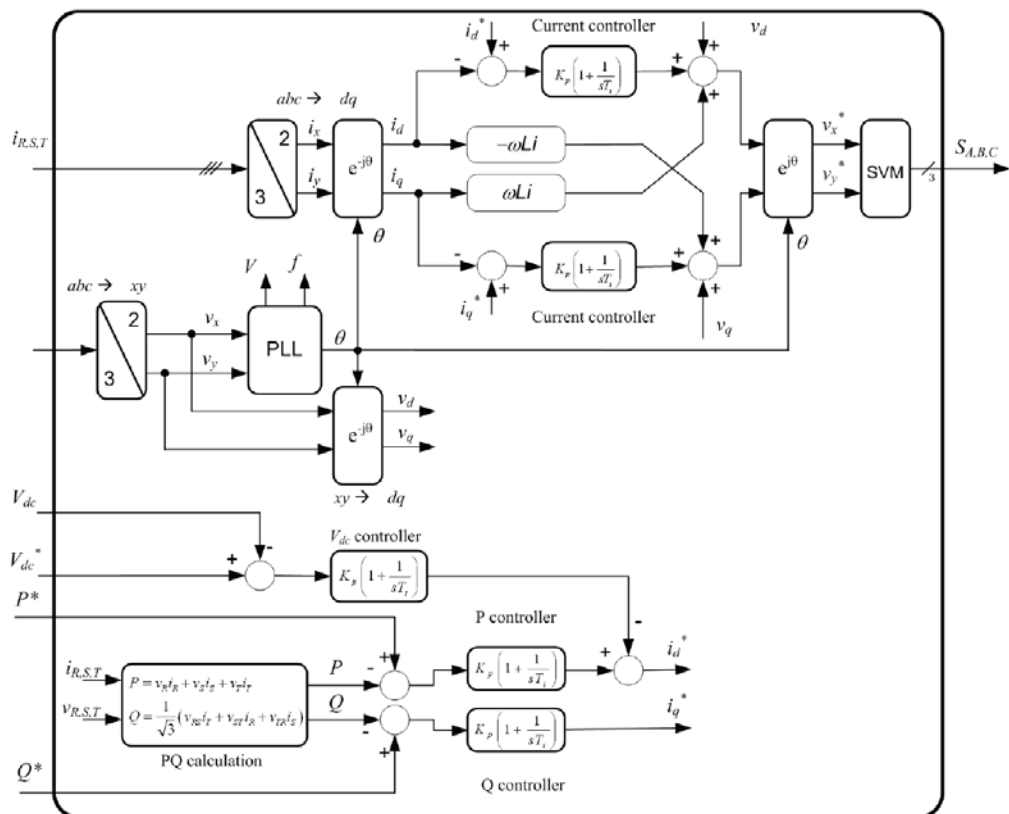


Fig.2.23 Control structure for VOC-PI with PLL

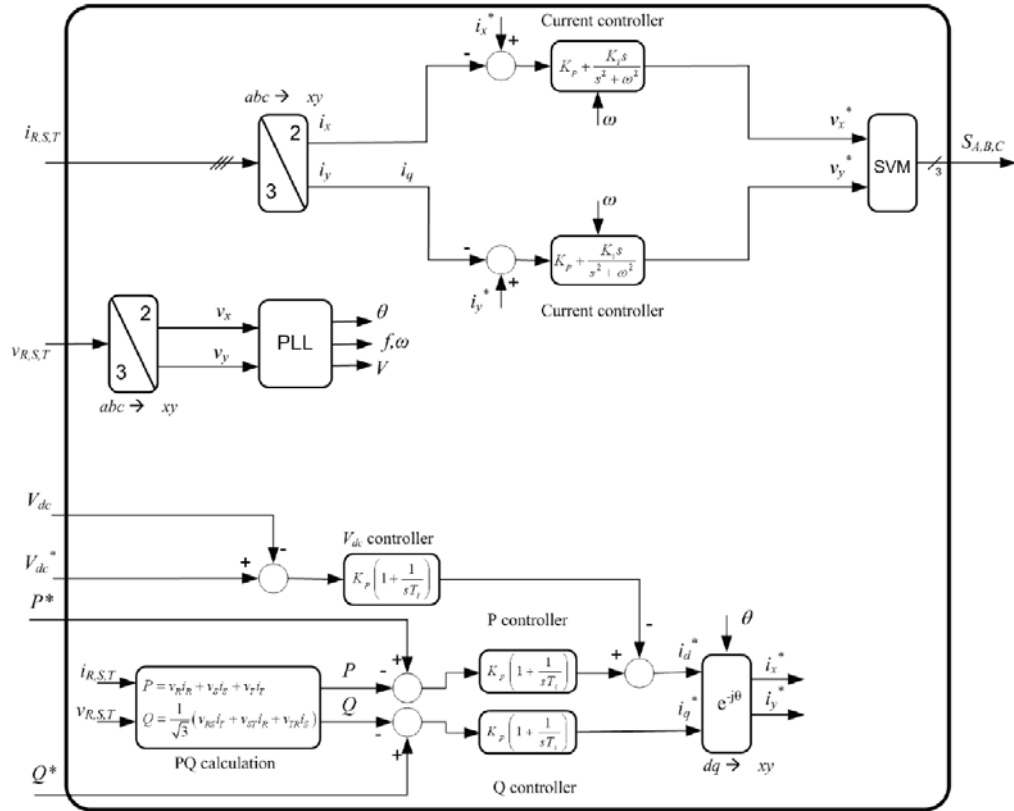


Fig.2.24 Control structure for VOC-PR with PLL

2.3.3 Synchronous VFOC-PI without PLL

VFOC proposes the use of a virtual flux by integrating the grid voltage. The angle of this flux will be in quadrature with the grid angle but will be less sensitive to grid disturbances due to the low-pass filter effect of the integrator. The performances of the grid angle estimator are limited and the dynamic is difficult to tune. More flexibility can be obtained with PLL where the dynamic can be adjusted by tuning the PI controller. VFOC will exhibit the same performances as VOC with PLL except for the much distorted grid case (THD=8%) where it produces grid angle error. VFOC is more robust for disturbed grid but can not outperform the PLL.[18][26]

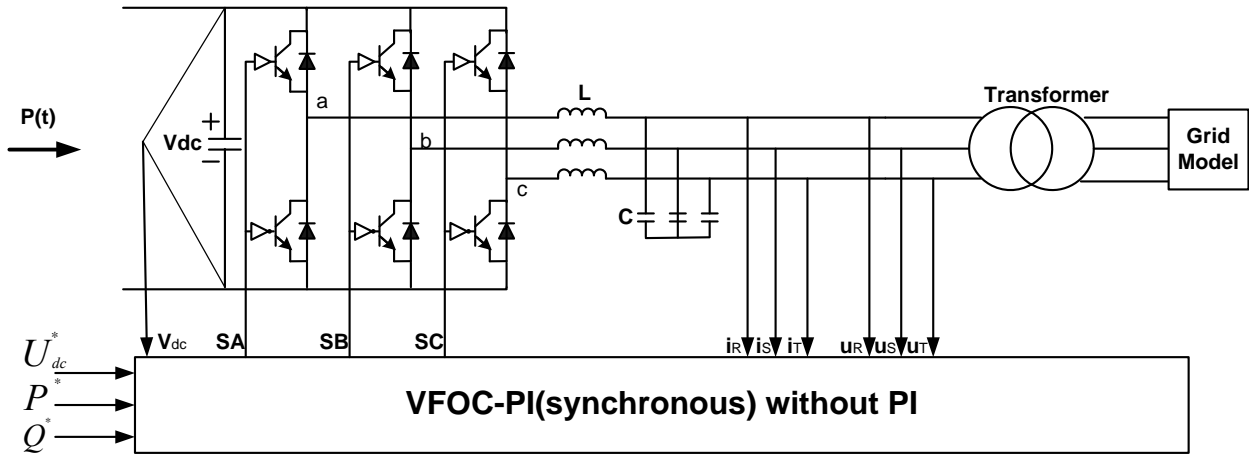


Fig.2.25 Diagram of the VFOC-PI control without PLL

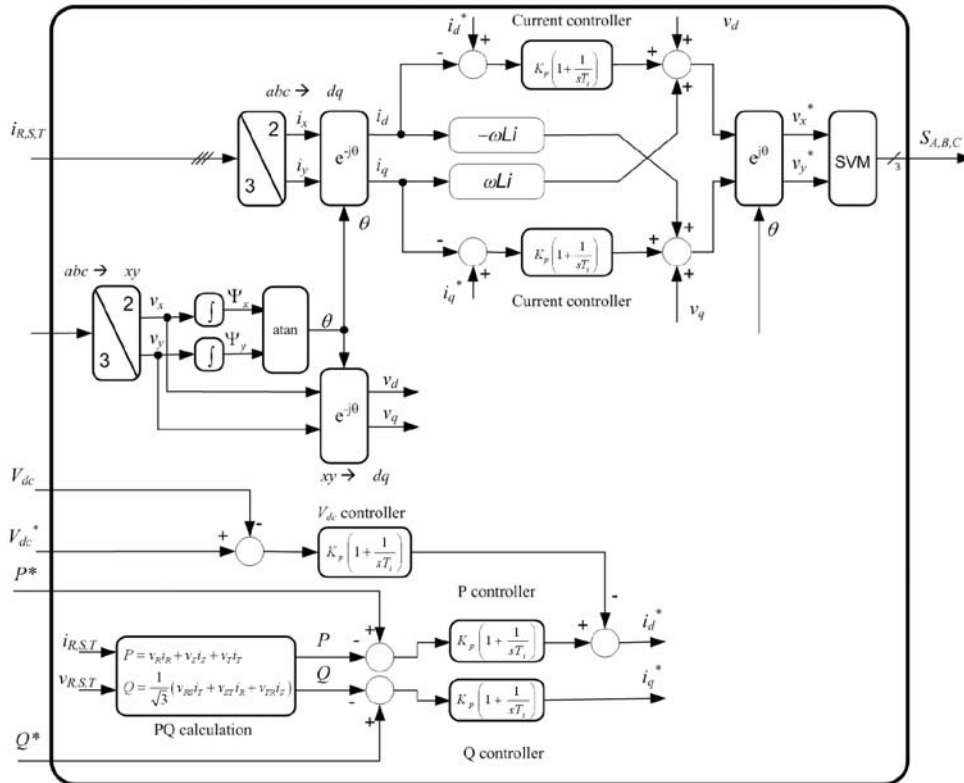


Fig.2.26 Control structure for VFOC-PI control without PLL

2.3.4 Adaptive Band Hysteresis (ABH) control with PLL

This control strategy is based on indirect PQ power control with adaptive band hysteresis (ABH). The diagram of the ABH control is similar with the diagram of the VFOC-PI control strategy from Fig.2.22 and the control structure is presented in Fig.2.27.

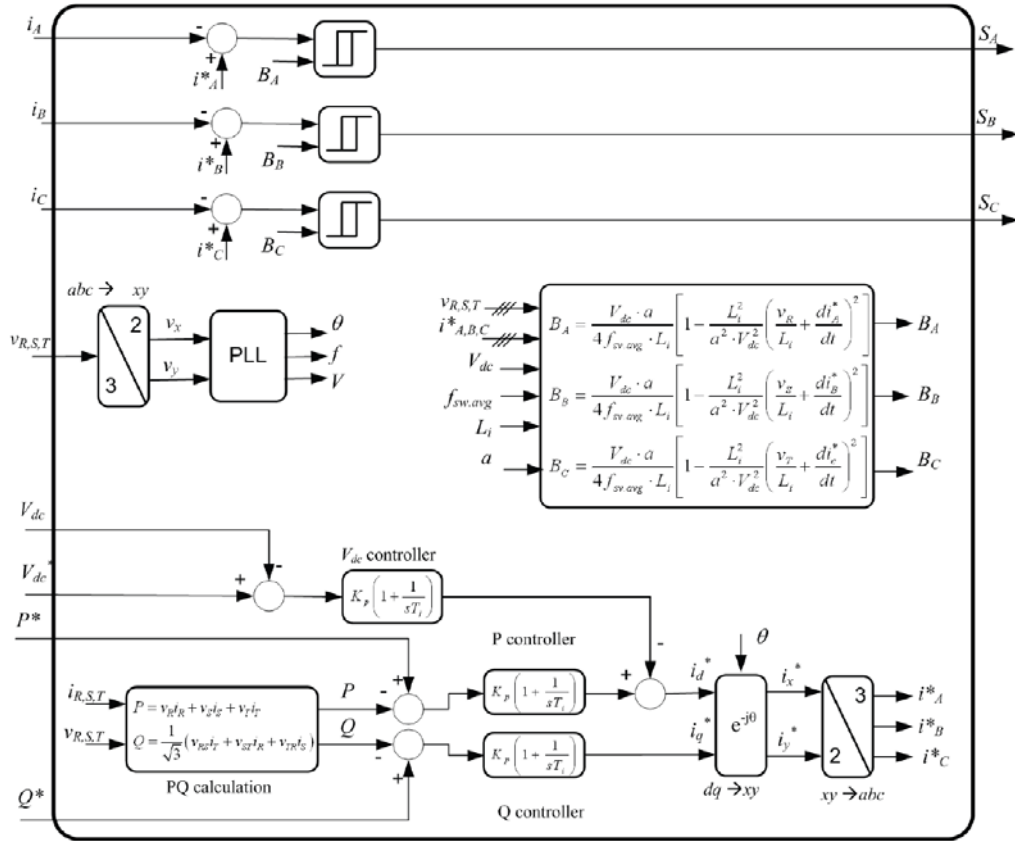


Fig.2.27 Control structure for ABH current control

Hysteresis control is known to exhibit high dynamic response as the concept is to minimize the error in one sample. As the typically sampling frequencies are in the range of 50-100 kHz, this means a very high bandwidth. A constant band for the hysteresis comparator leads to variable switching frequency. An on-line adaptation of the band can be done in order to keep the switching frequency quasi-constant. The PLL is used in order to orientate the output of the P and Q controller with grid angle and for grid monitoring. [18]

Even if this strategy is using a PLL for orientation of the reference currents, it will exhibit improved performances under grid voltage variations due to the higher bandwidth of the current controller that help in order to keep the currents under the trip limits.[26]

2.3.5 Direct Power Control (DPC) with SVM and PLL

The control structure for this strategy is presented in Fig.2.28 while the diagram of this control method is similar with the one from Fig.2.25.

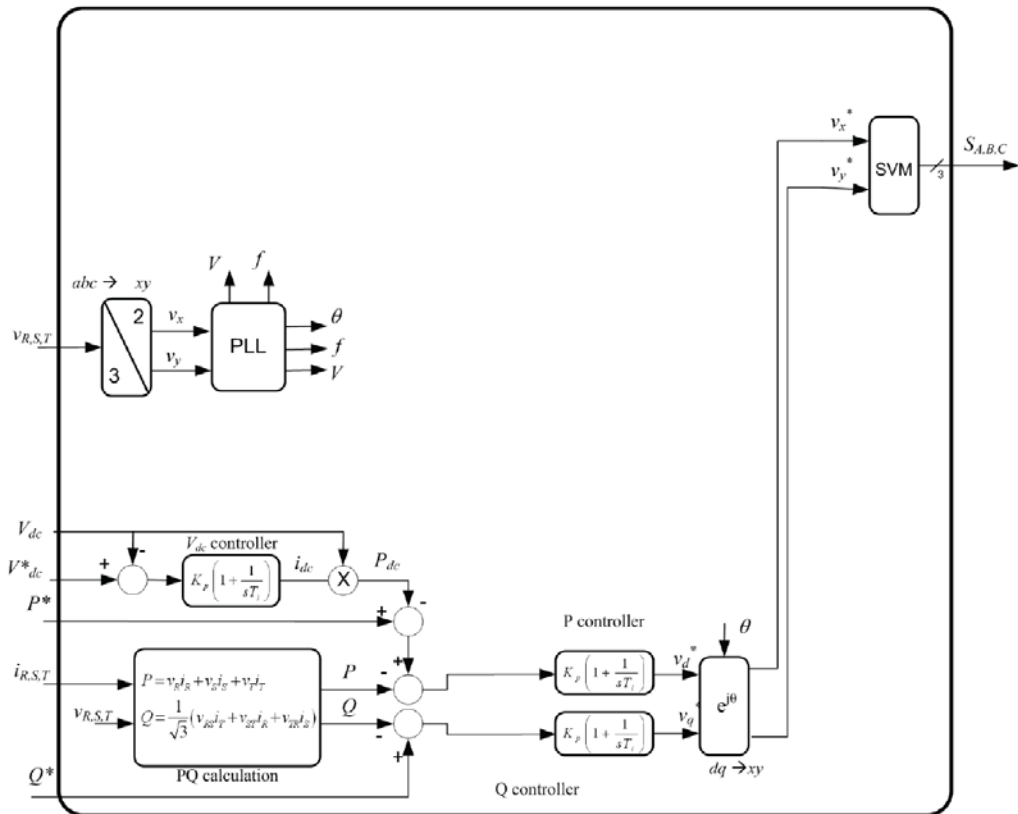


Fig.2.28 Control structure for DPC-SVM with PLL

This control method is a simplified VOC strategy. The difference between this two control strategies is that the current controllers are eliminated. The power controllers produce directly the voltage references for the space vector modulator (SVM) and this can be also the reason why this method is called direct power control. A conventional PLL is used also in this strategy in order to detect the grid phase angle ϑ , grid frequency f and grid voltage V from the grid voltages.

The power used to balance the DC voltage is estimated using the DC voltage controller output and other PI controllers are used for active and reactive power controllers.

DPC can be also implemented using hysteric control yielding in more robustness over for distorted grid conditions but with the price of very high computation intensity, difficult to implement in low-cost DSP technology [26]. The control structure for VFDP-SVM with PLL is represented in Fig.2.29.

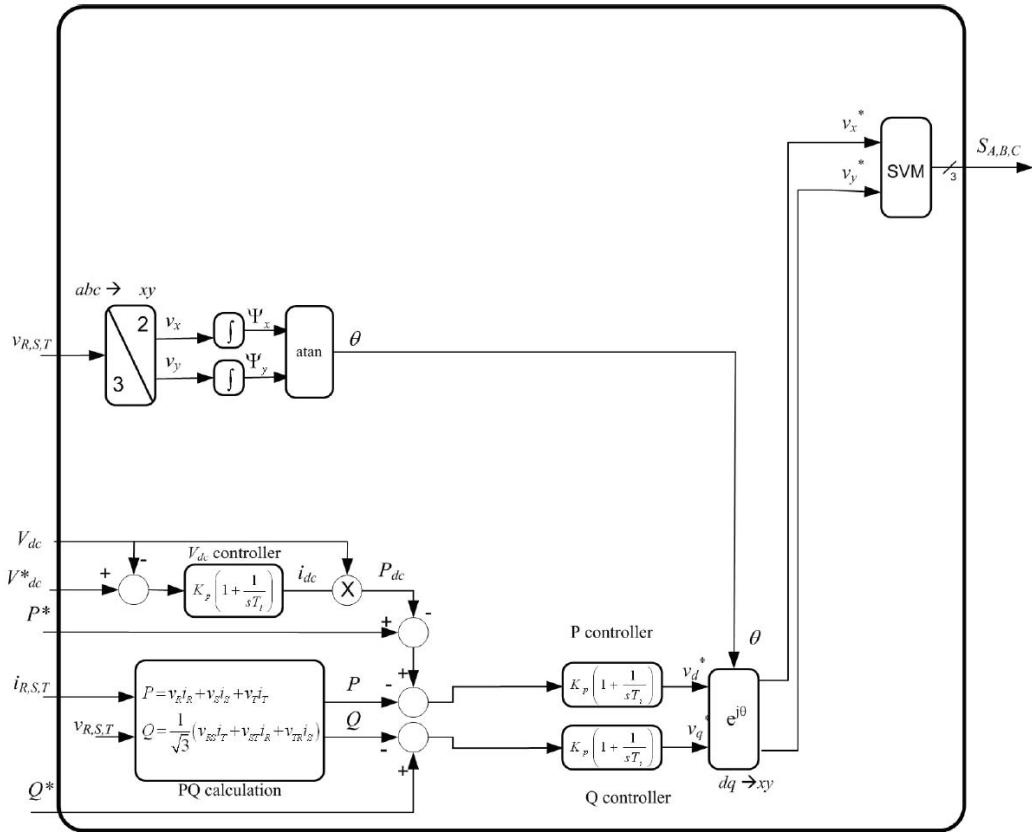


Fig.2.29 Control structure for VFDPC-SVM with PLL

Chapter 3

Modeling

Abstract

In this chapter, a description of the whole plant model, including grid, DC link capacitor, ideal three-branches six-switches LCL-filter connected inverter implemented and its control system is given, together with theoretical explanations about the implementation methods adopted.

3.1. Introduction.....	Page 40
3.2. Plant model	Page 40
3.2.1 Grid side converter.....	Page 41
3.2.2 Space vector modulation.....	Page 43
3.2.3 LCL filter.....	Page 45
3.2.4 Grid model.....	Page 49
3.2.5 DC link circuit.....	Page 50

3.1. Introduction

Since that the wind turbine and generator side converter are not the main issue for this project the modified layout of the modeling system can be seen again in Fig 3.1 where is represented the plant model which is compose by the grid side converter feed by the DC link and connected to the grid by means of a passive filter and the model for the control of the grid side.

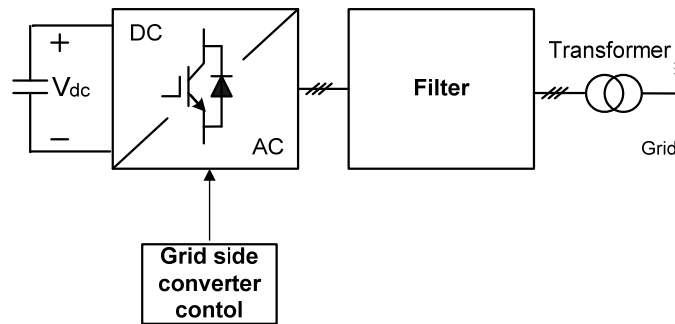


Fig.3.1 Layout of the model system

First, the model of the plant will be described and after the model of the grid side converter control will be presented.

3.2. Plant model.

The plant is represented in Fig 3.2 and its model is simulated using Matlab Simulink models.

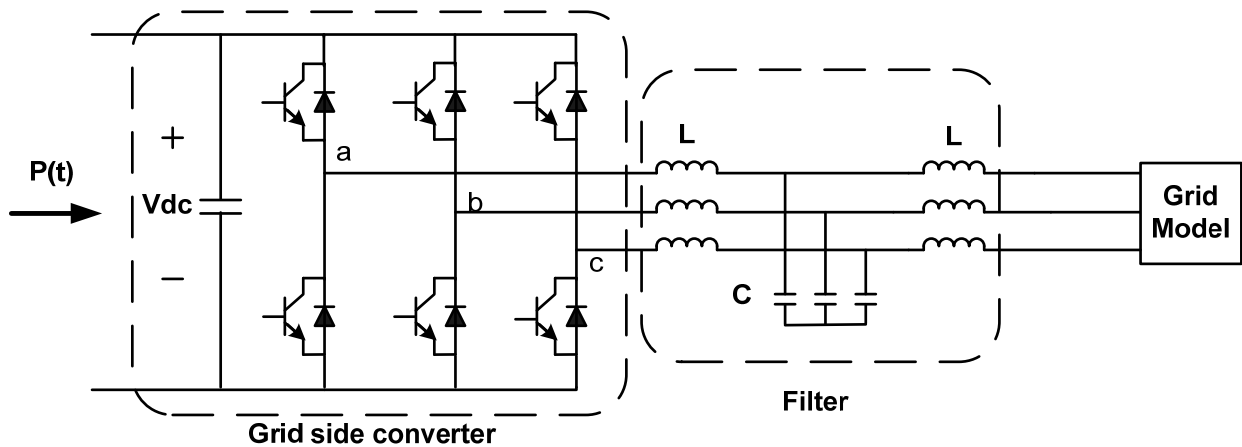


Fig.3.2 Layout of the plant model

3.2.1 Grid side converter

A back-to-back converter consists of two voltage source converters (VSC) and a capacitor as shown in Fig.3.3. When operating in generator mode, the generator side converter operates as a rectifier and the grid side converter as an inverter. But as both converters are identical, power flow can be bi-directional [17][18].

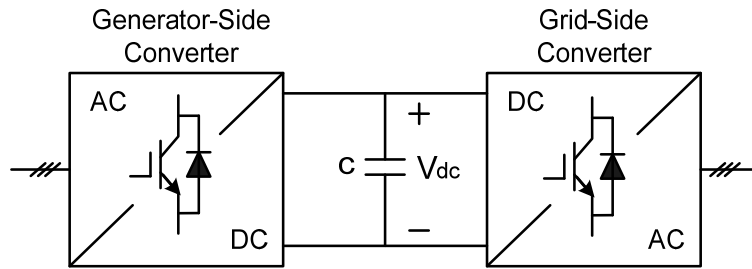


Fig.3.3. Back-to-back converter

Model of the back-to-back converter is necessary in simulation to feed the generator and grid model. But as the grid side is only considered in simulations, the model of the whole back-to-back converter is not needed. Consequently, the model of the grid side VSC is sufficient to carry out the simulations and is the only part considered in this section. The model of the VSC is an average model as the system includes a mechanical system making the time-frame of interest much longer than the switching time of the converter. Therefore, there is no need to have a switching model where the effect of switching adds little significance to the result.

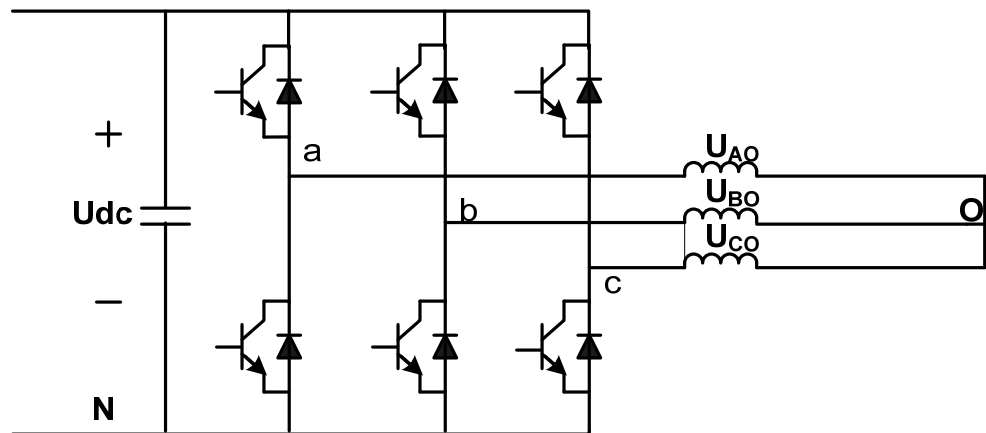


Fig.3.4 Grid side VSC

The inverter implemented is a mathematical function, which represents the behaviour of an ideal six-switch inverter without any physical limitation or dissipation or lag or non-linearity.

Its logical scheme was implemented as two sub-blocks, one for calculating the voltages and one for the currents. The two switches on the same branch will be commanded by a boolean signal (da, db, dc): a 1 value on the input will turn on the upper switch and turn off the lower, a 0 value will turn on the lower and turn off the upper one. In every instant three switches, one per leg, will be on.

Considering the equivalent circuit of the inverter-filter system Fig.3.4, the output line voltages of the inverter have the expression:

$$\begin{cases} u_{abinv} = u_{AN}(t) - u_{BN}(t) \\ u_{bcinv} = u_{BN}(t) - u_{CN}(t) \\ u_{cainv} = u_{CN}(t) - u_{AN}(t) \end{cases} \quad \text{Eq.3.1}$$

In Fig.3.4 the O point represents the centre-star of the star-connected capacitors in the filter, while N is the reference voltage point on the DC side.

The difference in voltages between the reference point and the centre-star will then be expressed as $u_{ON}(t)$.

Phase voltages can be written as:

$$\begin{cases} u_{ainv} = u_{AN}(t) - u_{ON}(t) \\ u_{binv} = u_{BN}(t) - u_{ON}(t) \\ u_{cinv} = u_{CN}(t) - u_{ON}(t) \end{cases} \quad \text{Eq.3.2}$$

From the above equations voltage of the centre-star is derived as:

$$u_{ON} = \frac{u_{ainv} + u_{binv} + u_{cinv}}{3} \quad \text{Eq.3.3}$$

Having the pulses for each inverter leg (da, db, dc), the inverter's leg voltages can be evaluated as:

$$\begin{cases} u_{AN} = u_{DC} \cdot da \\ u_{BN} = u_{DC} \cdot db \\ u_{CN} = u_{DC} \cdot dc \end{cases} \quad \text{Eq.3.4}$$

considering Eq.3.1-3.4 the resulting line voltages will have the expression:

$$\begin{cases} u_{AB} = u_{DC} \cdot (da - db) \\ u_{BC} = u_{DC} \cdot (db - dc) \\ u_{CA} = u_{DC} \cdot (dc - da) \end{cases} \quad \text{Eq.3.5}$$

Similarly, considering Eq.3.1-3.5 the phase voltages can be found as:

$$\begin{cases} u_{ainv} = u_{DC} \cdot (da - (da + db + dc)/3) \\ u_{binv} = u_{DC} \cdot (db - (da + db + dc)/3) \\ u_{cinv} = u_{DC} \cdot (dc - (da + db + dc)/3) \end{cases} \quad \text{Eq.3.6}$$

The inverter is a voltage source; this means that currents in the AC side will be a function of the voltages impressed by the inverter and the configuration of the grid it is connected to. Current on the DC side can be calculated as a function of phase currents and switches configuration:

$$i_{DC} = da \cdot i_{ainv} + db \cdot i_{binv} + dc \cdot i_{cinv} \quad \text{Eq.3.7}$$

3.2.2 Space vector modulation (SVM)

To find switching instants S_a, S_b, S_c for the converter is used Space Vector Modulation (SVM). SVM is based on the fact that every vector \vec{v}_{ref} can be expressed as a weighted average combination of two adjacent active space vectors and the null-state vectors 0 and 7. In the three-phase system, the reference voltage vector is defined as [9], [6]:

$$v_{ref} = \frac{2}{3} (v_a + av_b + a^2 v_c) \quad \text{Eq.3.8}$$

where V_a, V_b, V_c denote phase voltages.

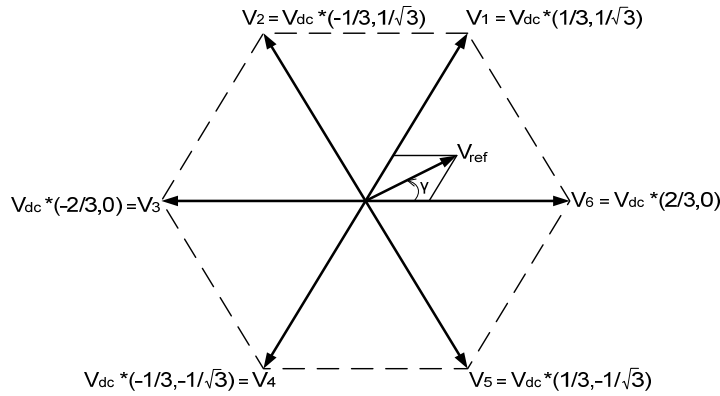


Fig.3.5 The space-vector diagram

The two adjacent voltage vectors are chosen from $\vec{v}_1 - \vec{v}_6$ according to the six active switching states ([011], [001], [101], [100], [110], [010]), plus two passive switching ([000] and [111]).

If the null-state vectors \mathbf{v}_0 and \mathbf{v}_7 are assumed equal with 0 and $\bar{\mathbf{v}}_{ref}$ is considered constant (for high switching frequency), the on-duration of active vectors $\bar{\mathbf{v}}_k$ and $\bar{\mathbf{v}}_{k+1}$ can be founded by solving the vectorial equation [10]:

$$v_{ref} \frac{T_s}{2} = v_k t_k + v_{k+1} t_{k+1} \quad \text{Eq.3.9}$$

$$t_0 = \frac{T_s}{2} - t_k - t_{k+1} \quad \text{Eq.3.10}$$

where t_0 is used by the null voltage vectors using a pattern that ensure that only one leg is switched at every state transition [11].

Thus $\bar{\mathbf{v}}_{ref}$ in sector 1 can be expressed as:

$$v_{ref} \frac{T_s}{2} = v_{100} \frac{t_1}{\frac{T_s}{2}} + v_{110} \frac{t_2}{\frac{T_s}{2}} \quad \text{Eq.3.11}$$

where the state voltages are:

$$v_{100} = \frac{2}{3} (a^0 V_{dc} \cdot \mathbf{1} + a^1 V_{dc} \cdot \mathbf{0} + a^2 V_{dc} \cdot \mathbf{0}) = \frac{2}{3} V_{dc} \quad \text{Eq.3.12}$$

$$v_{110} = \frac{2}{3} (a^0 V_{dc} \cdot \mathbf{1} + a^1 V_{dc} \cdot \mathbf{1} + a^2 V_{dc} \cdot \mathbf{0}) = \frac{2}{3} V_{dc} \left(\frac{1}{2} + j \frac{\sqrt{3}}{2} \right) \quad \text{Eq.3.13}$$

Replacing Eq.3.12 and 3.13 in the Eq.3.11 and splitting final equation to real and imaginary part, the time widths t_1 and t_2 are:

$$t_1 = \frac{V_{ref} \sqrt{3}}{V_{dc}} \sin(60^\circ - \gamma) \quad \text{Eq.3.14}$$

$$t_2 = \frac{V_{ref} \sqrt{3}}{V_{dc}} \sin \gamma \quad \text{Eq.3.15}$$

Finally the duty cycles can be calculated:

$$S_a = \frac{t_1 + t_2 + \frac{t_0}{2}}{\frac{T_s}{2}} \quad \text{Eq.3.16}$$

$$S_b = \frac{t_2 + \frac{t_0}{2}}{\frac{T_s}{2}} \quad \text{Eq.3.17}$$

$$S_c = \frac{\frac{t_0}{2}}{\frac{T_s}{2}} \quad \text{Eq.3.18}$$

3.2.3 LCL Filter

The connection of an inverter to the utility grid is typically done by the use of a filter. As a filter it can be used an inductor or an LCL module; the LCL filter, though, provides good performances with lower encumbrance and costs [19][20]. This is the main reason why this filter has been chosen. The LCL filter implemented is composed by three reactors with resistance R_i and inductance L_i on the converter side and three capacitors C_f (damped with a resistor R_d); a further branch of the filter, represented as three reactors with resistance R_g and inductance L_g , comes from taking in account the impedance of the transformer adopted for connection to the grid and the grid impedance. Effect of the filter is the reduction of high frequency current ripple injected by the inverter. [19],[20]

The chosen LCL three-phase filter has star-connected capacitors, and the centre-star is not connected to the ground. The inverter output voltages are not referred to the ground either, but to the centre-star of the capacitors, as demonstrated in the inverter description paragraph. A graphical description of the equivalent circuit of the filter and the theoretical explanation and calculations for its implementation are given in the following pages.

The components for every phase of the filter are supposed to be identical, so Fig.3.6 is a suitable description also for phase b and c. The main requirements for the LCL-filter are:

- to decouple energy between grid voltage and voltage source inverter
- to filter differential mode inverter switching noise from mains
- to filter common mode inverter switching noise from mains
- to have low losses and compact size

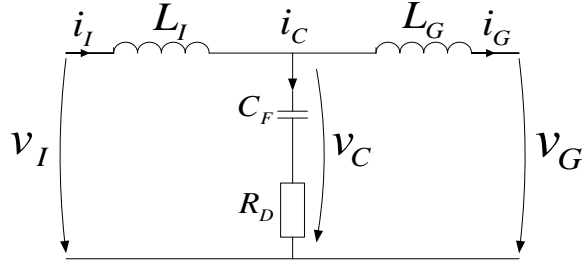


Fig.3.6 LCL filter

From the above figure, the filter model in the s-plane can be written as:

$$\begin{aligned}
 i_I - i_C - i_G &= 0 \\
 v_I &= i_I L_I s + v_C \\
 v_G &= -i_G L_G s + v_C \\
 v_C &= i_C \left(\frac{1}{C_F s} + R_D \right)
 \end{aligned}
 \tag{Eq.3.19}$$

Where: v_I is the inverter voltage

i_I is the inverter current

L_I is the inverter side inductance

L_G is the grid side inductance

C_F is the grid side capacitance

R_D is the damping series resistor

From the above equations can be written the expressions of the inverter- and grid side currents:

$$\begin{aligned}
 i_I &= \frac{1}{L_I s} (v_I - v_C) \\
 i_G &= \frac{1}{L_G s} (v_C - v_G) \\
 v_C &= (i_I - i_G) \left(\frac{1}{C_F s} + R_D \right)
 \end{aligned}
 \tag{Eq.3.20}$$

The set equations 3.8 and 3.9 can be represented as an LCL model, suitable for implementation in simulation:

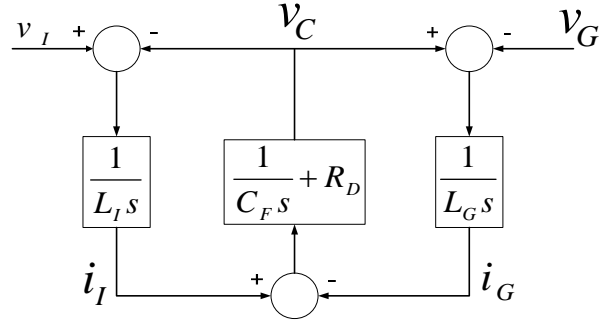


Fig.3.7 Single phase LCL model in s-plane

In order to determinate the transfer function of the above LCL model, using Fig.3.7 can be also written:

$$v_I = z_{11}i_I + z_{12}i_G \quad \text{Eq.3.21}$$

$$v_G = z_{21}i_I + z_{22}i_G$$

where

$$z_{11} = L_I s + \frac{1}{C_F s} + R_D, \quad z_{12} = -\left(\frac{1}{C_F s} + R_D\right) \quad \text{Eq.3.22}$$

$$z_{21} = \frac{1}{C_F s} + R_D, \quad z_{22} = -\left(L_G s + \frac{1}{C_F s} + R_D\right)$$

Grid voltage is assumed as ideal voltage source and represents short circuit for harmonic frequencies, and for filter analysis it is set to zero.

$$v_G = 0 \quad \text{Eq.3.23}$$

Then, the following transfer function can be written:

$$H(s) = \frac{i_I(s)}{v_I(s)} = \frac{L_I C_F s^2 + R_D C_F s + 1}{L_I L_G C_F s^3 + R_D C_F (L_I + L_G) s^2 + (L_I + L_G) s} \quad \text{Eq.3.24}$$

The following design considerations are taken into account [22]:

- the capacitor value is limited by the decrease of the power factor at rated power (less than 5%). The total value of the inductance should be lower than 10% to limit the DC-link voltage.
- the voltage drop across the filter during operation in order to limit the DC-link voltage.
- the resonant frequency should be included in a range between ten times the line frequency and one half of the switching frequency in order to do not create resonance problems in the lower and higher parts of the harmonic spectrum. The passive resistor should be chosen as a compromise between the necessary damping and the losses in the system.

The values used for filter parameters are:

$$R_l = 0.2\Omega ; L_l = 6mH ; R_G = 0.1\Omega ; L_G = 3mH ; C_F = 2\mu F ; R_D = 0.05\Omega ; \quad \text{Eq.2. 25}$$

In order to obtain the frequency response and the pole-zero position of the LCL filter the Bode diagram and pole-zero map have been done and is presented below:

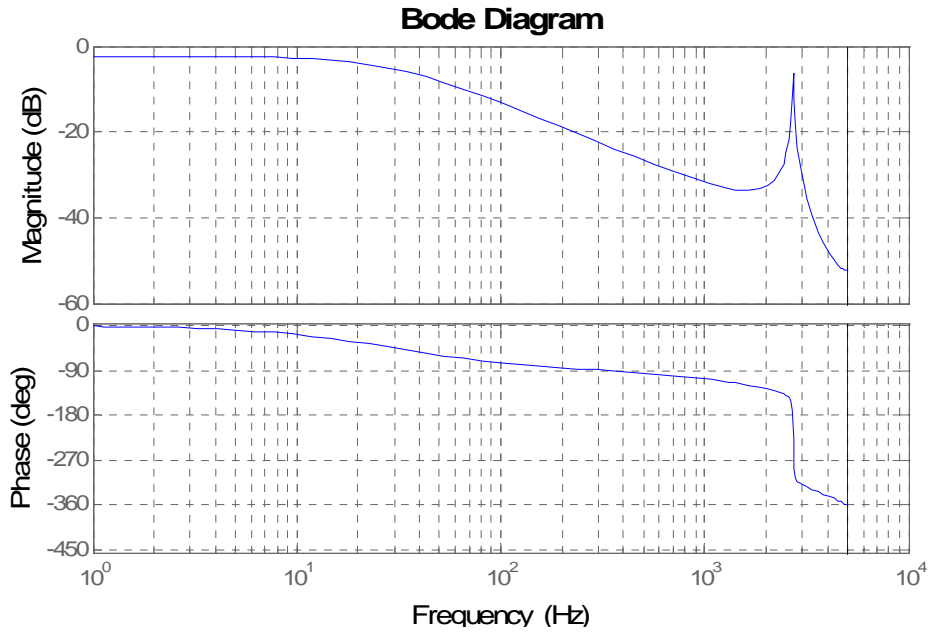


Fig.3.8 Bode plot for LCL filter

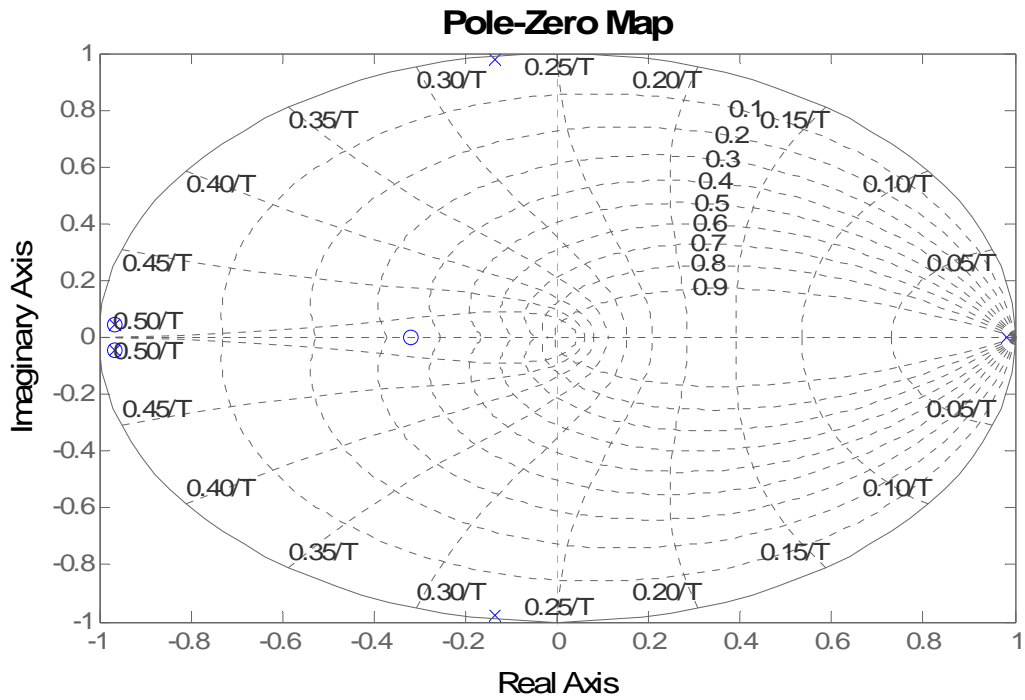


Fig.3.9 Pole-zero map

3.2.4 Grid model

In this section will be describe the mathematical model of the grid model [21].

The grid is represented as an ideal symmetrical three-phase voltage source shown in the next figure.

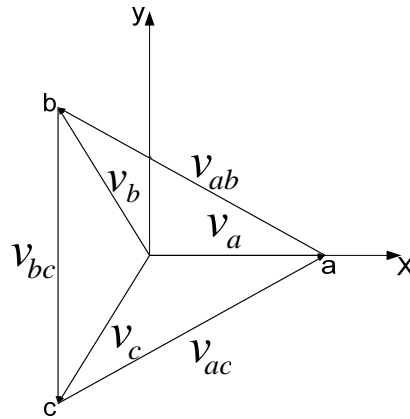


Fig.2. 10 Symmetrical three-phase system

The three phase voltages of the symmetrical system are defined as:

$$v_a = E_m \cos(\omega \cdot t) \quad \text{Eq.3.26}$$

$$v_b = E_m \cos\left(\omega \cdot t - \frac{2\pi}{3}\right) \quad \text{Eq.3.27}$$

$$v_c = E_m \cos\left(\omega \cdot t - \frac{4\pi}{3}\right) \quad \text{Eq.3.28}$$

where E_m is the amplitude of the phase voltage and ω is the angular frequency .

The three phase currents of the symmetrical system are defined as:

$$i_a = I_m \cos(\omega \cdot t) \quad \text{Eq.3.29}$$

$$i_b = I_m \cos\left(\omega \cdot t - \frac{2\pi}{3} + \varphi\right) \quad \text{Eq.3.30}$$

$$i_c = I_m \cos\left(\omega \cdot t - \frac{4\pi}{3} + \varphi\right) \quad \text{Eq.3.31}$$

where I_m is the amplitude of the phase current and φ is the phase between the voltage and the current.

We also have the line-to-line voltages which are defined as:

$$v_{ab} = v_a - v_b \quad \text{Eq.3.32}$$

$$v_{bc} = v_b - v_c \quad \text{Eq.3.33}$$

$$v_{ca} = v_c - v_a \quad \text{Eq.3.34}$$

In case there is no neutral connection we will have the following equations:

$$i_a + i_b + i_c = 0 \quad \text{Eq.3.35}$$

$$v_a + v_b + v_c = 0 \quad \text{Eq.3.36}$$

Active and reactive power is:

$$P = \text{Re}(\underline{v} \cdot \underline{i}^*) = v_a i_a + v_b i_b + v_c i_c \quad \text{Eq.3.37}$$

$$Q = \text{Im}(\underline{v} \cdot \underline{i}^*) = -\frac{1}{\sqrt{3}}(v_{bc} i_a + v_{ca} i_b + v_{ab} i_c) \quad \text{Eq.3.38}$$

3.2.5 DC link circuit

The input DC current of the DC link is calculated by dividing the reference power to the DC voltage.

$$V_{dc} = \frac{1}{C_{dc}} \int (i_{dc} - i_{inv}) dt + R_{dc} (i_{dc} - i_{inv}) \quad \text{Eq.2.39}$$

Chapter 4

Control strategies design

Abstract

This chapter presents the study of the grid control strategy. First part will describe the main requirements for the strategy chose for the design and implementation. The chosen strategy is VOC PI synchronous with PLL and the functionality together with the mathematical model is presented in this section.

4.1 Introduction.....	Page 52
4.2 Control method.....	Page 52
4.3 Phase locked loop.....	Page 56
4.4 The d axis and q axis current controller.....	Page 58
4.5 DC voltage controller.....	Page 60

4.1. Introduction

One of the goals of this project is to control the grid currents by using a convenient strategy which can highlight the behavior of the grid in different operating modes.

In this chapter will be described one method for controlling the grid currents, VOC-PI synchronous with PLL. The control strategy should meet the following demands:

- The bandwidth of the controllers should be sufficiently high to inject 5th and 7th harmonic currents into a 50Hz grid
- Frequency change rate up to 5Hz/sec
- Power factor $\cos(\varphi)$ range from 0.9 inductive to 0.9 capacitive at full load. Reactive power up to 0.85 time rated power when no active power is produced.
- Ease of implementation and controller tuning

4.2. Control method -VOC-PI synchronous with PLL

Voltage oriented control is based on coordinate transformation between stationary $\hat{\alpha}\beta$ and synchronous rotating d-q reference systems. According to [18] this strategy guarantees fast transient response and high static performance via an internal current control loops. Consequently, the final configuration and performance of the system largely depends on the quality of the applied current control strategy. One of the solutions is hysteresis current control. This current control provides a fast dynamic response, good accuracy, no dc offset and high robustness but the price for all of this is its average switching frequency which varies with the dc load current; this makes the switching pattern uneven and random, thus resulting in additional stress on switching devices and difficulties of LCL input filter design.

Among the presented regulators, the widely used scheme for high-performance current control is the d-q synchronous controller, where the currents being regulated are dc quantities, which eliminates the steady-state error [18].

The block diagram of this strategy is illustrated in Fig.4.1:

- In this strategy, a conventional PLL is used to detect the phase grid angle θ and the grid frequency f . The frequency is needed in order to monitor the grid condition and to comply with the requirements while the grid angle θ is required for Clark and Park transformations. This frame transformations are describe in the Appendix A.

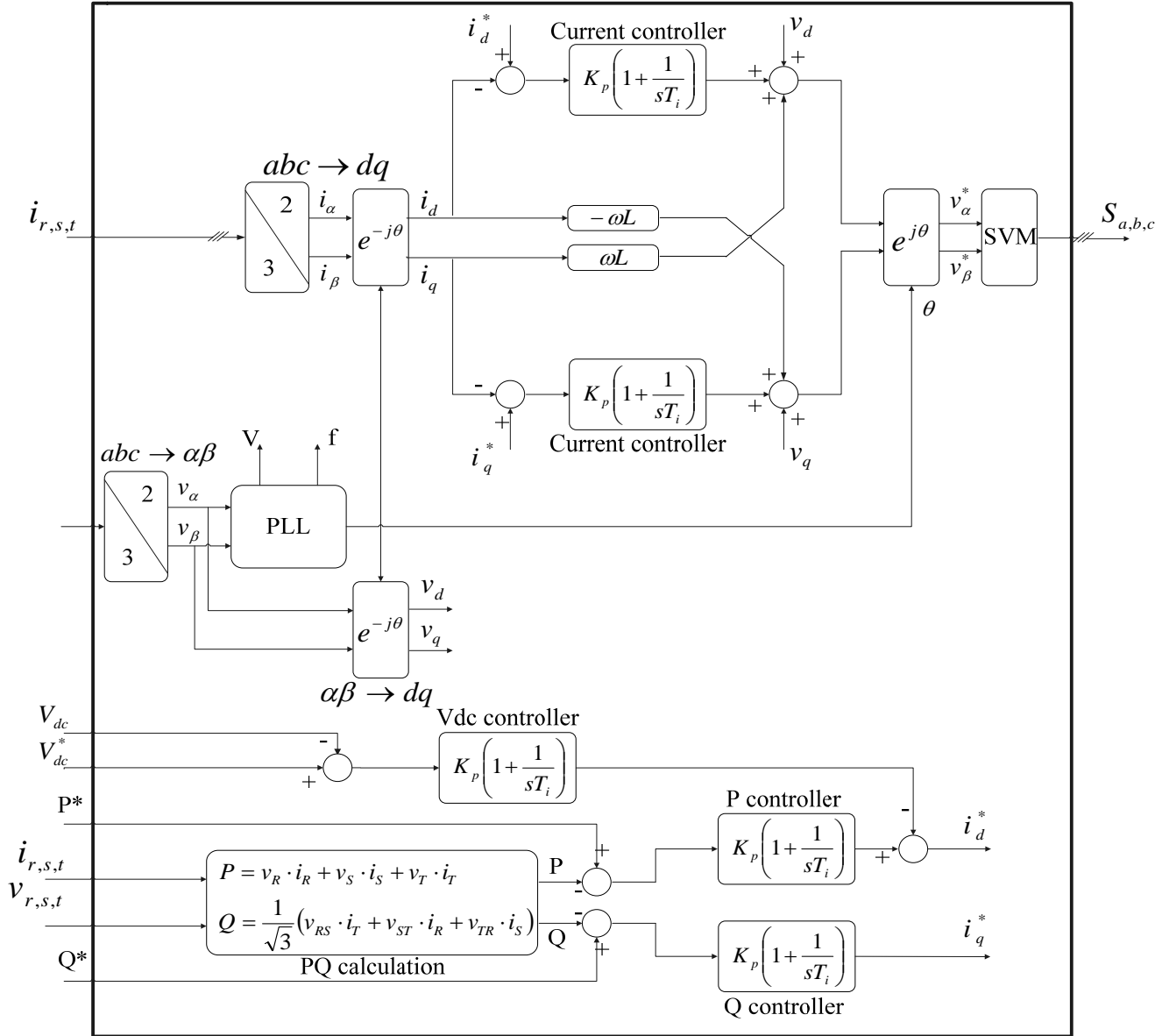


Fig.4.1 VOC-PI synchronous with PLL

- Conventional PI controllers are used, that are standard structures which contain the basic proportional (P) component and the integrative (I) component. The P component makes a frequency characteristic with the same gain for all the frequencies and is related to the amount of the ripple. The I component minimizes errors at low frequencies.
- The transfer function of a PI controller is:

$$H(s) = K_p \left(1 + \frac{1}{T_i \cdot s}\right) \quad \text{Eq.4.1}$$

where K_p is the high frequency gain of the controller and T_i is the integral time constant.

- PI controllers are universally known because of their flexibility combined with the relatively easy tuning. Due to the capabilities of the integral action to estimate load

disturbance, a certain stability margin in the closed-loop is obtained. That is, the integral variable provides an estimate of the load disturbances, which is counteracted in the feedback loop.

- A PI controller is also used for the DC voltage and its output is feed-forwarded to the output of PQ controller to obtain the reference for the active current i_d and the reactive current i_q . The actual powers P and Q are calculated using the conventional instantaneous power definition in ‘abc’ systems.
- In order to obtain a synchronous control, we need the transformation in ‘dq’ frame, which is obtained by using the Park transformations. The three phase currents and voltages from ‘abc’ frame are transformed in ‘dq’ frame currents and voltages.
- The equations used for these transformations are:

$$\begin{pmatrix} i_d \\ i_q \end{pmatrix} = \frac{2}{3} \begin{pmatrix} \cos \gamma & \cos\left(\gamma - \frac{2\pi}{3}\right) & \cos\left(\gamma + \frac{2\pi}{3}\right) \\ \sin \gamma & \sin\left(\gamma - \frac{2\pi}{3}\right) & \sin\left(\gamma + \frac{2\pi}{3}\right) \end{pmatrix} \begin{pmatrix} i_a \\ i_b \\ i_c \end{pmatrix} \quad \text{Eq.4.2}$$

for the currents and

$$\begin{pmatrix} u_d \\ u_q \end{pmatrix} = \frac{2}{3} \begin{pmatrix} \cos \gamma & \cos\left(\gamma - \frac{2\pi}{3}\right) & \cos\left(\gamma + \frac{2\pi}{3}\right) \\ \sin \gamma & \sin\left(\gamma - \frac{2\pi}{3}\right) & \sin\left(\gamma + \frac{2\pi}{3}\right) \end{pmatrix} \begin{pmatrix} u_a \\ u_b \\ u_c \end{pmatrix} \quad \text{Eq.4.3}$$

for the voltages.

- In this strategy, the currents and voltages in ‘ $\alpha\beta$ ’ frame are rotated with $e^{-j\gamma}$ resulting a split of the AC line currents into two rectangular components $i = [i_d, i_q]$. The component i_q determines reactive power while i_d decide the active power flow. Thus the active and reactive power can be controlled independently.
- The UPF condition is met when the line current vector, i_L , is aligned with the line voltage vector, u_L [18]. By placing the d-axis of the rotating coordinates on the line voltage vector a simplified dynamic model can be obtained. The voltage equations in the d-q synchronous reference frame are presented below:

$$u_d = R i_d + L \frac{di_d}{dt} + u_d - \omega_s L i_q \quad \text{Eq.4.4}$$

$$0 = u_{Lq} = R i_{Lq} + L \frac{di_{Lq}}{dt} + u_q + \omega_s L i_{Ld} \quad \text{Eq.4.5}$$

- The q-axis current is set to zero in all conditions for unity power factor control while the reference current i_d is set by the DC-link voltage controller and controls the active power flow between the supply and the dc-link [18]. For $R \approx 0$ Eq.4.4-4.5 can be reduce to:

$$E_m = L \frac{di_{Ld}}{dt} + u_d - \omega_s L i_{Lq} \quad \text{Eq.4.6}$$

$$0 = L \frac{di_{Lq}}{dt} + u_q + \omega_s L i_{Ld} \quad \text{Eq.4.7}$$

Assuming that the q-axis current is well regulated to 0, the following equation hold true:

$$E_m = L \frac{di_{Ld}}{dt} + u_d \quad \text{Eq.4.8}$$

$$0 = u_q + \omega_s L i_{Ld} \quad \text{Eq.4.9}$$

- The tracing performance for a PI controller is not so good especially for the coupled system described by Eq.4.6-4.7. Therefore, in order to obtain a high performance for the system, a decoupled controller is used [18]. The block diagram is presented in Fig.4.2

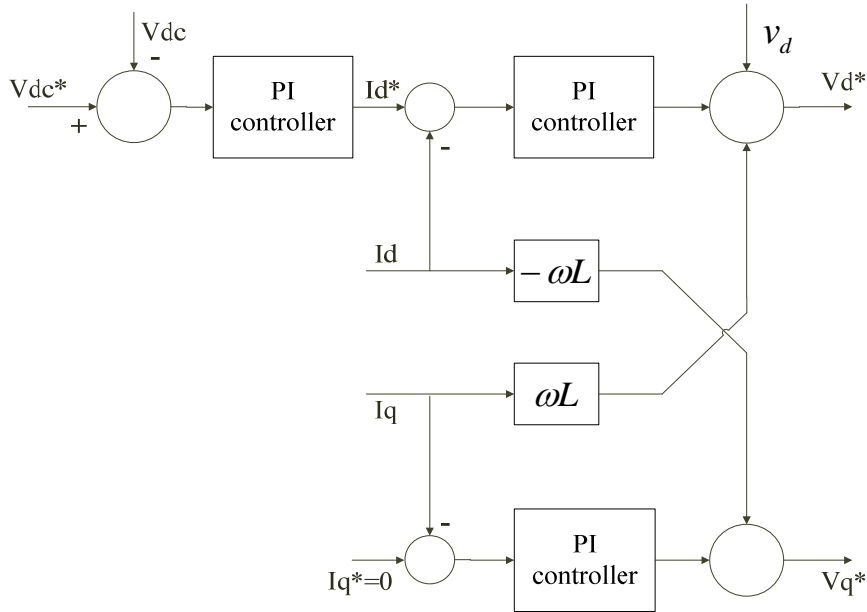


Fig.3.2 Compensation of the cross coupling between axes

The output of the decoupled system has the following form:

$$u_d = E_m + \omega L i_{Lq} + \Delta u_d \quad \text{Eq.4.10}$$

$$u_q = \Delta u_q - \omega L i_{Ld} \quad \text{Eq.4.11}$$

Where Δ are the output signals of the current controllers.

- In order to get a good dynamic response and to decouple the grid voltage from the output of the current controllers, a grid voltage feed-forward is used. [18]
- The output signals from PI controllers are transformed in $\alpha - \beta$ and is used for switching signal generation by a space vector modulator described in section 3.2.2.

4.2.1 Phase locked loop (PLL)

As it is describe in section 2.3.1 the PLL is used in order to determine the phase angle θ and the frequency of the grid. The block diagram of the used PLL is further shown in Fig.4.3:

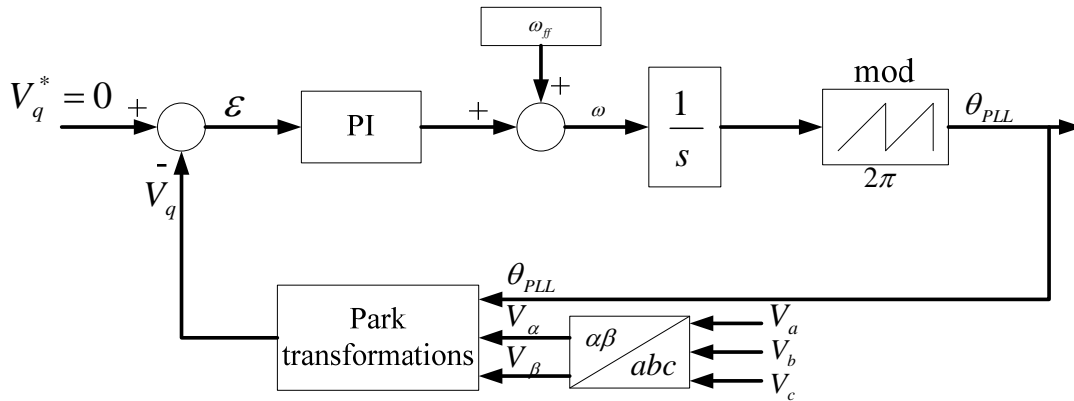


Fig.4.3 Block diagram of a three-phase PLL

As it can be observed that is used a PI controller in order to reduce the error between the reference and measured values of V_q . The measured value V_q is determined by applying the Park transformations to the three-phase voltages V_a, V_b, V_c .

The form of the PI controller from Fig.4.3 can be presented:

$$P(s) = K_p \left(\frac{T_I s + 1}{T_I s} \right) \quad \text{Eq.4.12}$$

which can be written like:

$$P(s) = \frac{K_p T_I s + K_p}{T_I s} \quad \text{Eq.4.13}$$

The transfer function of the linearised model of the PLL is a second order transfer function:

$$H(s) = \frac{K_p s + \frac{K_p}{T_I}}{s^2 + K_p s + \frac{K_p}{T_I}} \quad \text{Eq.4.14}$$

where: K_p is the proportional gain and K_I is the integral gain

The overshoot is set to 5%, which gives a damping ratio of $\zeta \approx 0.7$. A settling time t_s inside of 1% band is chosen to be a 50 Hz period or $t_s = 20\text{ms}$. The undamped natural frequency ω_n of the transfer function is obtained:

$$t_s = \frac{4}{\zeta \omega_n} = 329 \text{ rad / s} \quad \text{Eq.4.15}$$

Comparing the transfer function of the PLL with a standard transfer function it is possible to calculate the proportional gain K_p and integral gain K_I :

$$K_p = 2\zeta \omega_n = 461 \quad \text{Eq.4.16}$$

$$\omega_n^2 = \frac{K_p}{T_I} \Rightarrow T_I = 0.0043 \quad \text{Eq.4.17}$$

A settling time of 20 ms was considered in order to get a satisfied high bandwidth of the PLL controller.

The output of our PI controller in addition with the feed forward frequency ω_{ff} is modulated and gives the phase angle θ .

The grid phase angle is represented in Figure 4.4:

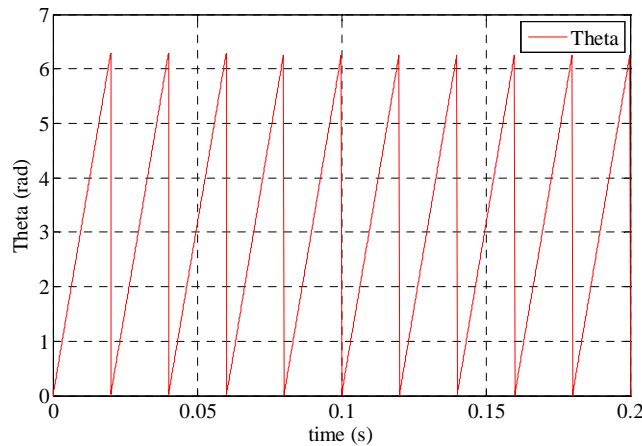


Fig.4 4 Grid phase angle θ

4.2.2 The d-axis and q-axis current controllers

Both current loops have the same dynamics. The tuning will be made only for one current controller, assuming for the other current loop the same parameters for the controller.

The block diagram of the synchronous current controller working in d-q coordinates is shown in Fig.4.5. It includes [22][23][24].

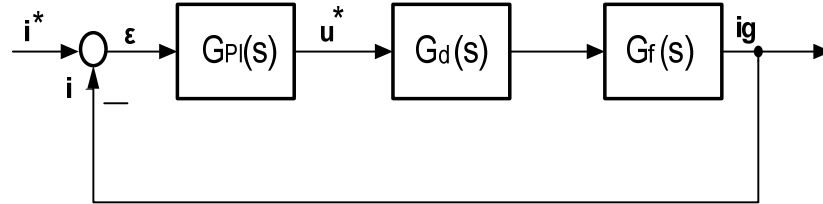


Fig.4. 5 Block diagram of the current loop in s-domain

$G_{PI}(s)$ is the PI controller transfer function which has the following expression:

$$G_{PI} = K_P \left(1 + \frac{1}{T_I s} \right) \quad \text{Eq.4.18}$$

- $G_d(s)$ is the $1.5T_s$ delay due to the elaboration of the computation device (T_s) and to the PWM ($0.5T_s$), indicating with T_s the sampling period. This delay time is taking into account by means of a first order transfer function.

$$G_d(s) = \frac{1}{1 + 1.5T_s s} \quad \text{Eq.4.19}$$

- $G_f(s)$ is the transfer function of the LCL filter.

$$G_f(s) = \frac{L_I C_F s^2 + R_D C_F s + 1}{L_I L_G C_F s^3 + R_D C_F (L_I + L_G) s^2 + (L_I + L_G) s} \quad \text{Eq.4.20}$$

The values of the filter parameters are listed in chapter 3.

The open-loop transfer function is given by the equation:

$$G_{OL}(s) = K_P \frac{1 + sT_i}{sT_i} \frac{1}{1 + 1.5T_s s} G_f(s) \quad \text{Eq.4.21}$$

All the transfer function of the design have been discretized using a zero-order-hold method at a sampling frequency at 10 kHz.

The requirements for the design of the current controller should be[23][24]:

- the current loop should be stable, (closed loop) with a phase margin larger than 45° .
- the bandwidth of the system should be minimum 500 Hz.

Because of the complex filter transfer function in order to determine the PI controller parameters the pole placement method is used. An integrator time constant $T_I = 8ms$ is selected as a trade-off between a good dynamics and still a good noise rejection. The gain K_p is selected using root locus method so that the dominant poles have a damping factor of 0.7.

In Fig.4.6 can be seen that the dominant poles have a damping factor of 0.7 at 600Hz. From the Bode diagram a gain margin of 12.6dB and a phase margin of 63° are obtained and the design of the controller gives a stable loop with the proportional gain $K_p = 14$.

From the closed loop Bode diagram (Fig.4.7) it can be seen that the bandwidth of the current controller has the value of 586Hz.

The requirements for the current loop are fulfilled giving a phase margin larger than 45° and a bandwidth of minimum 500 Hz.

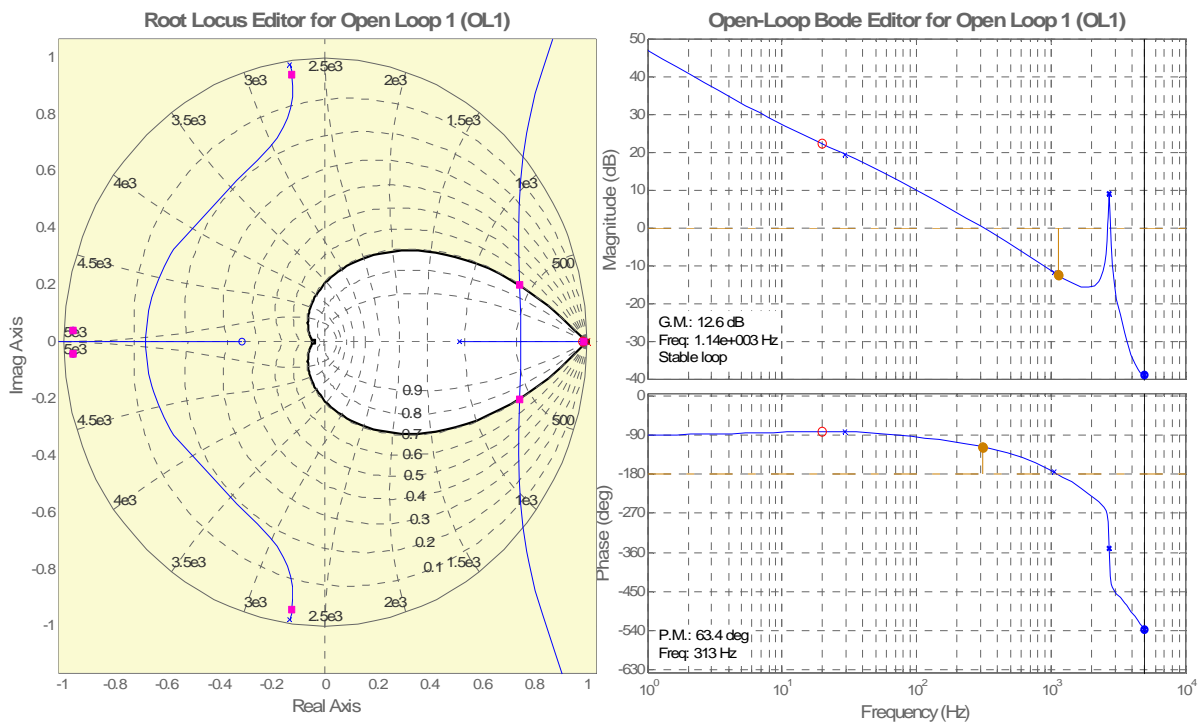


Fig.4.6 Root locus and Bode diagram of the open loop current controller

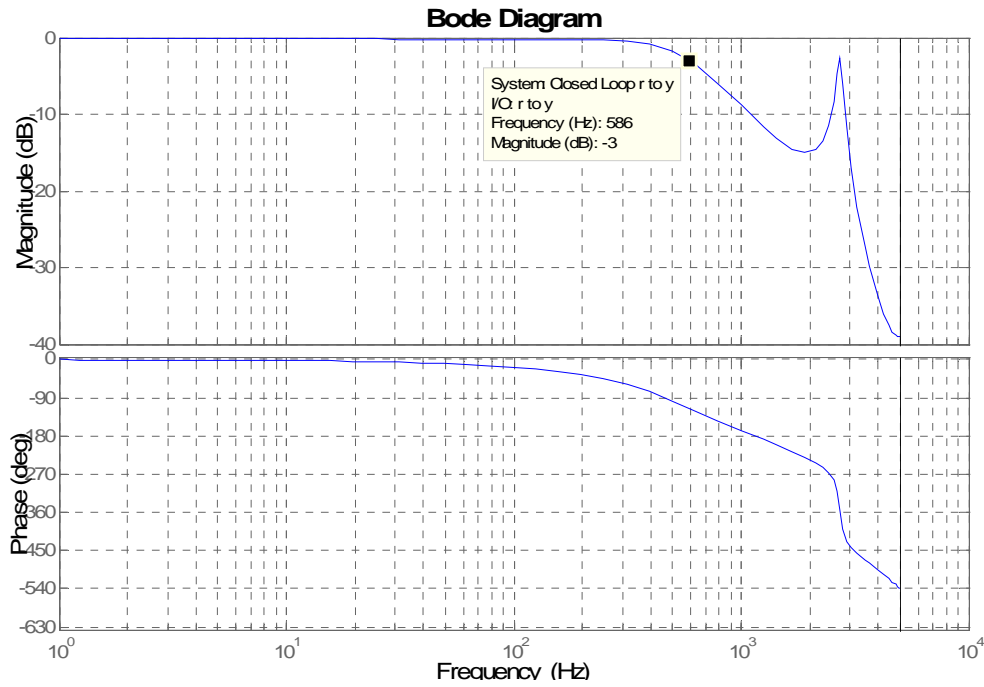


Fig.4.7 Bode diagram of the closed loop current controller

4.2.3 DC voltage controllers

The DC voltage controller is used to produce the reference current value for the current controller. Its aim is to keep the voltage constant on the DC side in normal condition or during grid faults or changes in input power. The DC link voltage control is changed according to the balance of power exchanged by the converter.

The DC voltage loop is an outer loop while the current loop is an inner loop. The internal loop have been designed to achive a short settling times in order to a fast corection of the error. The outer loop can be design to be slower. Thus, the inner loop and the outer loop can be considered decoupled and they can be liniarized.

The DC-link voltage is controlled by means of the converter side DC current and the plant is given by [23]:

$$G_{DC} = \frac{3S_d}{4} \frac{1}{C_{dc}s} \tag{Eq.4.22}$$

Where: S_d is the switching steady state signal on d-axis which is averaged in the following computation to a value of 1 and C_{dc} is the vlue of the DC link capacitor.

The block diagram of the DC link controller is presented in Fig.4.8:

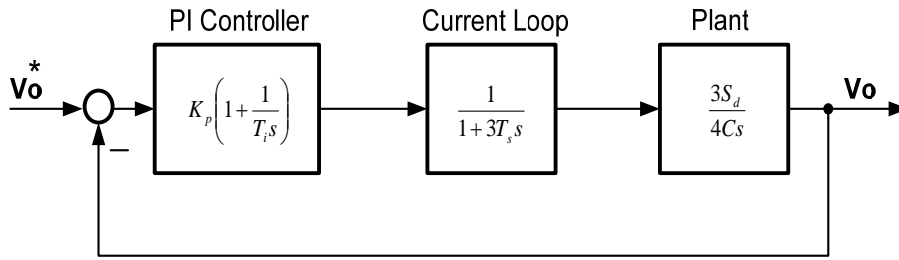


Fig.4.8 Dc voltage loop

In Fig4.8 the voltage control loop in S-domain is represented, including also the delay of the current loop and the DC link plant.

The transfer function in continuous domain for the PI controller is given by:

$$G_{PI} = K_P \left(1 + \frac{1}{T_I s} \right) \quad \text{Eq.4.23}$$

This transfer function can be tuned following the „optimum symmetrical”[23]. In order to obtain the parameters, according to this criterion the phase margin can be impose at 45°. Thus the controller parameter can be obtain as follows:

$$K_P = \frac{4C_{dc}}{9aS_d T_s} = 0.33 \quad \text{Eq.4.24}$$

$$T_i = 3a^2 T_s = 0.0017 \quad \text{Eq.4.25}$$

where:

$$a = \frac{1 + \cos \psi}{\sin \psi} = 2.4 \quad \text{Eq.4.26}$$

ψ -phase margin

The root locus of the voltage contro loop is represented in Fig.4.8 and shows that the design gives a stable loop and leads to a phase margin of 35.8° and a step response characterise by (see Fig.4.9):

- overshoot of 43%
- rise time of 0.00071s
- settling time of 0.005s

From the closed loop Bode diagram (Fig.4.10) it can be seen that the bandwidth of the voltage controller has the value of 396Hz which will give a loop slowest that the current loop.

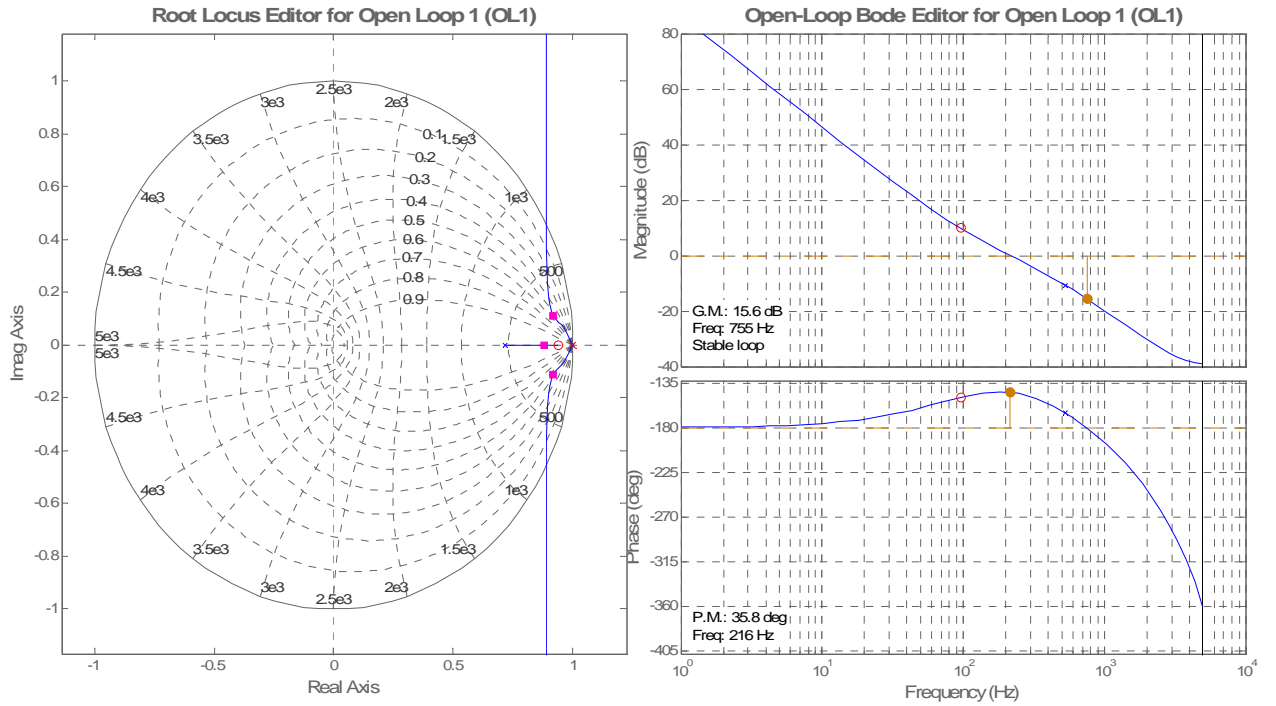


Fig.4.9 Root Locus and open loopBode diagram

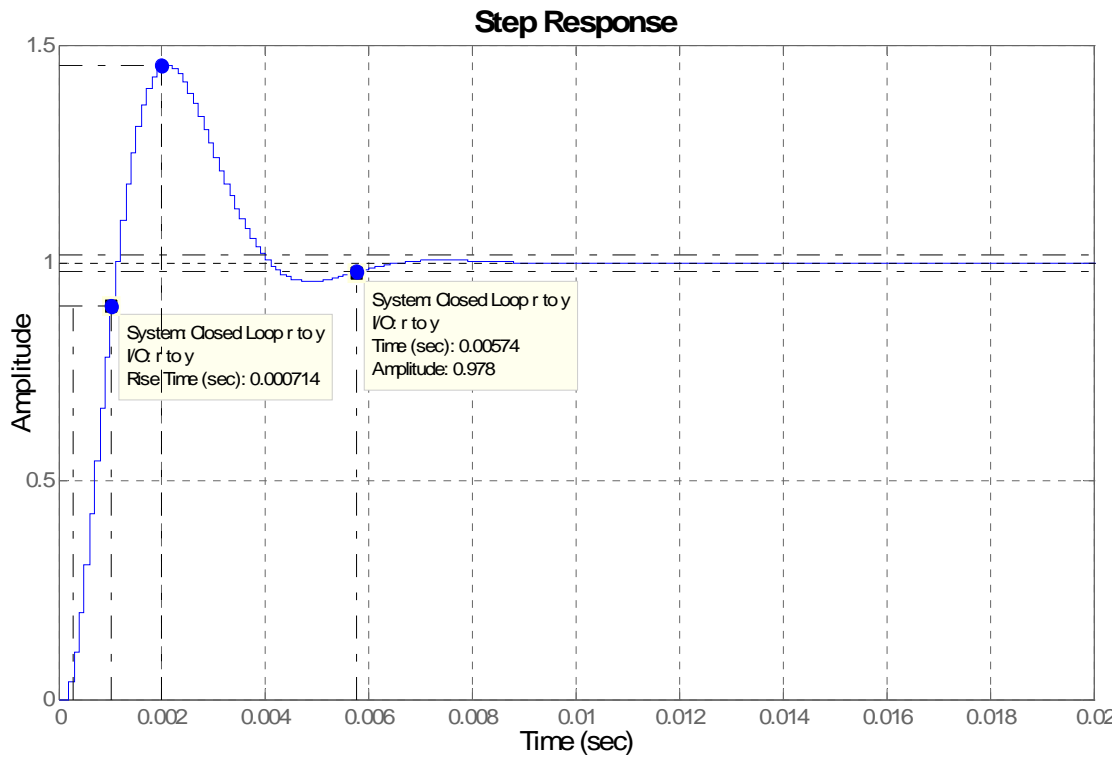


Fig.4.10 Step response

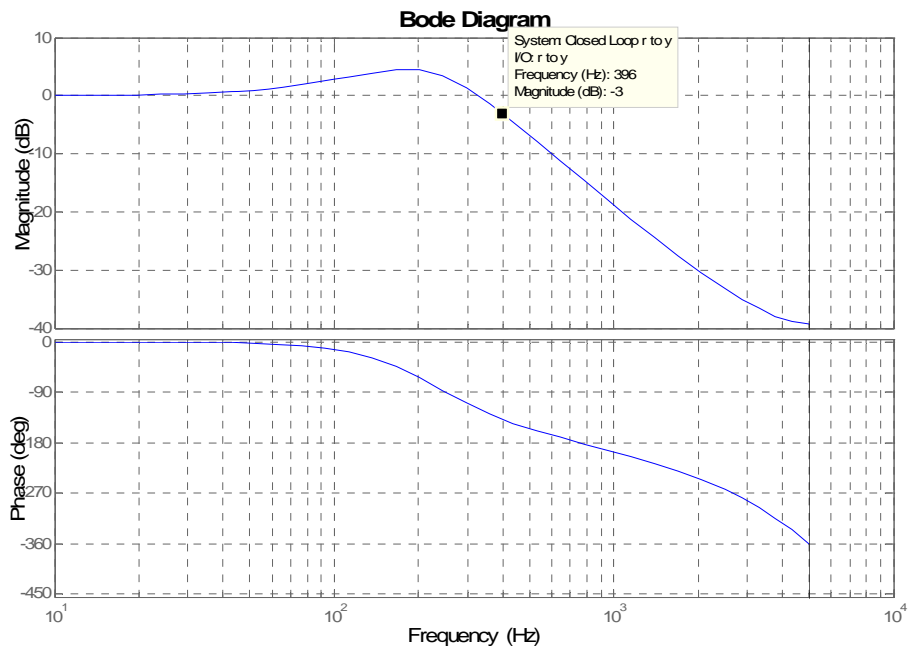


Fig.4.11 Closed loop Bode diagram

Chapter 5

Simulation and experimental results

Abstract

In this chapter the simulations of the active rectifier with LCL-filter are presented. Simulations have been done using Matlab-Simulink toolbox. The results are shown the behavior of the grid current which is controlled in the inner loop with an adequate control for the DC-link voltage in the outer loop. Second part of this chapter consists from a description of the experimental setup used to validate the simulation results. Experimental results will be presented in the end of this section.

5.1 Introduction.....	Page 66
5.2 Simulation results	Page 66
5.3 Implementation and experimental evaluation.....	Page 70
5.4 Experimental results.....	Page 74

5.1. Introduction

The purpose of this chapter is to validate the models used in developing the control strategy, described before in chapter 3 and 4. The simulation work was carried out by using the software package Matlab-Simulink. The simulation results will be used and verified during the practical implementation.

5.2. Simulation results: Reference power step signal

This study case proves that the control strategy developed in this project is well performed. In this simulation case it has been applied a step variation in the reference input power as can be seen in Fig.5.1. This step is increased every 0.5s with 500W. It can be analyzed how the control parameter are varying in function of the input power variation.

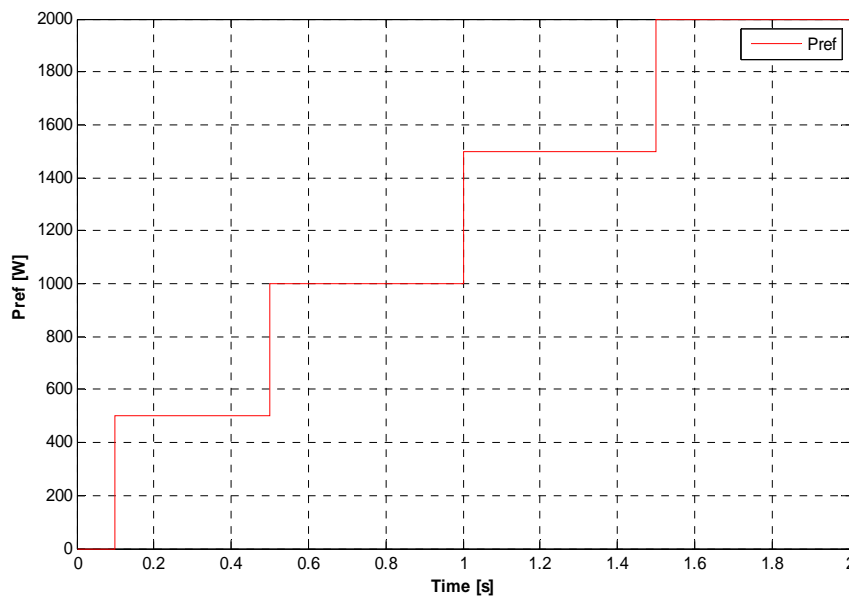


Fig.5.1 Step variations in input reference power

In Fig.5.2 and Fig.5.3 the current loop controller is validate and can be seen that the i_d and i_q measured signals are tracking very well their references. From this two figures it can be analyze also that the current controller is very fast and is reaching the reference in a very short time Because the i_d current determines the active power this is increasing direct proportional with the step variation of active power while the i_q current which decides the reactive power is fixed to 0.

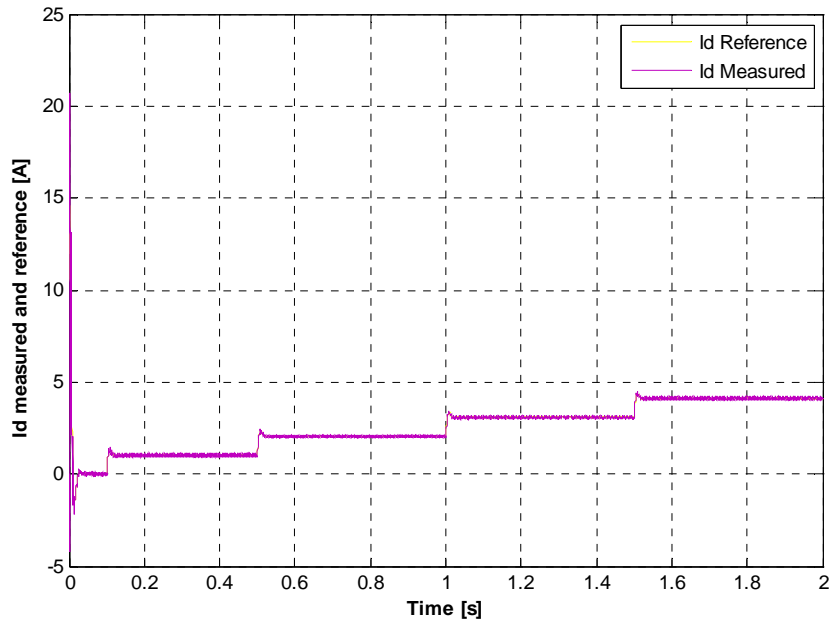


Fig.5.2 Id current reference and measured

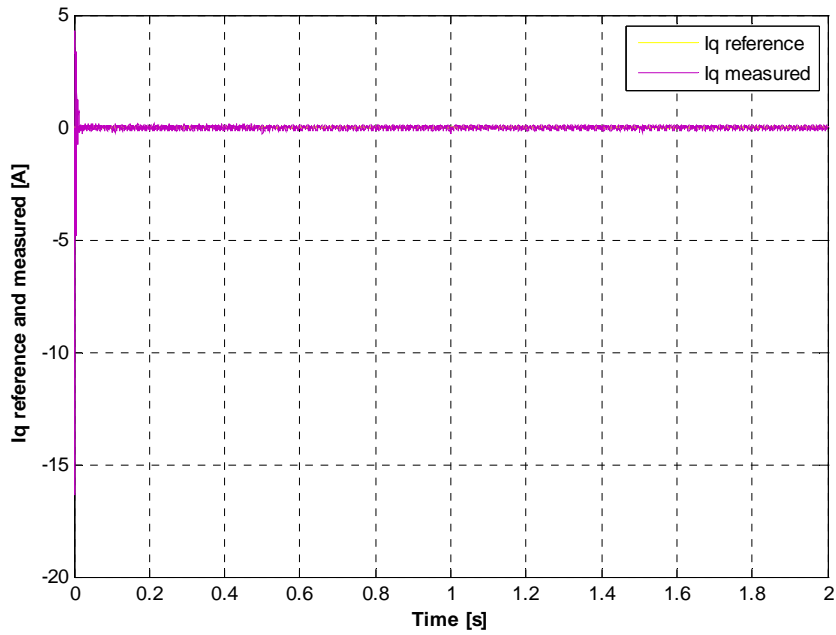


Fig.5. 3 Iq current reference and measured

In Fig.5.4 and 5.5 it can be seen the grid currents which are increasing in function of the i_d current variation and respectively active power variation. The values for the grid currents are starting from 1.2A at 500W and are increasing until 4A at 2kW. In Fig.5.5 it can be view the shape of the grid currents.

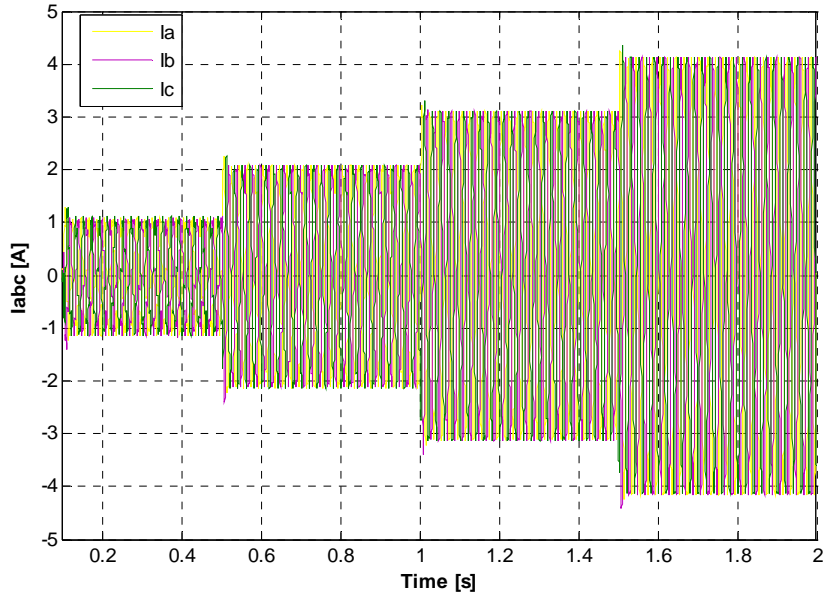


Fig.5.4 Grid currents

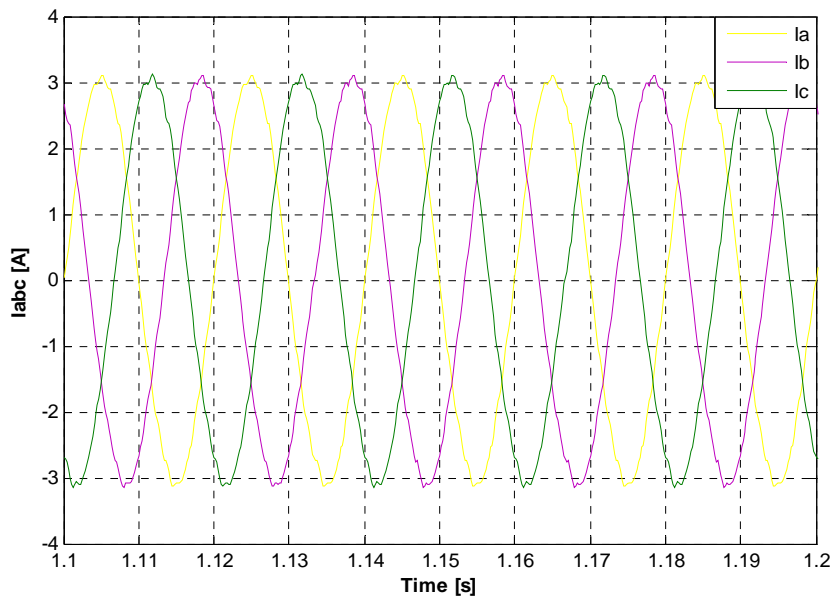


Fig.5.5 Grid currents

In the next figure it is represent the variation of the measured active power- P_{meas} - in function of its reference- P_{ref} . It can be seen that the measured active power is tracking very well the reference. The reactive power is also plotted in the same figure and is equal with its reference which is set to 0. In order to check if the unity power factor is achieve in Fig.5.7 the first phase of the grid voltage is plotted together with the first phase of the grid current. It can be notice that the grid current and voltage are in phase for the value of the reactive power fixed to 0.

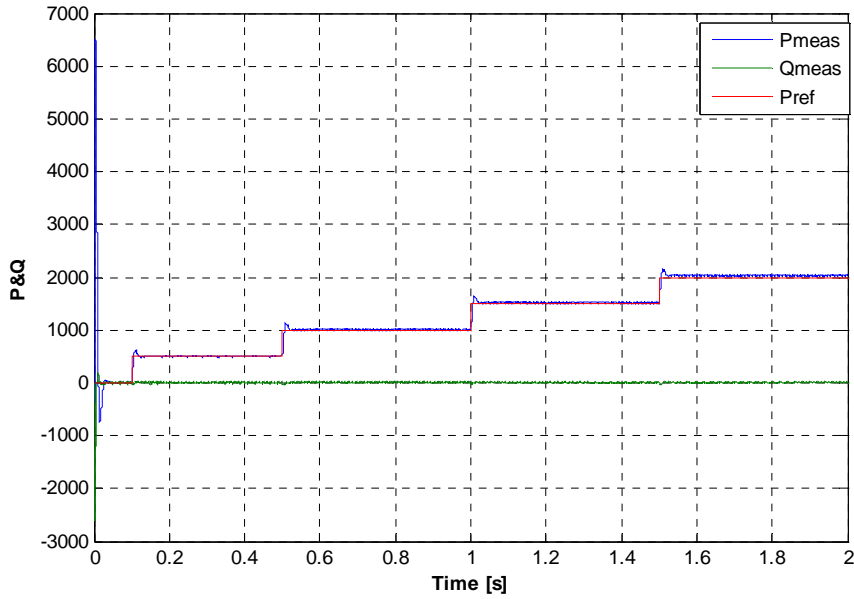


Fig.5.6 Active & reactive power variation.

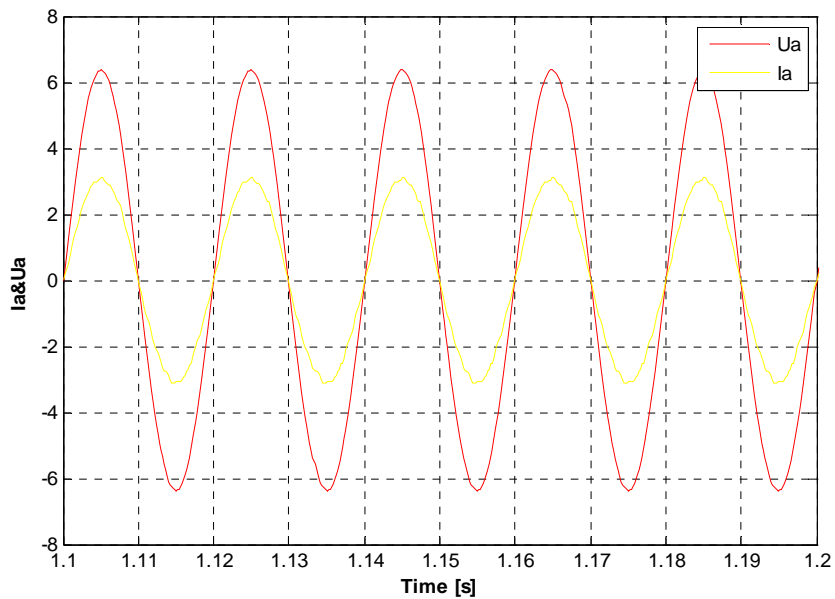


Fig.5.7 Ia&Ua current and voltage phase

One of the purposes of the grid side converter control strategy is to keep the DC link voltage stable in functions of the power variation. Fig.5.8 is validating the DC-link voltage controller which provides a good tracking of the measured dc voltage to its reference. It can be notice that at the same time when the active power is increasing the DC voltage is trying also to increase. The DC controller is reducing very fast the error and is keeping always the DC link at the same constant value.

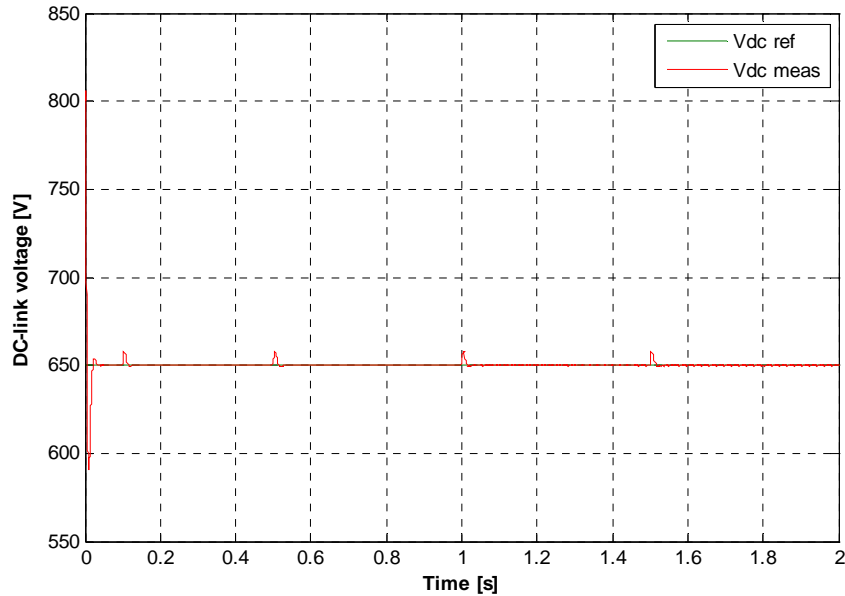


Fig.5.8 DC-link voltage

5.3. Implementation and experimental evaluation

The control of the grid side converter has been implemented in dSPACE platform and tested for the evaluation of performance. Due to the time constraints, the model for the compensation of the harmonics has not been implemented yet. Experimental results support the design of the control system presented in Chapter 4.

5.2.1 Experimental setup

A block diagram of the experimental test setup is shown in Fig.5.9. The experimental test setup is presented also in Fig.5.10 and as it can be seen, is composed by:

- Danfoss inverter FC302
 - Rated power:3.9 kVA
 - Rated input voltage:3x360 Vrms-500 Vdc
 - Rated input current:5.0/4.3 A
 - Rated input frequency:50-60 Hz
 - Rated output voltage:3x0-Vin
 - Rated output current:5.6/4.8A
 - Rated output frequency:0-1000Hz

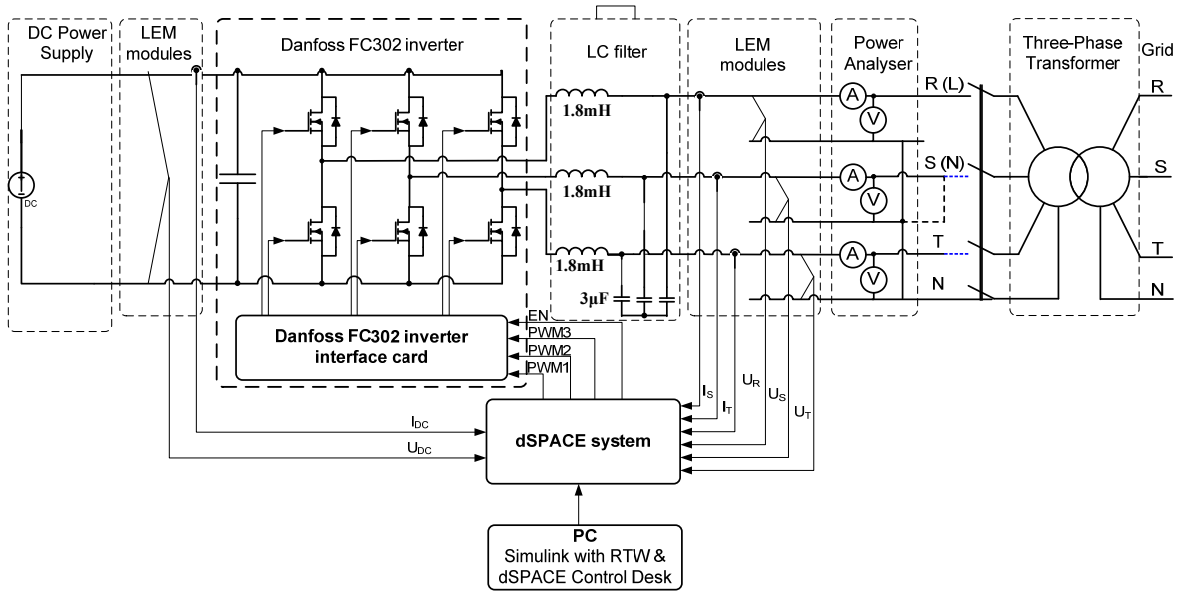


Fig.5.9 Experimental setup block diagram

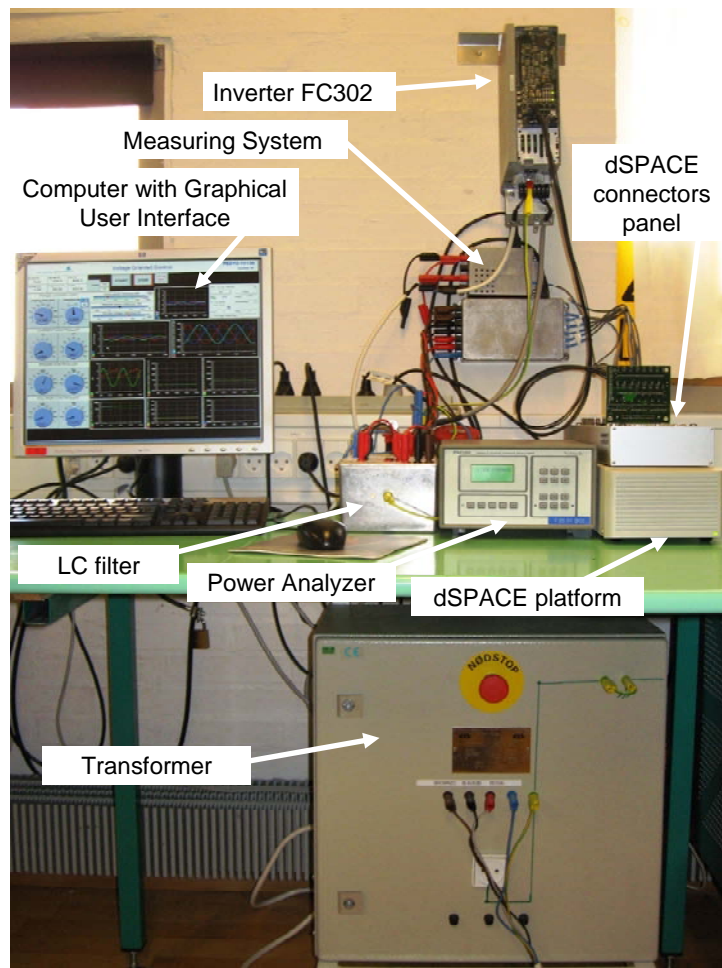


Fig.5.10 Experimental setup

- 2 x Delta Elektronika DC power supply connected in series
 - Type: SM300 D10
 - Rated power: 3kW
 - Rated voltage: 300V
 - Rated current: 10A

- The measuring system includes:
 - LEM box for measurement of U_{dc} (1 x voltage transducer LV25-800, LEM)
 - LEM box for measurement of grid currents i_a , i_b , i_c (3 x current transducer LA55-P, LEM)

- Power analyzer
- Three-phase transformer
- dSpace system

5.2.2 Digital implementation

The control system has been implemented in the dSPACE DS1103 PPC system [25]; it is a mixed RISC/DSP digital controller providing a powerful processor for floating point calculations. The DS1103 PPC card is plugged in one of the ISA slots of the mother-board of the host computer. The control system has been developed using Matlab/Simulink and then automatically processed and run in the DS1103 PPC card [25]. As shown in Fig.6.1, the control system includes:

- the control of the grid side converter based on the VOC;
- the Space Vector Modulation (SVM) technique, which calculates duty-cycles provided to the grid side converter.

A Graphical User Interface (GUI) has been built using the software Control Desk of dSPACE. It allows the real-time evaluation of the control system. The Control Desk GUI is presented in Fig.5.10.

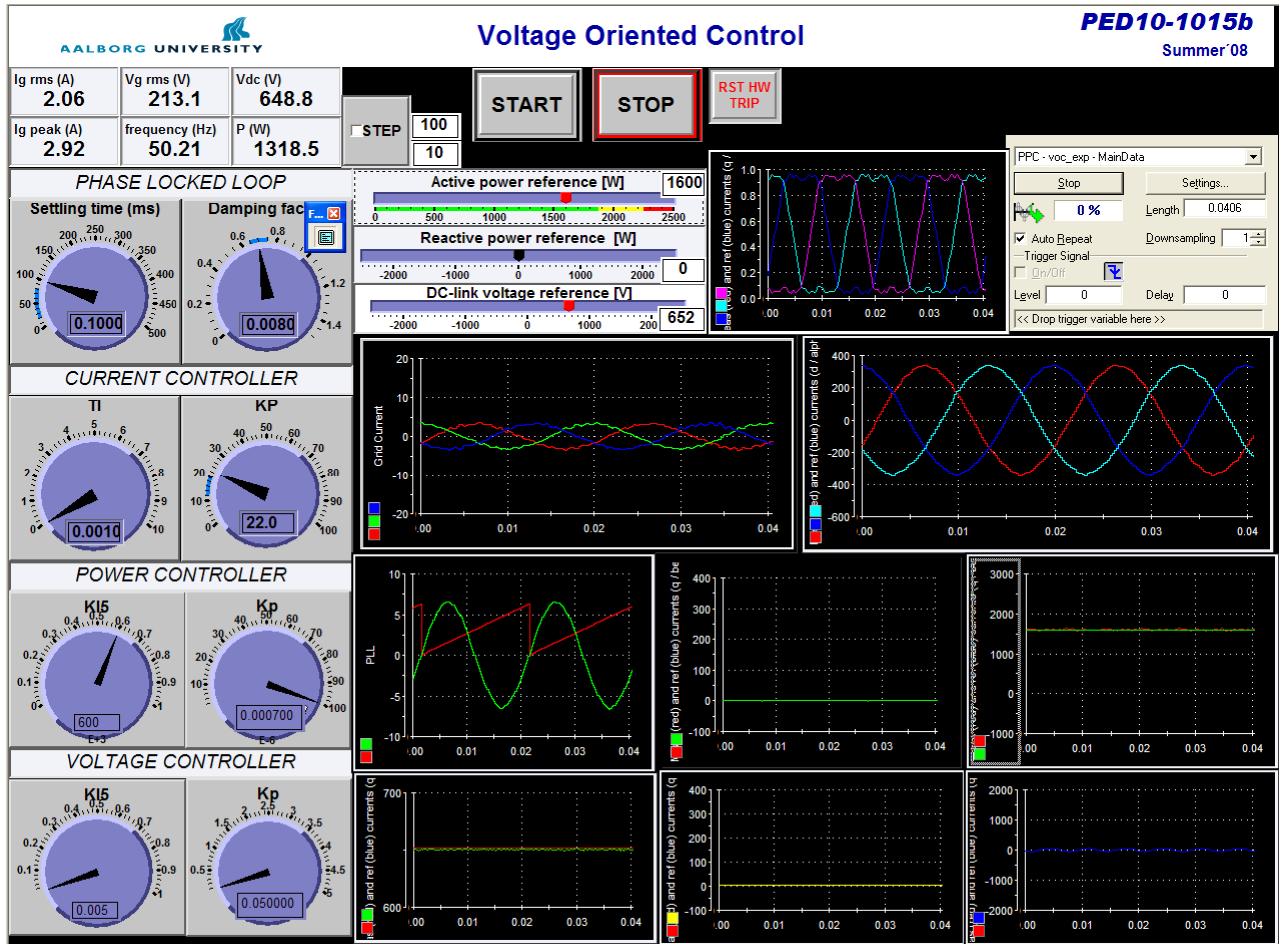


Fig.5. 11 Control Desk Graphical User Interface for real-time evaluation of the control system

It can be used to provide inputs such as:

- active and reactive power reference
- DC-link voltage reference

It can be used to visualize outputs such as:

- DC voltage reference and measured
- Active & reactive power reference and measured
- Grid synchronization(theta provided by the PLL which is in phase with the grid voltage)
- dq-axes currents reference and measured
- grid currents and voltages
- duty cycles D_a , D_b , D_c

5.2.2 Experimental results

The control of the grid side converter has been tested using the experimental test setup presented in Section 5.2.1. The study case which is analyzed is similar with the simulation case from Section 5.1 and it proves that the control system is well performed when the reference input active power is changed with step variations.

In order to validate the design of the PLL system and to prove the synchronization with the grid voltages, Fig.5.13 is represented where it can be seen that the PLL is extracting without errors the phase angle of the grid voltages and is providing the synchronization with the grid.

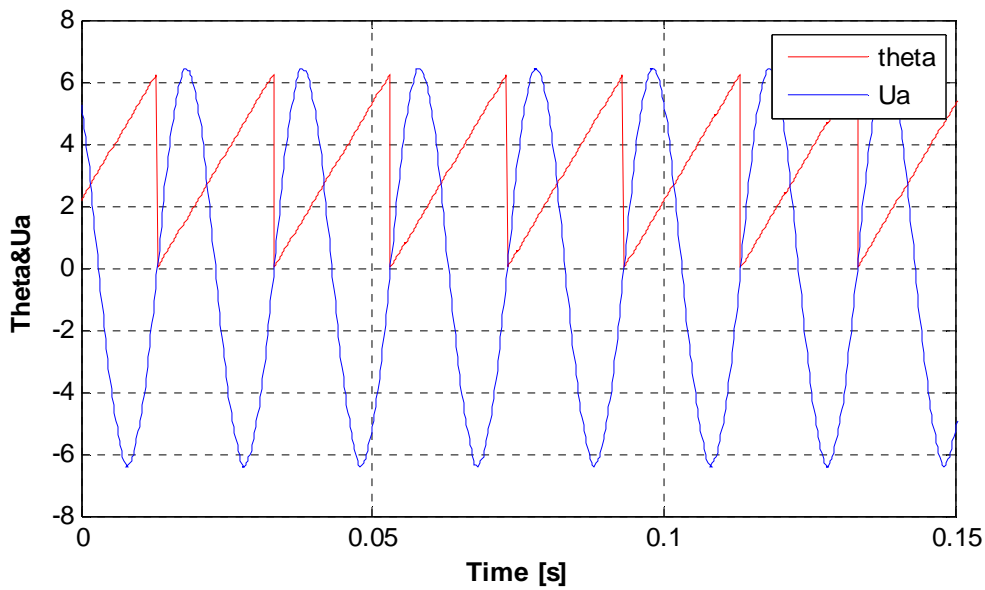


Fig.5.12 Grid phase voltage & Theta PLL

The duty cycle provided to the inverter is represented in Fig.5.14

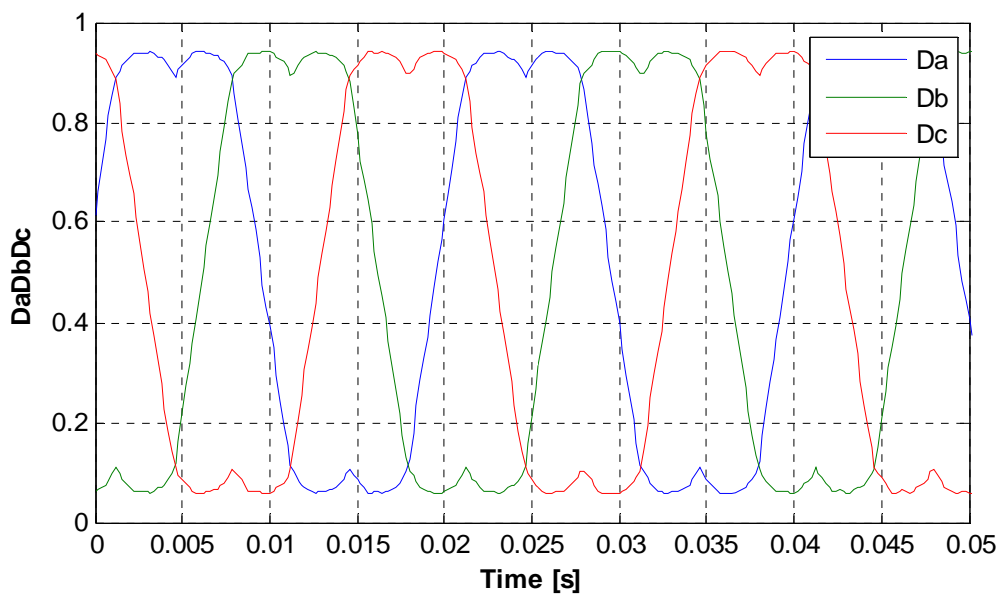


Fig.5.13 Duty cycle

The reactive energy being set to 0 can be seen that the grid phase voltage is in phase with grid phase current.

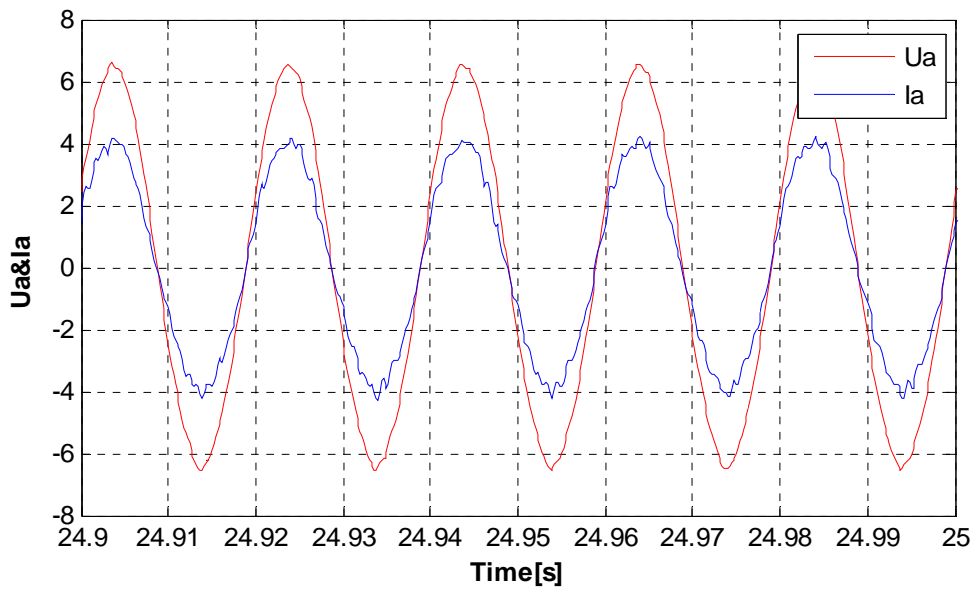


Fig.5. 14 Ua&Ia

As can be seen in Fig.5.14 the reference active power is following a step which is starting from 100W and is increasing every 5s to the nominal power of the inverter (2200kW). It also can be notice that the measured power is following very well the reference. The i_d measured current is represented in Fig.5.15. It can be notice that it follows very well the reference which means that the current controller is very well performed.

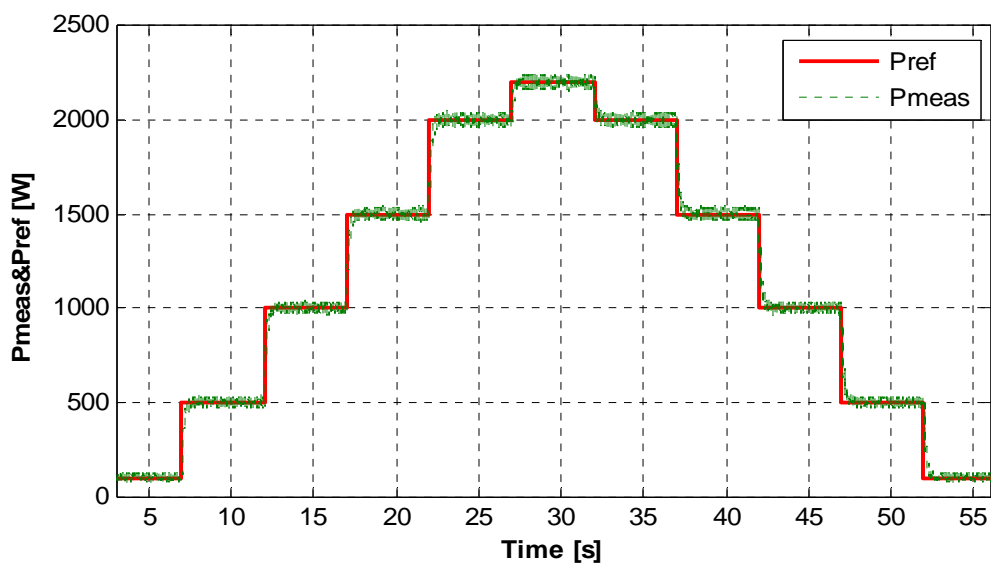


Fig.5.15 Active power reference and the active power

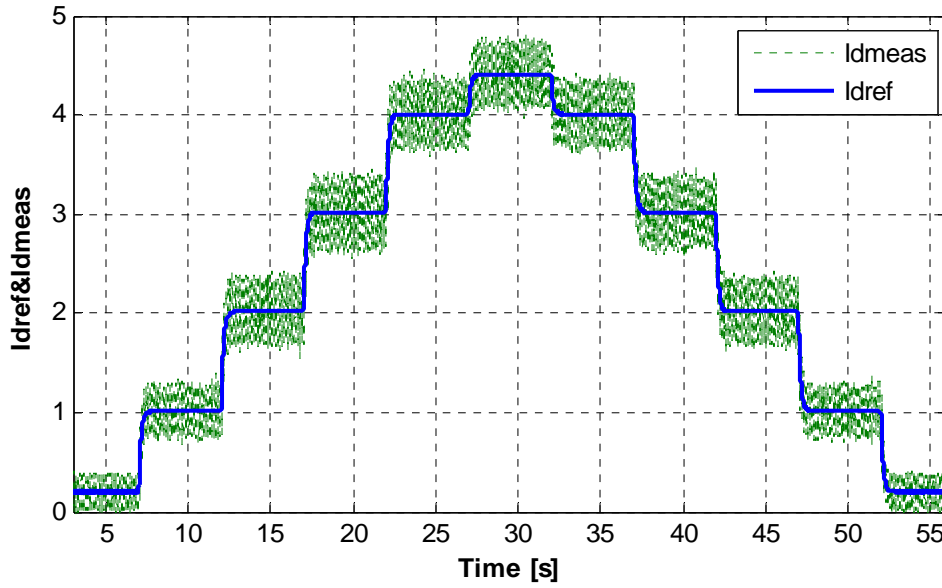


Fig.5.16 Id measured & reference current

In Fig.5.16 the grid currents are represented and it can be seen that are increasing direct proportional with the active power reference step variation.

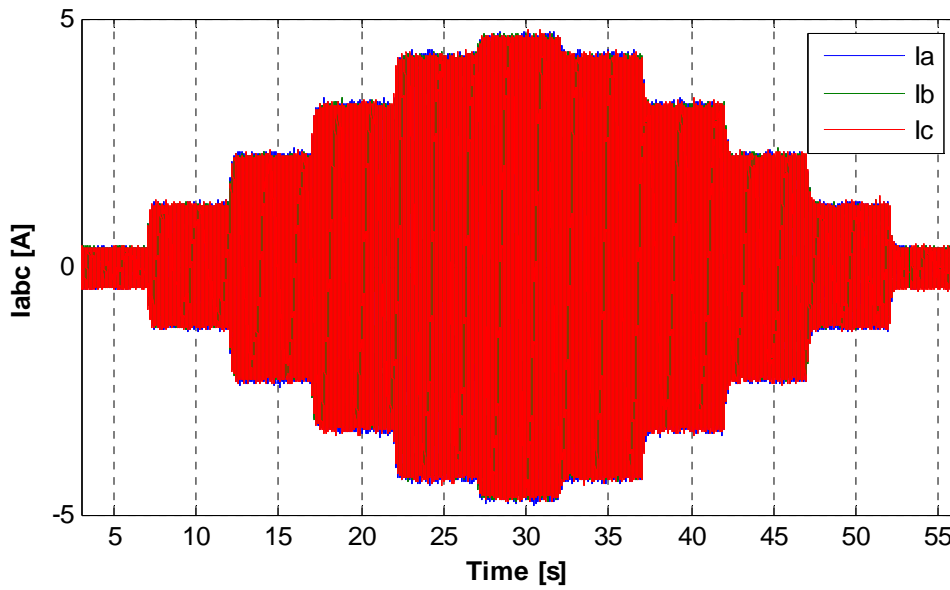


Fig.5.17 Grid currents

A zoom in the grid currents is done and can be seen in Fig.5.17 the behavior of these currents following the step in power reference.

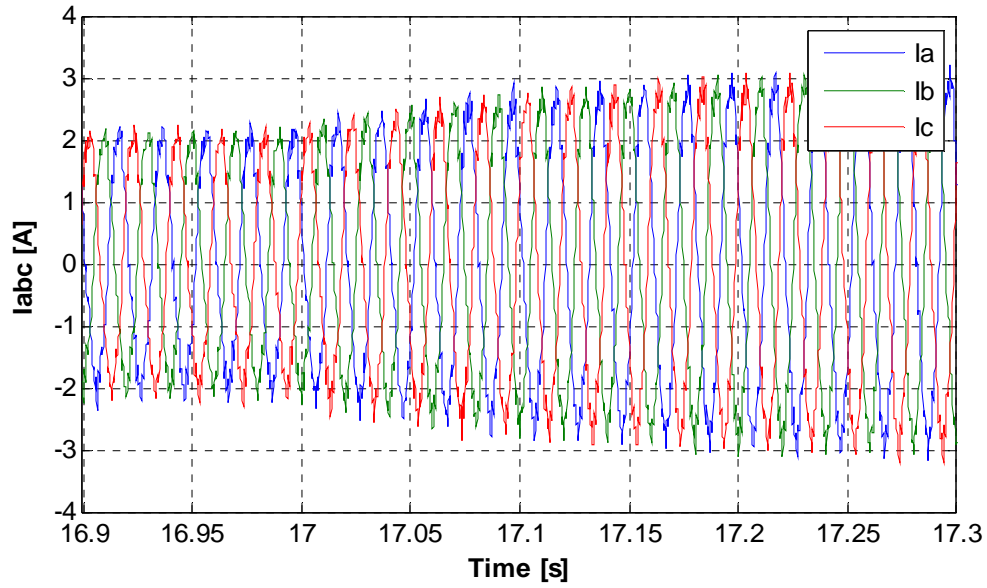


Fig.5. 18 Grid currents-zoom

Summary

In this chapter the simulation results have been presented together with their implementation. A description of the experimental test setup is included in the second part and the experimental results are described in the end of this chapter.

Chapter 6

Conclusion and future work

6.1. Conclusions

This project is focused on the control of the grid side converter in a back-to back configuration and can be organized into four main parts:

1. Background and project definition
2. Modelling
3. Control system design
4. Implementation and experimental evaluation

In the first part, the project is defined. First a short background about the wind energy technology is provided; different concepts for variable-speed wind turbines are presented and a description of the project and goals is given. It can be including in the first part also the overview of the grid codes and control strategies for the grid side converter which are presented in Chapter 2.

The second part of the project is focused on modelling each component of the considered system. In order to simulate the entire system for the assessment of the control system, the models of the following items are required:

- model of the DC-link capacitor
- model of the grid side converter
- model of the LCL-filter
- model of the grid

Model of the DC-link capacitor is used to obtain the DC-link voltage provided to the grid side inverter and to the control system. The model of the grid side inverter is composing by an ideal six-switch inverter without any physical limitation or dissipation or lag or non-linearity. The grid side converter is connected to the grid model by means of an LCL filter which effect is to reduce the high frequency current ripple injected by the inverter. The grid model is represented as an ideal symmetrical three-phase voltage source. All this four main parts of the system are composing the plant model.

The third part of the project is focused on the design of the control system required to control the grid side power converter. The control method chosen for the design is voltage oriented

control which is a control strategy for the grid side converter where the active and reactive power are regulated by controlling the i_d and i_q current components.

Here the following items are designed:

- Phase locked loop
- DC voltage controller
- Q controller
- dq-axes controller

PLL is the most extended frequency adaptive technique for grid synchronization of the WT. Is also a very useful method that enables the grid invertors to create a current reference synchronized with the grid and also to comply with the grid monitoring standards. Grid synchronization allows a right instantaneous interaction between the power converter and the grid.

The aim of the DC voltage controller is a outer loop current controller which will keep the voltage constant on the DC side in normal condition or during grid faults or changes in input power. The inputs for this block are the reference and measured values for the DC voltage. The error between these two values will be the input for a PI controller which will put on the output the reference signal for the i_d -axis current. The design of the controller is presented in section 4.2.3.

For the reactive power it has been implemented another PI controller which will keep the measured reactive power following the reference. The output from this block will be the reference signal for the i_q -axis current.

The dq-axes controller is the inner loop which will correct the error between the reference i_d , i_q and the measured values for this two current axis. The references are providing by the voltage controller respectively reactive power controller while the measured values are derived from the grid currents which are transformed by means of the frame transformations in d-q-axes currents. On the output of this block the references for the d-q voltages axes will be transformed in \hat{v}_d and \hat{v}_q and applied to the duty cycle generator block.

The last part of the project is focused on the implementation of the designed control system and experimental validation; the control system is implemented in a dSPACE platform and tested with an experimental test setup. The experimental evaluations have led to the following considerations:

- the simulation results have been validate by the experimental results
- the design of the controller is well performed

Due to time constraints, the harmonics compensation techniques is not a part of this project but this topic will be one of the tasks for the future work.

A Graphical User Interface (GUI) is built for the real-time evaluation of the control performance.

6.2. Future work

Future work of the present project includes:

- design and implementation of other control strategies for the grid side converter in order to do a comparison between methods of control.
- implementation of the harmonic compensation techniques
- grid inverter control in case of line voltage asymmetry
- low voltage ride through (grid codes compliance)
- this work has been focused and implemented only on the grid side converter. A complete implementation of the control strategy for the generator side together with the control for the grid side convertor could be build
- implementation of the entire control system in a C-S Function to reduce the computational time.

References:

- [1] F. D. Bianchi, H. D. Battista, and R. J. Mantz, *Wind Turbine Control System*. Springer, 2007. ISBN 1-8462-8492-9
- [2] F. Blaabjerg and F. Iov, "Wind power - a power source now enabled by power electronics," 30 September - 4 October 2007. Keynote paper in Proc of 9th Brazilian Power Electronics Conference COBEP 07, Blumenau Santa Catarina, Brazil, ISBN 978-85-99195-02-4.
- [3] F. Blaabjerg, F. Iov, Z. Chen, and R. Teodorescu, "Power electronics in renewable energy systems," Keynote paper at EPE-PEMC 2006 Conference, August 30 - September 1 2006, Portoroz, Slovenia, p.17, IEEE Catalog Number: 06EX1405C, ISBN 1-4244-0449-5.
- [4] F. Iov and F. B. UNIFLEX-PM, "Advanced power converters for universal and flexible power management in future electricity network - converter applications in future European electricity network," tech. rep., 2007.
- [5] F. Blaabjerg, R. Teodorescu, M. Liserre, and A. Timbus, "Overview of control and grid synchronization for distributed power generation systems," IEEE Transactions on Industrial Electronics, 2006.
- [6] J.G.Slootweg, H. Polinder, and W.L.Kling, "Dynamic modelling of a wind turbine with doubly fed induction generator," IEEE, 2001.
- [7] F. Hansen, L. Helle, F. Blaabjerg, E. Ritche, S. Munk-Nielsen, H. Bindner, P. Sørensen, and B. Bak-Jensen, *Conceptual survey of Generators and Power Electronics for Wind Turbines*. RISØ National laboratory, December 2001.
- [8] J. H. O. Carlson and K. Thorborg, "Survey of variable speed operation of wind turbines," in European Union Wind Energy Conference, pp. 496–409, 1996.
- [9] A report by EWEA, "Large scale integration of wind energy in the European power supply". Published by EWEA, December 2005.
- [10] J. C. Ausin, D. N. Gevers and B. Andresen, "Fault Ride-Through Capability test unit for Wind Turbines"
- [11] Lícia Neto Arruda, Sidélmo Magalhães Silva, Braz J. Cardoso Filho, *PLL Structures for Utility Connected Systems*,
- [12] Mihai Ciobotaru, Remus Teodorescu, Vassilios G Agelidis, *Offset rejection for PLL based synchronization in grid-connected converters, APEC-2008*
- [13] UNIFLEX-PM "Advanced Power Converters for Universal and Flexible Power Management in Future Electricity Network" 019794 (SES6)
- [14] F. Blaabjerg and F. Iov, "Wind power - a power source now enabled by power electronics," 30 September - 4 October 2007. Keynote paper in Proc of 9th Brazilian Power Electronics Conference COBEP 07, Blumenau Santa Catarina, Brazil, ISBN 978-85-99195-02-4.

- [15] A. Timbus, R. Teodorescu, F. Blaabjerg “*Independent Synchronization and Control of Three Phase Grid Converters*” SPEEDAM 2006 International Symposium on Power Electronics, Electrical Drives, Automation and Motion
- [16] A. Timbus, R. Teodorescu, F. Blaabjerg *Synchronization Methods for Three Phase Distributed Power Generation Systems. An Overview and Evaluation* 0-7803-9033-4/05/\$20.00 ©2005 IEEE.
- [17] F. Iov, A. Hansen, P. Sørensen, and F. Blaabjerg, Wind Turbine Blockset in Matlab/Simulink. General Overview and Description of the Model. Aalborg University, March 2004. ISBN 87-89179-46-3.
- [18] M. P. Kazmierkowski, R. Krishnan, and F. Blaabjerg, *Control in Power Electronics*. Academic Press, 2002. ISBN 0-12-402772-5.
- [19] M. Liserre, A. Dell’Aquila, F. Blaabjerg “Genetic Algorithm-Based Design of the Active Damping for an LCL-Filter Three-Phase Active Rectifier” *Power Electronics, IEEE Transactions on power electronics*, Volume 19, No 1, Jan. 2004 Pp: 76 - 86
- [20] M. Liserre, A. Dell’Aquila, F. Blaabjerg “*Design and Control of an LCL-filter based Three-phase Active Rectifier*”, Industry Applications Conference, 2002. 37th IAS Annual Meeting Volume 2, 13-18 Oct. 2002 Page(s):1181 - 1188 vol.2
- [21] N. Mohan, *Advanced electric drives*. MNPERE, 2001. ISBN -9715-2920-5.
- [22] R Teodorescu, F. Blaabjerg “*Flexible control of small wind turbines with grid failure detection operating in stand-alone and grid-connected mode*” *IEEE Transactions on power electronics*, Volume 19, No 5, Sept. 2004 Pp: 1323 - 1332
- [23] M. Liserre, A. Dell’Aquila, F. Blaabjerg “*Design and control of a three-phase active rectifier under non-ideal operating conditions*” *IEEE Transactions on power electronics*, 2002 Pp: 1181 - 1188
- [24] M. Liserre, F. Blaabjerg, R Teodorescu “*Grid impedance estimation via excitation of LCL-filter resonance*” *IEEE Transactions on industry applications* Volume 43, No 5, Sept/Oct. 2007 Pp: 1401 - 1407
- [25] dSPACE, Real-Time Interface (RTI and RTI-MP): Implementation Guide, November 2005. Release 5.0.

- [26] R. Teodorescu, F. Iov, F. Blaabjerg "Modeling and control of grid converter. Phase 1a: Basic grid inverter control" February 2006

Nomenclature

C_{dc}	DC-link capacitor
C_F	three phase LCL filter capacitance
d_a, d_b, d_c	switching states for the voltage source
E_m	amplitude of the phase voltage
i_a, i_b, i_c	three phase currents
i_d, i_q	current in 'dq' rotating frame
i_C	capacitor current
i_L	line current vector
i_G	grid side current
i_I	inverter side current
I_m	amplitude of the phase current
i_α, i_β	current in stationary frame
K_I	integral gain for the PI controller
K_P	proportional gain for the PI controller
L	total inductance
L_G	grid side inductance
L_I	inverter side inductance
P, Q	active and reactive powers
R_D	damping resistance
R_G	grid side resistance
R_I	inverter side resistance
s	continuous operator
t	time

T_I	integral time constant
T_s	sampling time
t_s	settling time
S_d	switching steady state signal
u_a, u_b, u_c	three phase voltages
$u_{abinv}, u_{bcinv}, u_{cainv}$	output line voltages of the inverter
u_{AN}, u_{BN}, u_{CN}	inverter's leg voltages
u_L	line voltage vector
u_C	capacitor voltage
u_{DC}	DC-link voltage
u_d, u_q	voltages in 'dq' rotating frame
u_G	grid side voltage
u_I	inverter side voltage
γ	angle between 'abc' and 'dq' frames
φ	phase between voltage and current
θ	grid phase angle
ω	angular frequency
ω_n	natural frequency
ω_{ff}	feed-forward frequency
Ψ	phase margin
ζ	damping factor

Abbreviations

AC	Alternating Current
DC	Direct Current
DFIG	Doubly Fed Induction Generator
DFIGWT	Doubly Fed Induction Generator Wind Turbine
DPC	Direct Power Control
EMI	Electromagnetic Interference
FRS	Frequency Response System
FRT	Fault-Ride-through Capability
FSPCWT	Full Scale Power Converter Wind Turbine
FSWT	Fixed Speed Wind Turbine
GC	Grid Codes
HV	High Voltage
IG	Induction Generator
LCL	Inductance-Capacitance-Inductance
LV	Low Voltage
MV	Medium Voltage
NPC	Neutral-Point Clamped
PCC	Point-of Common-Coupling
PI	Proportional-Integral Controller
PLL	Phase-Locked Loop
PMSG	Permanent Magnet Synchronous Generator
PVSWT	Partial Variable Speed Wind Turbine
PWM	Pulse Width Modulation
SCIG	Squirrel Cage Induction Generator
SO	System Operator
SVC	Static VAR Compensators
SVM	Space Vector Modulation
THD	Total Harmonics Distortion

TSO	Transmission System Operator
UPF	Unity Power Factor
VFDPC	Virtual Flux Direct Power Control
VFOC	Virtual Flux Oriented Control
VOC	Voltage Oriented Control
VRS	Voltage Regulator System
VSC	Voltage Source Converter
VSI	Voltage Source Inverter
WECS	Wind Energy Conversion System
WFPS	Wind Power Stations
WT	Wind Turbine
WRIG	Wound Rotor Induction Generator
ZCD	Zero Cross Detection

Appendix

Abstract

In this section are presented the reference frame transformations (see Appendix A) and all simulation and implementation blocks (Matlab Simulink and dSPACE) used in the control of the grid side converter (see Appendix B).

Appendix A: Reference Frame Theory.....	Page 92
Appendix B: Simulation and Implementation Models.....	Page 95

Appendix A

Reference Frame Theory

The aim of this section is to introduce the essential concepts of reference frame theory.

Three-phase to two-phase transformation (Clarke transformation)

The Clarke transform is using three time varying variables $f_a(t), f_b(t), f_c(t)$ to calculate their two-components in orthogonal axis. The three time varying variables $f_a(t), f_b(t), f_c(t)$ can be represented by means of the space vector \underline{f}_{abc} which is defined as follows [21]:

$$\underline{f}_{abc} = \frac{2}{3}(f_a(t) + \alpha f_b(t) + \alpha^2 f_c(t)) \tag{A.1}$$

where $\alpha = e^{j\frac{2\pi}{3}}$. The representation of the space vectors is shown in the figure A1

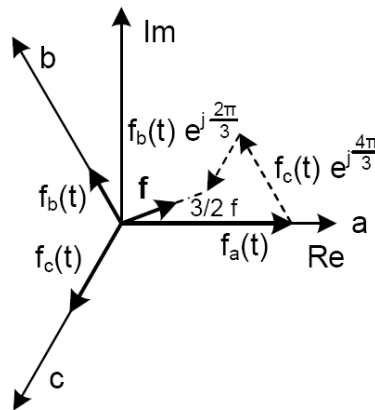


Figure A.1. Space vector concept in abc reference frame

By means of Clarke transformation \underline{f}_{abc} can be represented in a stationary reference frame $\alpha\beta$ (α is the real axis and is aligned with a-axis, β is the imaginary axis) as in figure A.2.

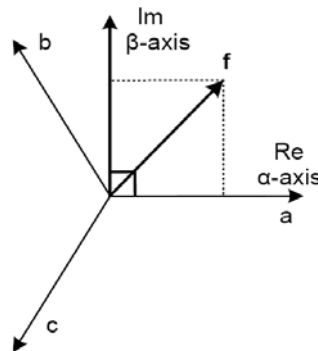


Figure A.2. Space vector concept in $\alpha\beta$ reference frame

The space vector $\underline{f}_{\alpha\beta}$ is defined as the complex quantity:

$$\underline{f}_{\alpha\beta} = f_{\alpha}(t) + jf_{\beta}(t) \quad (\text{A.2})$$

where the components $f_{\alpha}(t)$, $f_{\beta}(t)$ can be calculated as follows:

$$f_{\alpha} = \frac{2}{3} \left(f_a(t) - \frac{1}{2}f_b(t) - \frac{1}{2}f_c(t) \right) \quad (\text{A.3})$$

$$f_{\beta} = \frac{2}{3} \left(0 + \frac{\sqrt{3}}{2}f_b(t) - \frac{\sqrt{3}}{2}f_c(t) \right) \quad (\text{A.4})$$

Vector rotation (Park transformation)

When we deal with vector control of electrical machines, it is generally necessary to use a common reference frame for both the rotor and the stator [21].

$\underline{f}_{\alpha\beta}$ can be represented in a rotating reference frame dq by means of the Park transformation where the d-axis is the real-axis which is shifted by an angle θ_{dq} with respect to the a-axis [21].

The space vector \underline{f}_{dq} in this new reference frame is given by:

$$\underline{f}_{dq} = f_d(t) + jf_q(t) \quad (\text{A.5})$$

where the components $f_d(t)$, $f_q(t)$ can be calculated as follows:

$$f_d(t) = f_{\alpha}(t)\cos\theta_{dq} + f_{\beta}(t)\sin\theta_{dq} \quad (\text{A.6})$$

$$f_q(t) = -f_{\alpha}(t)\sin\theta_{dq} + f_{\beta}(t)\cos\theta_{dq} \quad (\text{A.7})$$

The space vector concept in the rotating reference frame is shown in the figure A.3.

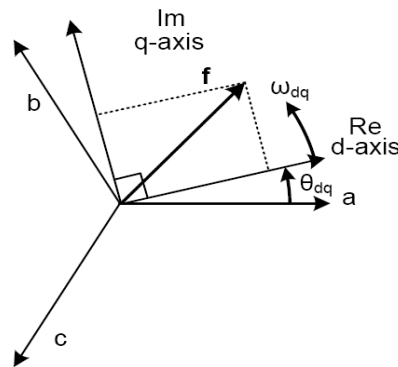


Figure C.3. Space vector concept in dq reference frame

The space vector \underline{f}_{dq} can be directly obtained from \underline{f}_{abc} as follows:

$$\underline{f}_{dq} = T_{dq}\underline{f}_{abc} \quad (\text{A.8})$$

where

$$T_{dq} = \frac{2}{3} \begin{bmatrix} \cos(\theta_{dq}) & \cos\left(\theta_{dq} - \frac{2\pi}{3}\right) & \cos\left(\theta_{dq} + \frac{2\pi}{3}\right) \\ -\sin(\theta_{dq}) & -\sin\left(\theta_{dq} - \frac{2\pi}{3}\right) & -\sin\left(\theta_{dq} + \frac{2\pi}{3}\right) \\ \frac{1}{2} & \frac{1}{2} & \frac{1}{2} \end{bmatrix} \quad (\text{A.9})$$

The transformation from dq frame to abc frame is shown below:

$$\underline{f}_{abc} = T_{dq}^{-1} \underline{f}_{dq} \quad (\text{A.10})$$

$$T_{dq}^{-1} = \frac{2}{3} \begin{bmatrix} \cos(\theta_{dq}) & -\sin(\theta_{dq}) & 1 \\ \cos\left(\theta_{dq} - \frac{2\pi}{3}\right) & -\sin\left(\theta_{dq} - \frac{2\pi}{3}\right) & 1 \\ \cos\left(\theta_{dq} + \frac{2\pi}{3}\right) & -\sin\left(\theta_{dq} + \frac{2\pi}{3}\right) & 1 \end{bmatrix} \quad (\text{A.11})$$

Appendix B

In this section the simulation and implementation models are presented. The simulation models are designed using Matlab Simulink.

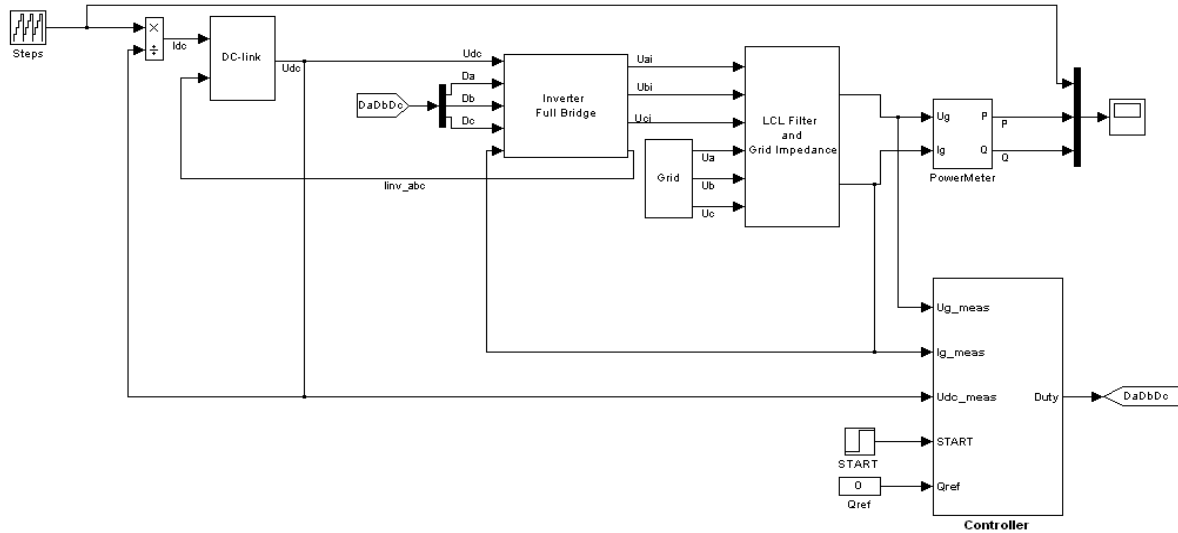


Fig. B1. Simulation model

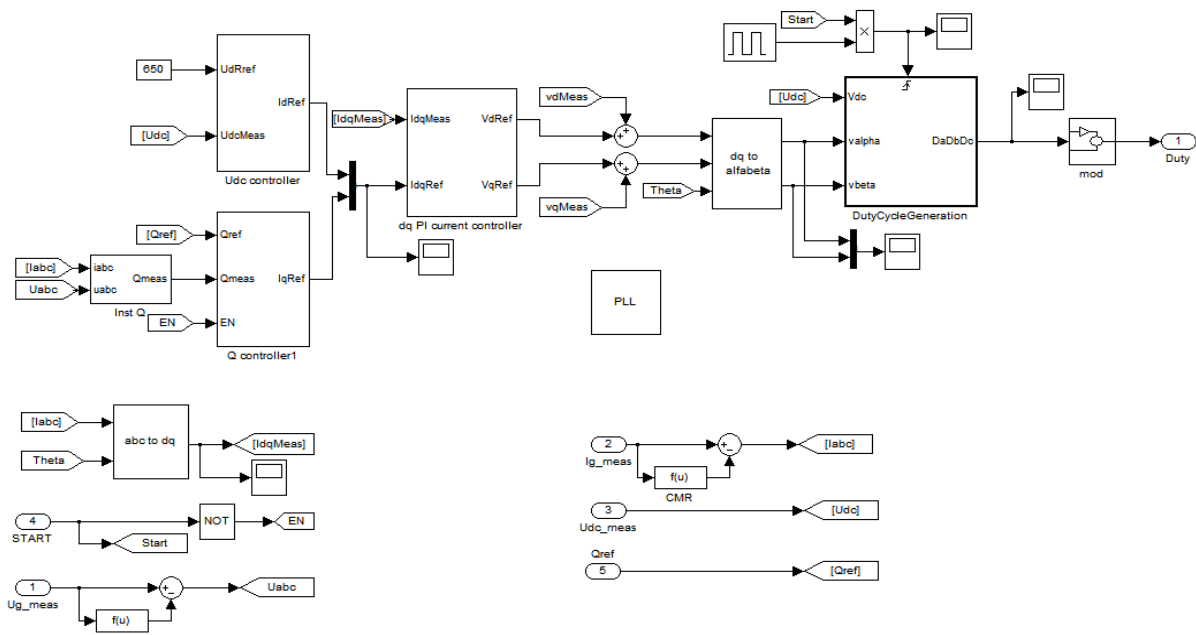


Fig. B2. Control System (VOC)

Phase-Locked Loop (PLL)

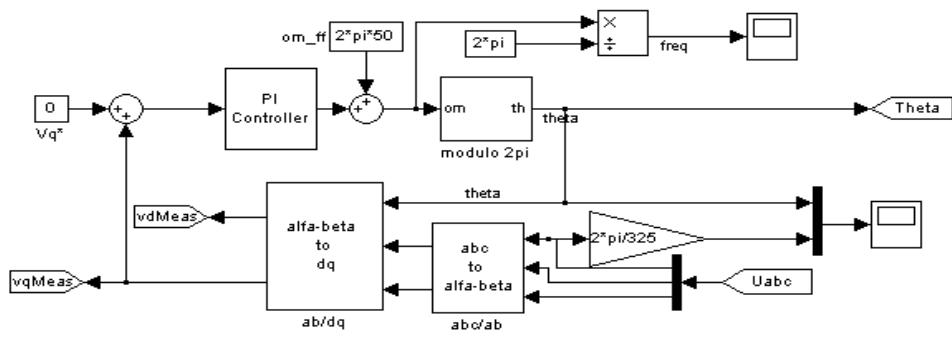


Fig. B3. PLL model

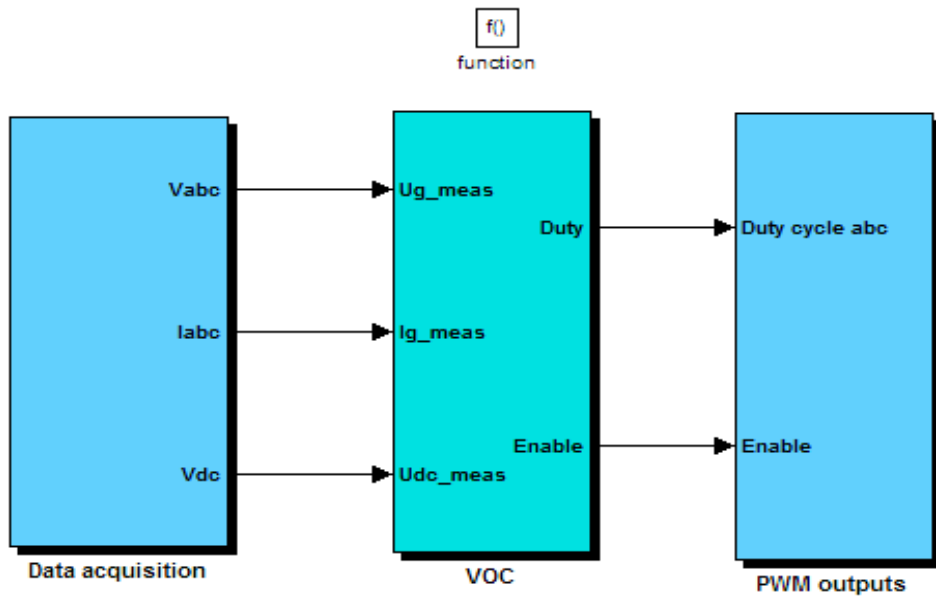


Fig B4. Experimental model